GEOMAR REPORT

NIELS NØRGAARD-PEDERSEN

LATE QUATERNARY ARCTIC OCEAN SEDIMENT RECORDS: SURFACE OCEAN CONDITIONS AND PROVENANCE OF ICE-RAFTED DEBRIS

65

GEOMAR REPORT

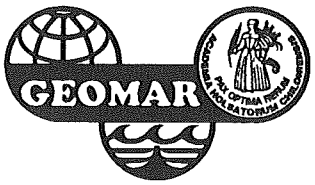

NIELS NØRGAARD-PEDERSEN

LATE QUATERNARY ARCTIC OCEAN SEDIMENT RECORDS: SURFACE OCEAN CONDITIONS AND PROVENANCE OF ICE-RAFTED DEBRIS

GEOMAR
Forschungszentrum
für marine Geowissenschaften
der Christian-Albrechts-Universität
zu Kiel

Kiel 1997

GEOMAR REPORT 65

GEOMAR
Research Center
for Marine Geosciences
Christian Albrechts University
in Kiel

Dissertation
zur Erlangung des Doktorgrades
der Mathematisch-Naturwissenschaftlichen Fakulät
der Christian-Albrechts-Universität zu Kiel
Zum Druck genehmigt am 13.11.1996

Redaktion der Serie: Gerhard Haass
Umschlag: Kerstin Kreis, Harald Gross, GEOMAR Technologie GmbH

Managing Editor: Gerhard Haass
Cover: Kerstin Kreis, Harald Gross, GEOMAR Technologie GmbH

GEOMAR REPORT
ISSN 0936 - 5788

GEOMAR REPORT
ISSN 0936 - 5788

GEOMAR
Forschungszentrum
für marine Geowissenschaften
D-24148 Kiel
Wischhofstr. 1-3
Telefon (0431) 600-2555, 600-2505

GEOMAR
Research Center
for Marine Geosciences
D-24148 Kiel / Germany
Wischhofstr. 1-3
Telephone (49) 431 / 600-2555, 600-2505

CONTENTS

[1] Original data in doctoral thesis (Nørgaard-Pedersen, 1996) at GEOMAR Research Center for Marine Geosciences, Wischhofstraße 1-3, D24148 Kiel, Germany

Summary

Sediment cores from the Eurasian Basin and the central part of the Arctic Ocean, spanning the last glacial-interglacial cycle, have been studied to search for evidence of changes in surface ocean environment in relation to climate controls and interaction with surrounding continents, ice sheets and oceans. The basic approach has been stratigraphic work on stable isotope records of planktic foraminifers, radiocarbon datings, coarse fraction analysis, and carbonate content.

Major environmental changes reflected in the hemipelagic sediments seem to be in phase with the variation of Northern Hemisphere glaciation and summer insolation. During glacial maxima, in oxygen isotope stages 4 and 2, the Arctic Ocean was characterised by a dense cover of sea ice with decreased seasonal variation limiting planktic productivity and bulk accumulation rates. Mapping of $\delta^{18}O$ values and reconstruction of surface ocean salinity distribution for the last glacial maximum (LGM) indicate that salinities in the central Arctic Ocean were several permille lower than the moderate high and relative constant values reported for the Norwegian-Greenland Sea. Assuming that the Arctic hydrological cycle was significantly reduced during the LGM (cf. Alley et al., 1993), the reconstructed low central Arctic surface salinities appear to reflect a higher residence time of the central Arctic surface water layer rather than a high influx of river run-off/glacial meltwater. The controlling factor (apart from salinity stratification and mixing processes) was possibly the balance between inflowing saline Atlantic water and outflowing surface water and sea ice through the Fram Strait, as other gate-ways were subarially exposed or blocked by ice sheets during the LGM.

Major deglaciations of circum-Arctic regions, following the peak glacials, can be traced almost synchronously by studying the stable isotope signatures of planktic foraminifers. For early oxygen isotope stage 3, a deglacial event (?isotopic event 3.31) in connection with an insolation maximum can be traced from the central Arctic Ocean to the North Atlantic. Supported by radiocarbon datings, a more detailed scenario has been reconstructed for the last deglaciation (Termination I) involving a diachronic course of regional ice sheet degradation. Two peak deglacial meltwater episodes in the Arctic Ocean at 14-12 ^{14}C ka (Termination Ia) and 10-8 ^{14}C ka (Termination Ib) were apparently synchronous with the global record of maximum meltwater discharges. The early and rapid deglaciation of the marine-based Barents Sea Ice Sheet, associated with Termination Ia, can be traced over the southern Eurasian Basin to the Gakkel Ridge by a low-$\delta^{18}O$ spike leading a characteristic peak of ice-rafted debris (IRD). A separate Termination Ib meltwater event is most conspicuous in the central Arctic and is associated with abundant detrital carbonate IRD increasing in abundance toward the Makarov Basin and the Morris Jesup Rise. This supports an origin from northern Canada and northern Greenland where lower Paleozoic platform

carbonates extensively crop out. During the peak deglacial episodes, characterised by strongly reduced ventilation of surface waters, the flux of planktic foraminifers was apparently reduced. A higher planktic foraminifer productivity is suggested for substages 5c (105-95 ka) and 5a (85-74 ka), the middle part of stage 3 (50-35 ka), and the Holocene characterised by a moderate to high summer insolation. With reference to the present 'interglacial' environment these periods presumably were characterised by a high open-water (lead) fraction during summers, an increase of sea-ice rafted sediment incorporated on the wide Arctic shelves, and a moderate to high freshwater influx from circum-Arctic rivers.

The low hemipelagic sedimentation rates of central Arctic Ocean late Quaternary sediments (0.2-1.5 cm ky^{-1}) preclude resolution of shorter-scale climate oscillations (<1000 years) linked to North Atlantic ocean/atmosphere circulation changes.

Zusammenfassung

Sedimentkerne aus dem Eurasischen Becken und dem zentralen Arktischen Ozean wurden untersucht, um die Veränderlichkeit wichtiger Eigenschaften der Oberflächenwassermassen während des letzten Glazial-Interglazial-Zyklus festzustellen. Dabei sollten klimatische Einflüsse und die Wechselwirkungen mit den umgebenden Kontinenten, Eisschilden und Ozeanen herausgearbeitet werden. Die stratigraphische Grundlage bildeten Radiokarbondatierungen und Profile stabiler Isotope in planktischen Foraminiferen, sowie Grobfraktions- und Karbonatgehaltsanalysen.

Die bedeutendsten Umweltveränderungen, die in den hemipelagischen Sedimenten abgebildet sind, scheinen weitgehend synchron mit den Veränderungen der Nordhemispären-Vereisungen und der Sommer-Insolation zu verlaufen. Während der glazialen Maxima in den Sauerstoffisotopenstadien 4 und 2 war der Arktische Ozean durch eine dichte Eisdecke mit beschränkter jahreszeitlicher Variation charakterisiert, so daß die planktische Produktivität und die Gesamtakkumulationsraten stark reduziert wurden. Die Kartierung der $\delta^{18}O$-Werte und die Rekonstruktion der Oberflächenwasser-Salzgehalte für das letzte glaziale Maximum (LGM) zeigen, daß die Salzgehalte im zentralen Arktischen Ozean mehrere Promille niedriger waren als die mittelhohen und relativ konstanten Werte, die aus dem Europäischen Nordmeer bekannt sind. Unter der Annahme, daß der arktische hydrologische Kreislauf während des LGM stark reduziert war (vgl. Alley et al., 1993), wird vermutet, daß die rekonstruierten niedrigen Oberflächenwasser-Salzgehalte in der zentralen Arktis eher von einer längeren Verweilzeit des Oberflächenwassers herrühren als von einem verstärkten Einstrom von Flußwasser und/oder Schmelzwasser. Der regulierende Faktor (abgesehen von Wassermassenschichtung und Mischungsprozessen) war vermutlich das Gleichgewicht zwischen dem einströmenden salzreichen Atlantikwasser einerseits und dem ausströmenden Oberflächenwasser und Meereis durch die Framstraße andererseits. Andere Meeresstraßen waren während des LGM entweder subaerisch exponiert oder von mächtigen Eisschilden bedeckt.

Die Hauptdeglaziationsphasen in den zirkum-arktischen Gebieten sind nahezu gleichzeitig in den Sauerstoffisotopensignalen planktischer Foraminiferen abgebildet. Ein deglaziales Ereignis im frühen Sauerstoffisotopenstadium 3 (Isotopenereignis 3.31?), das parallel zu einem lokalen Insolationsmaximum auftrat, kann vom zentralen Arktischen Ozean bis in den Nordatlantik verfolgt werden. Ein weitaus detaillierteres Szenario konnte auf der Basis von ^{14}C-Datierungen für die letzte Deglaziation (Termination I) rekonstruiert werden. Dabei zeigte sich eine diachroner Verlauf im Zerfall der einzelnen Eisschilde. Zwei Schmelzwasserereignisse (14-12 ^{14}C ka und 10-8 ^{14}C ka, die Terminationen Ia und Ib)

während der Hauptdeglaziationsphase fanden offenbar gleichzeitig mit den bedeutendsten Schmelzwassereinträgen in den Weltozean statt. Der frühe und rasche Zerfall des "marine-based" Barentssee-Eisschildes während der Termination Ia kann über das südliche Eurasische Becken bis zum Gakkelrücken über ein niedriges $\delta^{18}O$-Signal verfolgt werden, dem unmittelbar ein charakteristischer Spitzenwert im Gehalt an eistransportiertem Material (IRD) folgt. Ein davon klar abgegrenztes Schmelzwasserereignis während der Termination Ib ist am stärksten im zentralen Bereich des Arktischen Ozeans ausgeprägt. Besonders dort erfolgte ein erhöhter Eintrag von detritischem Karbonat im IRD, mit steigenden Werten in Richtung Makarovbecken und Morris-Jesup-Rise. Diese Beobachtung bestärkt die Vermutung, daß dieses Material aus dem Bereich des nördlichen Kanada und Grönland stammt, wo frühpaläozoische Plattformkarbonate großflächig anstehen. Während der Hauptdeglaziationsphasen, charakterisiert durch eine stark reduzierte Durchlüftung des Oberflächenwassers, war die Ablagerung von planktischen Foraminiferen stark reduziert. Phasen erhöhter planktischer Produktivität lagen vermutlich in den Isotopensubstadien 5c (105-95 ka) und 5a (85-74 ka), im mittleren Stadium 3 (50-35 ka) und im Holozän, also in Zeiten mittlerer bis hoher Sommerinsolationswerte. Vergleichbar mit den heutigen "interglazialen" Verhältnissen waren diese Zeitabschnitte vermutlich (besonders im Sommer) durch einen relativ hohen Anteil an offenen Wasserflächen (Rinnen) im Eis gekennzeichnet. Es wurde dann verstärkt Meereis-transportiertes Sediment abgelagert, das auf den breiten arktischen Schelfen ins Eis eingetragen worden war. Der Einstrom von Süßwasser durch zirkum-arktische Flüsse war mittelhoch bis hoch.

Die allgemein niedrigen hemipelagischen Sedimentationsraten der spätquartären Ablagerungen im zentralen Arktischen Ozean (0,2-1,5 cm/1000 J.) verhindern leider die Auflösung von Klimaveränderungen im Bereich von 1000 oder weniger Jahren, die in Verbindung mit entsprechenden Veränderungen im System Ozean-Atmosphäre im Nordatlantik stehen können.

1. INTRODUCTION

During the last decades it has been realised that the Arctic Ocean plays a decisive role for the global climate and the dynamics of the world's ocean and atmosphere. The rapid fluctuations of the Arctic sea ice cover, and its consequences for global change, are therefore intensively being studied. Changes in ice production and freshwater budget of the Arctic Ocean and its shelf seas, or in the export of these products to the convective regions of the North Atlantic, might alter the large-scale Atlantic circulation cell and cause major changes for northwestern Europe climate in particular.

Sea ice covers and their margins have responded rapidly to the extreme climate changes during the most recent geological past. Geological data from the North Atlantic Ocean and the Norwegian-Greenland Sea reveal dramatic changes in marine ice cover, iceberg and melt water discharge between glacial and interglacial situations (Bond et al., 1992, 1993; Broecker et al. 1992; Grousset et al., 1993). Supporting information drawn from ice core data in Greenland suggests that the nature of the ice cover in the Norwegian-Greenland Sea, and probably also in the Arctic Ocean, can change over the time span of decades rather than centuries or millennia (Dansgaard et al. 1989; Johnsen et al. 1992; Alley et al., 1993; Taylor et al. 1993, Bond & Lotti, 1995). The consequences of the Quaternary global climatic cyclicity for the Arctic Ocean environment and interaction with adjacent seas and continents are less well known. Reconstructions of the last glacial Arctic Ocean, based on theoretical speculations rather than in situ data, hence reach from an icedome- or iceshelf-covered ocean (e.g. Hughes et al., 1977; Keigwin, 1982; Fillon, 1984) to an ice free, more saline Arctic Ocean (e.g. Olausson, 1985).

The sediments of the Arctic Ocean sea floor have recorded long- and short-term northern hemisphere cooling and warming during several million years (Clark et al., 1980; Aksu & Mudie, 1985; Thiede et al., 1990; Poore et al., 1993). Since the mid-sixties numerous sediment cores spanning the Pliocene and Quaternary periods of the Arctic Ocean history have been obtained from manned ice floe and icebreaker expeditions. Only little progress has been achieved in establishing a quantitative chronostratigraphic framework due to uncertainties in the interpretation of bio-, magneto-, aminoacid-, and isotope-stratigraphic data. Evidence from the Arctic Ocean of the last glacial period and subsequent deglaciation was until recently limited to cores from the southern part of the Eurasian Basin (Markussen et al. 1985; Zahn et al., 1985; Köhler, 1992). During the last decade, ODP initiatives as well as the Nansen Arctic Drilling Program and the cabability of research icebreakers to operate in unexplored regions of the Arctic Ocean have created the background for a better understanding of recent processes and paleoceanography. Better coring techniques and

improved dating methods of high latitude marine sediments with very little biogenic carbonate now cause that the Quaternary lithostratigraphic framework partly can be supplemented with a chronostratigraphic one.

Arctic Ocean Quaternary sediment sequences are characterised by strong lithological changes, which reflect changes in the supply of terrigenic and biogenic materials as well as different transport modes (ice-rafting, currents, turbidites). In order to translate the sedimentological and stable isotopic data into environmental proxies, the fluxes of the specific components have to be quantified. This can be done only if a high-resolution stratigraphy of the cores investigated can be established. For specific time slices, the spatial distribution of the sedimentological proxies can then mapped out as basis for an integrated environmental reconstruction. Major goals of the present work have been (a) to understand how the Arctic Ocean responded to major warming and cooling periods and subsequent growth and decay of circum-Arctic ice sheets during the last glacial-interglacial cycle, (b) to obtain more precise information on how the Arctic Ocean responded to varying influx of fresh water from rivers and deglacial melt water, and (d) to understand the climatic importance and effect of water mass exchange with the Norwegian-Greenland Sea (Fig. 1).

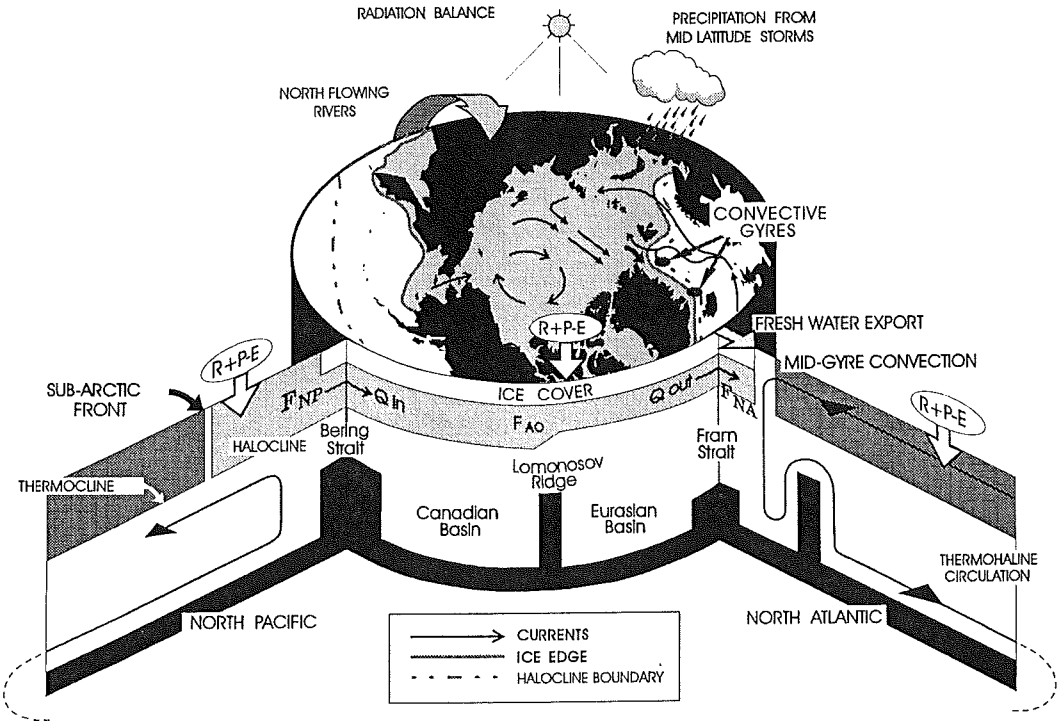

Fig. 1. Schematic Arctic Ocean climate connections. In the horizontal plane the extent of sea ice in winter is shown by the shaded region and the mean surface circulation by arrows. The subarctic front separates the salt-stratified upper water of the Arctic and subarctic oceans from the temperature-stratified upper waters of the subtropical oceans. From Aagaard & Carmack (1994).

1.1 Physiography, oceanography and ice cover of the Arctic Ocean

The Arctic Ocean is a strongly stratified enclosed sea with two major deep basins, the Amerasian and the Eurasian Basin, and extensive shallow shelves (Fig. 2). The up to 4500 m deep basins are separated by the 2000 km long Lomonosov Ridge extending from the north of Greenland to the New Siberian Islands. The Eurasian Basin north of the wide shelf areas of the Barents-, Kara-, and Laptev Sea is subdivided into the Nansen Basin and the Amundsen Basin by the active volcanic spreading ridge, the Gakkel Ridge. Four restricted passages connect the Arctic Ocean with the world oceans. The Barents Sea, Fram Strait, and the Canadian achipelago connect it to the North Atlantic, and Bering Strait connects it to the Pacific. Only Fram Strait permits exchanges of deep water over a sill at about 2500 m between the Arctic Ocean and the Norwegian-Greenland Sea.

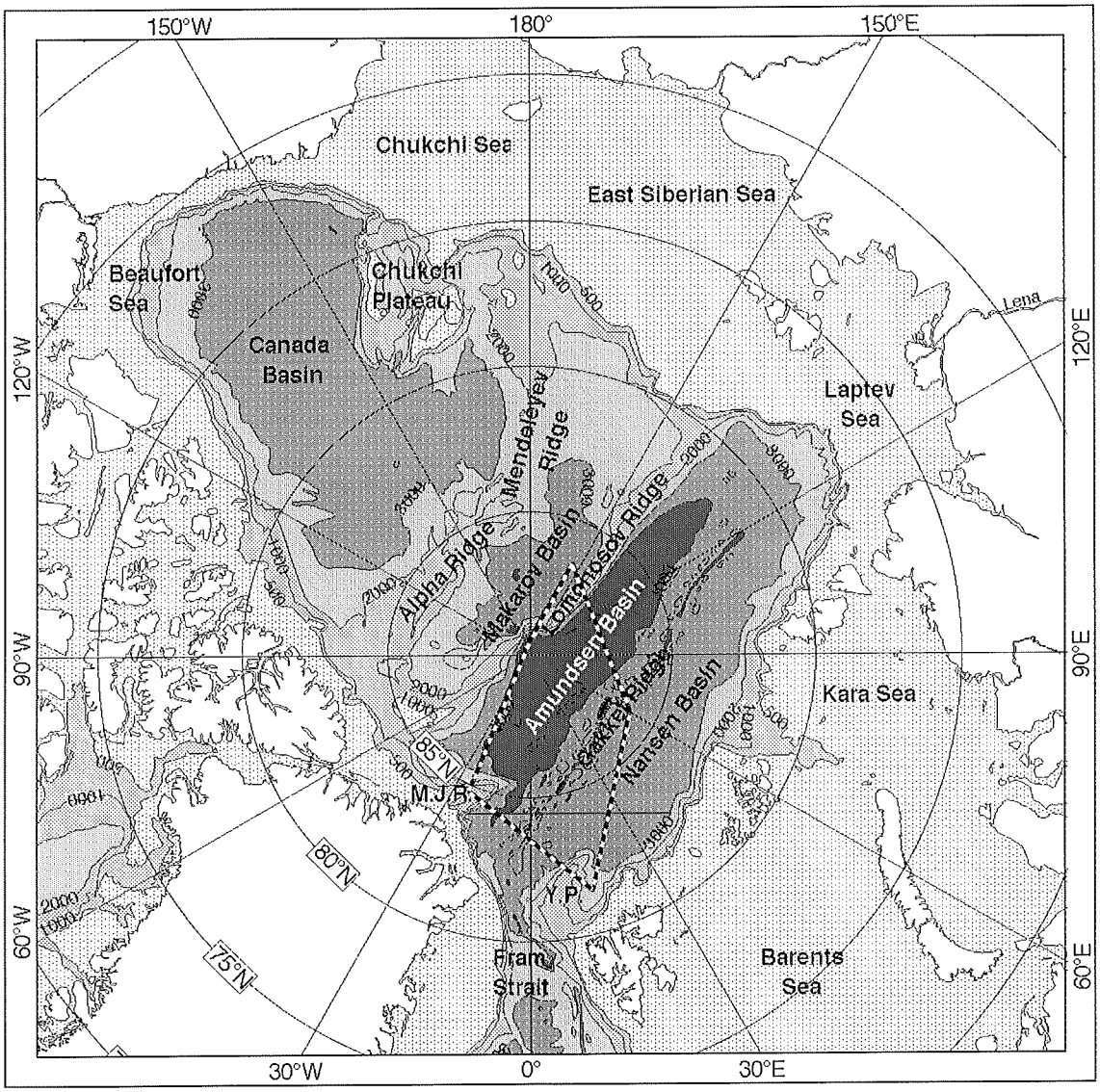

Fig. 2. General bathymetric map of the Arctic Ocean and adjacent seas. Y.P.: Yermak Plateau, M.J.R.: Morris Jesup Rise. The framed area delimits the region studied.

The Arctic Ocean is covered by permanent pack ice whose extent and borders fluctuate widely in response to seasonal changes in wind patterns, insolation, and resulting surface water temperatures (Fig. 3). The pack ice is a mixture of young (i.e. first year), second year, and multiyear ice with a highly variable thickness after undergoing several years of melting, refreezing, and deformation. The formation of sea ice mainly takes place on the wide Arctic shelves, where the inflow of freshwater from the large Siberian and North American rivers effectively reduces salinity. Leads and polynyas, which are kept open by wind effect during autumn and winter, are here acting as effective ice factories, in which new ice constantly is produced and exported to the major ice drift systems (Dethleff et al., 1993; Kassens & Thiede, 1994; Reimnitz, 1994). Glacier ice in the form of icebergs is only rarely observed in the present Arctic Ocean. Source areas for icebergs are Ellesmere- and Devon Island, Svalbard, Severnaya Zemlya, Franz Josef Land and Novaya Zemlya.

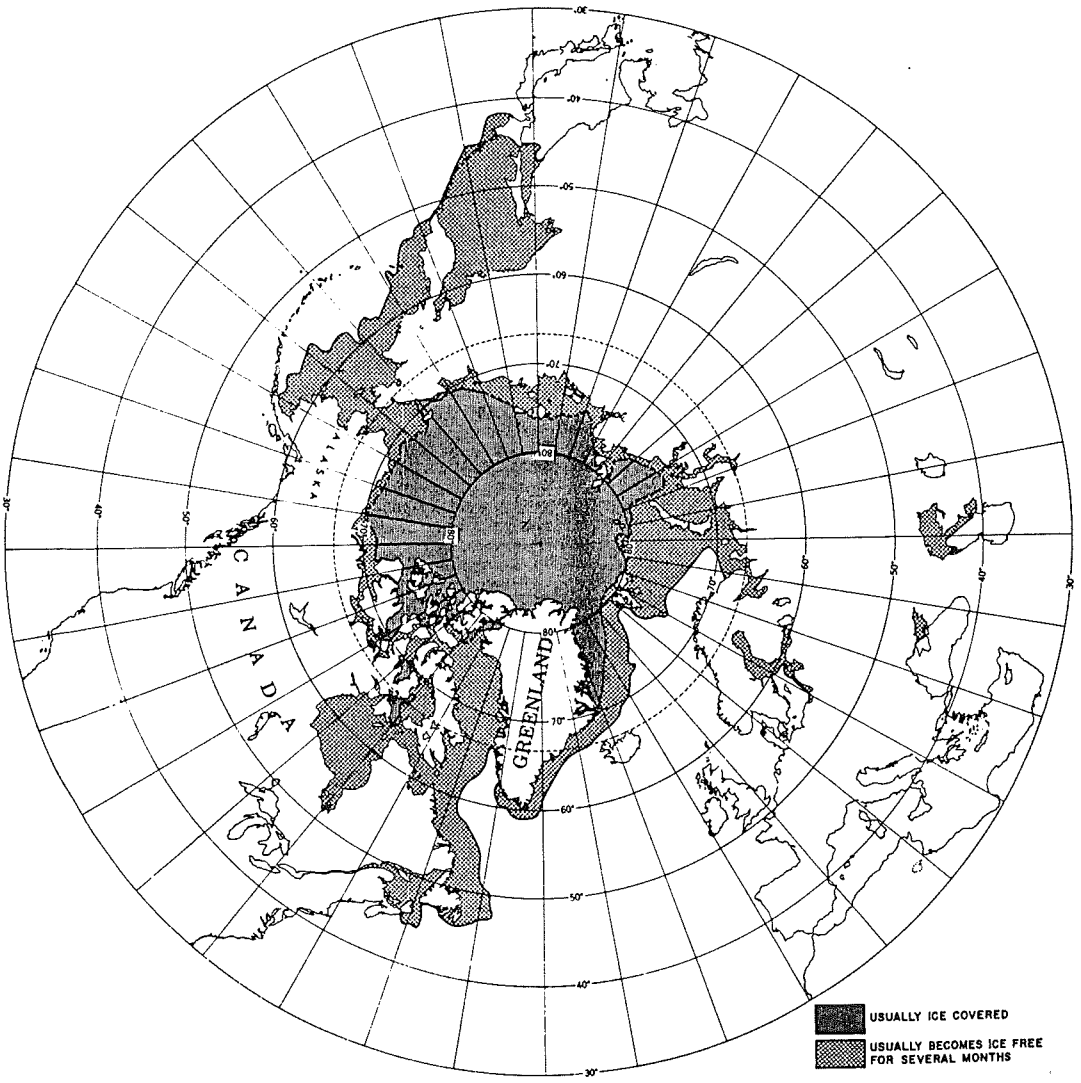

Fig. 3. Average minimum (August) and maximum (February) sea ice extent in the Northern Hemisphere. From Untersteiner (1990).

Two main features characterise ice drift and upper-ocean circulation patterns in the Arctic (Gordienko & Laktionov, 1969; Gloersen et al., 1992). Over the Canada Basin, the Beaufort Gyre, a clockwise circulation prevails (Fig. 4). The Transpolar Drift Stream extends northward from the East Siberian Sea across the Eurasian Basin continuing southward through the Fram Strait between Svalbard and Greenland, accounting for approximately 90% of the total ice export from the Arctic Ocean (Aagaard & Carmack, 1989). The circulation systems are driven by a complex balance of wind and water movements and a large seasonally and annually variability of the ice motion have been observed during the last decades where trajectory data of air-dropped drifting buoys, tracked by satellites have greatly expanded (Gloersen et al., 1992).

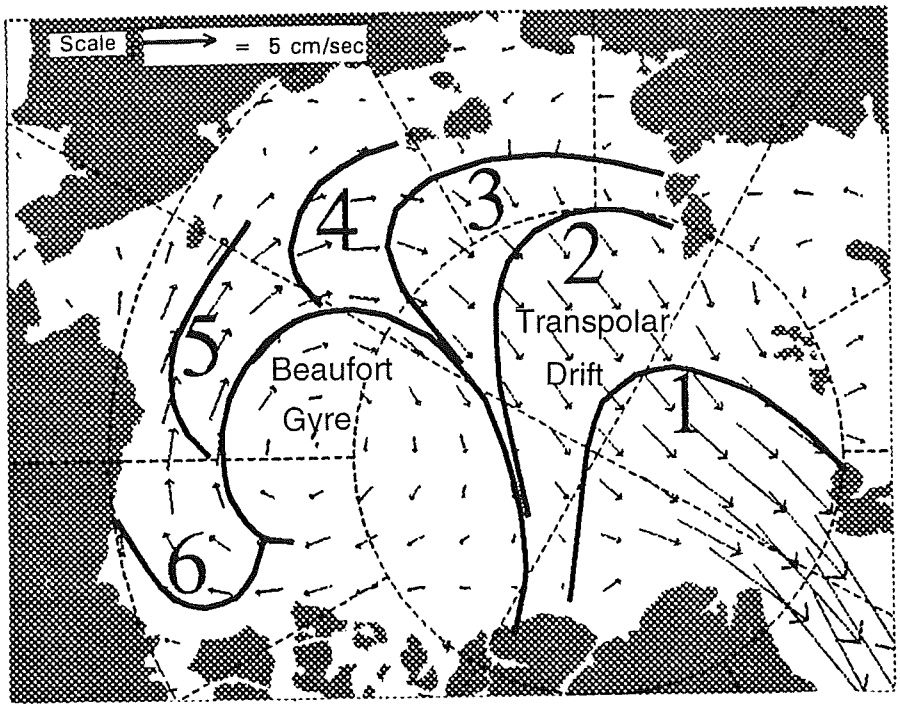

Fig. 4. Annual mean of ice motion in the Arctic Ocean based on 1979 through 1990 International Arctic Buoy Program data. The superimposed lines indicate the number of years the ice resides in the Arctic Ocean before exiting through the Fram Strait. From IABP Brochure (1994).

The Arctic Ocean is markedly stratified by a halocline between about 50-150 m (Fig. 5). This results in very low vertical heat diffusion rates in the upper water column and insulation of the underlying warm Atlantic Layer from the surface. The stratification also prevents winter convection and surface mixed layer deepening greater than about 50 m. This is fundamentally why the Arctic Ocean is more or less permanently ice covered (Aagaard & Carmack, 1994). The temperature of the surface water layer is almost constant and low (1.7°C), close to the freezing point. The surface salinity varies from about 33.5‰ close to Svalbard to less than 31.5‰ in the central Arctic Ocean (Gorshkov, 1983; Anderson et al.

1994). The salinity distribution is a reflection of the relative amount of the different source waters; Atlantic, Pacific, river run-off and sea ice melt water. Freshwater supply from Siberian and North American rivers and melting of sea ice during summer result in a pronounced density stratification in the uppermost 100-200 m of the water column. A lateral increase in the relative amount of riverine freshwater can be observed in cross sections from the Nansen Basin to the central Arctic Ocean (Bauch, 1995). Extensive sea ice formation on the shallow shelves during late autumn and winter causes the rejection of high saline, low temperature solutions (brines), which sink and flow from the shelves and down the slopes into the deep basins (Aagaard et al., 1985). This process in the Arctic, in addition to convective chimneys in the Norwegian-Greenland Sea, is very important for the supply of oxygen to and ventilation of the world deep oceans.

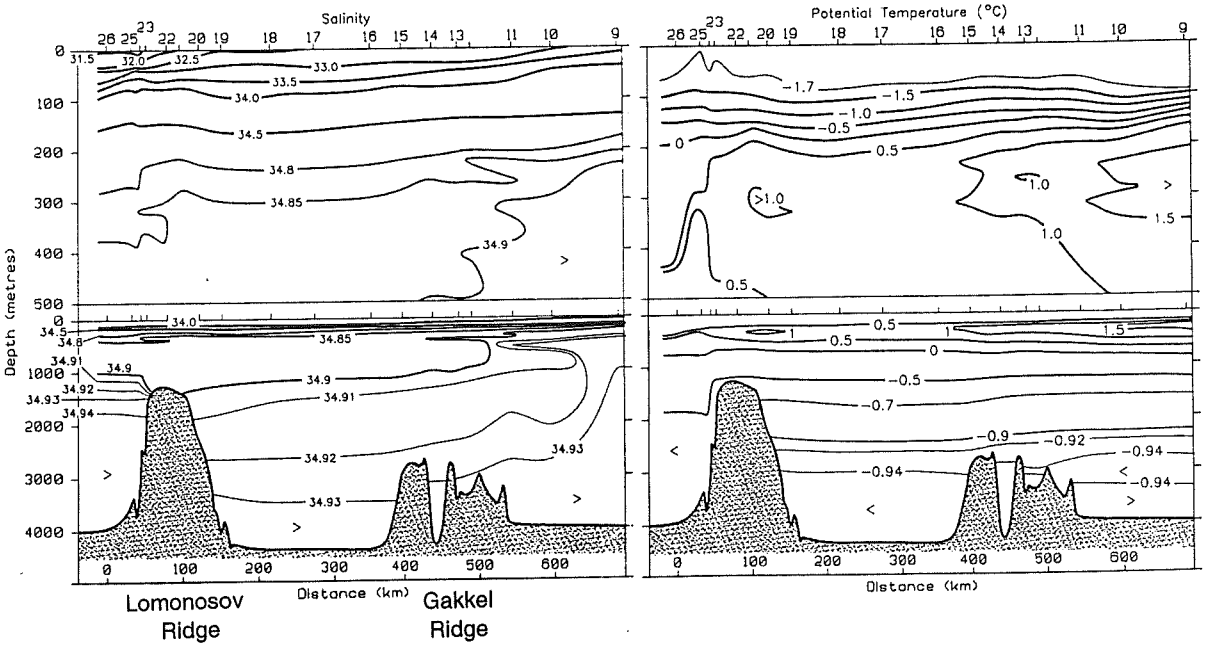

Fig. 5. Temperature and salinity distribution in the Eurasian Basin (from the Nansen Basin to the Makarov Basin). ARCTIC '91 transect from Anderson et al. (1994).

Warmer waters with temperatures above 0°C, found from about 200 m down to 600-800 m, have been denoted the Atlantic Layer (Nansen, 1902; Anderson et al., 1994; Rudels et al. 1994). One source is the West Spitsbergen Current, which enters the Arctic Ocean, mixes with low salinity waters and is transformed into low salinity Polar Waters north of Svalbard (Carmack, 1990). A second inflow of Atlantic Waters possibly of equal strength takes place

across the Barents Sea where it is cooled and made less saline (e.g. Rudels, 1987; Rudels et al. 1994; Schauer et al., 1995). The two branches meet north of the Kara Sea and further mixing processes take place along their flow paths by sinking shelf plumes. Recent oceanographic studies have come up with a detailed picture of the circulation of the Atlantic layer and intermediate depth waters, between 200 m and 1700 m round the Arctic Ocean (Anderson et al., 1994; Rudels et al., 1994; Aagaard et al., 1996). Several loops of cyclonic flows have been identified in the Eurasian and Amerasian Basins following continental slopes and flanks of submarine ridge systems. A considerable warming (0.5 -1.0°C) and shallowing of the Atlantic layer during the last 40 years was recently reported by Macdonald (1996).

The horizontal and vertical variations of temperature and salinity in the deep waters below approximately 1700 m water depth are small (Fig. 5). This water arrives in part from the Norwegian-Greenland Sea Bottom Water, the remainder is formed in the surface layer of the shelf seas (Rudels & Quadfasel, 1991; Anderson et al., 1994). Freezing during winter generates cold and saline waters which sink down the continental slopes.

1.2 Modern depositional environment

The surface sediments of the Arctic seafloor consist mainly of hemipelagic, fine-grained, clastic material derived by sea ice, river discharge and eolian influx from surrounding continents, as well as particles of biogenic origin (planktic and benthic organisms). The dominant part of the grain size fraction >63 µm is made up by well-preserved tests of calcite-shelled planktic foraminifers (almost 100% *Neogloboquadrina pachyderma* sin.) and indicate only weak carbonate dissolution (Markussen, 1986; Pagels, 1992). Sediments redistributed by muddy turbidite currents are common in the deep basins. On elevated highs local occurrences of sediments markedly enriched in coarse fraction may indicate bottom current activity and winnoving of fines. The colour of the uppermost Holocene sediments is brownish indicating an oxidizing bottom water environment.

Intensive research during the last decades has established that sea ice is an important transport agent of sediments from the shallow Arctic shelves to the deep ocean. Evidence for sediment entrainment into the sea ice cover is seen in large areas of seasonal ice containing silt- and clay-sized material disseminated throughout the upper part of ice floes (Nansen, 1897; Clark & Hanson, 1983; Kempena et al., 1989; Pfirman et al., 1990; Wollenburg, 1993; Nürnberg, 1994; Rachor, 1997). Large quantities of fine-grained sediment are discharged by the large Siberian rivers, Ob, Yenisei and Lena in the late spring and early summer months. At this time the pack ice cover in the marginal seas is either melting or the seas are ice free. Therefore, direct incorporation of river sediments may be limited to

shorefast ice near the river mouth which melts rapidly (Holmes & Creager, 1974). Clay-sized particles are likely to be transported in suspension by oceanic currents into the deep ocean and contribute to the hemipelagic sedimentation (Stein et al., 1994a). The major process of sediment entrainment into the sea ice occurs during initial ice formation (freeze-up in the autumn) on the shallow shelves by frazil ice formation (Reimnitz & Kempena, 1987; Wollenburg, 1993; Dethleff, 1995). By anchor ice formation (Reimnitz et al., 1987) and bonding of surficial sediments, even coarse sediment and large shells can be incorporated into the sea ice. Ice growth slows down after the ice has reached a thickness of a few cm to decimeters and large elongated crystals (columnar ice) continue to form on the underside of ice floes during the drift in the winter season. Along the drift path of the sea ice, sediment is released to the water column in only minor amounts during seasonal melting and rafting events. Major floe melting and disintegration, and potential for sediment release, occur during summer in the marginal ice zone, near polynyas and large leads (Hebbeln & Wefer, 1991).

Glacier ice is capable of transporting very coarse material eroded from continents or shelf bottoms into the central Arctic Ocean. Under the present 'interglacial' conditions the amount of sediments released from icebergs is expected to be very low. During glaciations and deglaciation, growth and subsequent decay of continental ice sheets in addition to rapid sea-level changes must have caused the episodic release of large amounts of icebergs from glacier fronts and ice shelves to the adjacent sea.

The magnitude of fine eolian material transported into the Arctic Ocean is still unter debate, but appears orders of magnitude too low to account for the particulate loads observed in Arctic sea ice (Larssen et al., 1987; Pfirman et al., 1990).

1.3 Arctic Ocean geology and paleoceanography

Comprehensive summaries on Arctic Ocean geology, paleoceanography, and paleoclimate are given by Herman (1989), Bleil & Thiede (1990), Grantz et al. (1990), and NAD Science Committee (1991). Recent data from ODP Leg 151 on the Yermak Plateau and in the Fram Strait indicate that the Arctic Ocean aquired its ice cover sometime between 5 to 15 million years ago related to a stepwise Northern Hemisphere cooling (Thiede & Myhre, 1995). About 3.5 Ma an intensification of glacial conditions took place marked by the first occurrence of dropstones. Furthermore, the data suggest episodical intensive ice rafting in the period 3.5 to 1.0 Ma and a major increase around 1 Ma.

Numerous cores from the Arctic Ocean documenting the Neogene and Quaternary intervals are available. Basin-wide lithostratigraphic units have been correlated in the Amerasian

Basin (e.g. Clark et al., 1980; Minicucci & Clark, 1983) but are based on a weak chronostratigraphic framework. Difficulties in the interpretation of bio-, magneto-, aminoacid- and isotope stratigraphic data have hampered a detailed dating of specific units. Recent progress in central Arctic Ocean chronostratigraphy has been achieved by the use of ^{10}Be and ^{230}Th radioisotope stratigraphy in combination with other methods (Eisenhauer et al. 1990, 1994; Bohrmann, 1991; Schäper, 1994; Molnar, 1995; Spielhagen et al., subm.). Hereby the identification of 100 ky glacial-interglacial cycles within the Brunhes magnetochron is possible. On the Northwind Ridge in the Amerasian Basin 100 ky glacial-interglacial cycles within the Brunhes have been suggested too (Phillips et al., 1992; Poore et al., 1994).

Recent advances in studies of sediment cores from from the eastern Arctic Basin allow a more detailed discussion of the upper Quaternary Arctic Ocean and its properties during the last deglaciation (Markussen, 1985; Zahn et al., 1985; Thiede, 1988; Bohrmann, 1991; Köhler, 1992; Pagels, 1992; Kubisch, 1992; Fütterer 1992; Letzig, 1995; Gard, 1993; Stein et al., 1994b; Elverhøi et al., 1995). Absolute dating by the AMS-^{14}C method of the last 40 ky record documents that hemipelagic sedimentation rates in the central Arctic are very low. Only turbidite influenced deep sea sites, continental margins (Nürnberg et al., 1995) and regions exposed to high summer ablation rates (e.g. Yermak Plateau, Fram Strait) show considerably higher sedimentation rates (Nowaczyk & Baumann, 1992). Markussen et al. (1985) and Zahn et al. (1985) documented in Fram Basin cores north of Greenland sedimentation rates in the range of 1-3 cm ky^{-1}, which were an order of magnitude higher than previous estimates for central Arctic Ocean sediments (e.g. Clark et al., 1984). The Fram-I cores, which were the first convincingly dated cores from the Arctic Ocean proper, document that planktic foraminifers *N. pachyderma* (sin.) were continuously deposited over the past 40 ky implying a modest planktic productivity even during fully glacial conditions. The planktic oxygen isotope records of the Fram cores were in close aggrement with lower latitude records demonstrating an active and efficient exchange of Arctic Ocean water masses with those of the global ocean.

A new milestone was reached by the RV *Polarstern* expedition to the Gakkel Ridge in 1987 (Thiede, 1988). The long and short sediment cores raised documented several glacial-interglacial cycles with highly variable accumulation rates (e.g. Bohrmann, 1991; Köhler, 1992; Mienert et al., 1990; Nowaczyk & Baumann, 1992; Eisenhauer et al., 1994). The combined studies show that the glacial oxygen isotope stage 6 was characterised by high sedimentation rates of coarse ice-rafted debris, including horizons rich in coal fragments (Kubisch, 1992; Bischof et al., 1990; Spielhagen & Thiede, 1994). The late Pleistocene Gakkel Ridge record from 45 to 13.5 ^{14}C ka, on the other hand, indicates low

sedimentation rates (0.3 to 0.5 cm ky^{-1}: Mienert et al., 1990; Bohrmann, 1991). An increase in sedimentation rates to about 1 cm ky^{-1} during Termination I into the Holocene was found. Stable isotope records of planktic foraminifers *N. pachyderma* (sin.) from the Gakkel Ridge and the Nansen Basin covering the last interglacial-glacial cycle were studied in detail by Köhler (1992). She found significant imprints on the global ice volume signal representing advection of meltwaters during the Termination I, isotope stage 3 and, during interglacials, by supply of isotopically light river water.

The circum-Arctic terrestrial and shelf margin deposits give a rather consistent picture of the extent of the Last Glacial Maximum (LGM: about 18 ^{14}C ka) ice sheets and the subsequent deglaciation. It is documented that an ice sheet centred over the Barent Sea reached to the shelf margin of the Arctic Ocean and proably coalesced with the Fennoscandian Ice Sheet to the south (Elverhøi et al., 1993; Lambeck, 1996; Vorren & Laberg, 1996). More isolated ice domes may have covered parts of the Kara Sea, Severnaya Zemlya and Taymyr Peninsula region, but this is still a matter of intense debate (Grosswald, 1980, 1993; Astakhov, 1992; Rutter, 1995; Lambeck, 1996). During the LGM the Greenland Ice Sheet and the Innutian Ice Sheet over the eastern Queen Elizabeth Islands probably had expanded to the present coastline, but the glaciers probably did not expand onto the Arctic Ocean shelf (Funder & Hansen, 1996; Hodgson, 1989). Ice cores from Greenland and northeastern Canada, with records spanning at least the last interglacial-glacial cycle, are direct evidence for the existence of ice sheets in that region throughout this period (Dansgaard et al., 1993; Hodgson, 1989). Geological evidence suggests that the glaciers that overran the Queen Elizabeth Islands an unknown number of times during the Quaternary were thickest and most extensive prior to the last glaciation (Hodgson, 1989). The huge Laurentide Ice Sheet that occupied much of northern North America during the last glaciation covered an area approximately equivalent to the present Antarctic Ice Sheet (Andrews, 1987). The northern extension was from the McKenzie River Delta in the northwest, across the Canadian Arctic archipelago through the Viscount Melville Sound and the Parry Channel to Baffin Island in the east (Hodgson, 1991). Dyke & Prest (1987) proposed for the LGM marine-based ice shelves reaching out onto the narrow Beaufort Sea Shelf through the deep (>400m) M'Clure Stait and Amundsen Gulf bordering Banks Island.

Our picture of older late Pleistocene glaciations and ice sheet extension in high northern latitudes is much more sporadic with conflicting hypotheses due to unprecise datings and reworking of deposits. From the climatically very dynamic Svalbard and Barents Sea area, as well as for Scandinavia, major glaciations and subsequent retreat have been suggested for the cold glacial oxygen isotope stage 6 (158-132 ka), substages 5d (118-108 ka) and 5b (93-85 ka), and stage 4 (74-59 ka) (Mangerud, 1991; Mangerud & Svendsen, 1992;

Mangerud et al., 1996; Baumann et al., 1995). A large stage 4 Laurentide Ice Sheet comparable to that of the LGM has been suggested by Dredge & Thorleifson (1987) and Porter (1989). Glacial deposits and erosional unconformities in the Mackenzie Trough of the Canadian Beaufort Shelf suggest that the Mackenzie Trough was excavated by ice tongues during the early and mid-(?), to late Weichselian (Blasco et al., 1990).

High resolution paleoclimate records from ice cores and marine and terrestrial sediments suggest climate variability at higher frequencies (10^3 yr) than those predicted by orbital forcing. Ice sheet variations and abrupt climate change at these millenial timescales are linked by data from the marine record of ice-rafted debris in the North Atlantic. Heinrich events, which are episodes of massive discharge of icebergs to the western North Atlantic (Broecker, 1992), and their newly discovered higher-frequency cousins (Bond & Lotti, 1995) indicate partial collapse of the Laurentide Ice Sheet during the Weichselian (possibly also other ice sheets in Europe and Iceland as well). The Greenland ice core record shows that the IRD events occurred at the end of cooling episodes in the North Atlantic region and are followed by rapid warming approaching interglacial conditions (Dansgaard-Oeschger events: Bond et al., 1993). Such rapid changes have not yet been documented for the Arctic Ocean, where the deep sea records in general show far too low sedimentation rates to resolve short-lived events.

1.4 Objectives

The present work intends to resolve temporal and spatial changes in the lithogenic and biogenic sediment deposition and stable isotope signals in the Eurasian and central Arctic Ocean for the last interglacial-glacial cycle, i.e. the past 130 ky. The basic approach has been high resolution stratigraphic and quantitative sedimentologic work on deep sea sediment cores to obtain proxy data for environmental parameters such as sea ice distribution, sediment rafting and surface water conditions (salinity, ventilation, plankton productivity).

Large volume box cores from the ARCTIC'91 expedition to the central Arctic Ocean (Fütterer, 1992) have been studied. Main emphasis has been put on cores from ridges and elevated sites with an undisturbed hemipelagic sediment record. To improve inter-core correlation over large distances, several deep basin cores, however, were also investigated and have proven to be useful for mapping of specific stratigraphic units. The sedimentological and isotope data gained shall be used as proxies for changes in the Arctic ice cover and drift pattern, the properties of the upper water column, and circum-Arctic glaciations/ deglaciations. A first step and prerequisite for paleoceanographic reconstructions is to establish a reliable stratigraphic framework by means of oxygen and carbon isotopes,

AMS-^{14}C dating, and lithologic inter-core correlation. The sediment composition and flux of ice-rafted debris (IRD), planktic foraminifers, and carbonate content yield information on the nature of the ice cover, the source areas, and the transport routes of terrigenic material. The isotopic records of planktic foraminifers are used for the evaluation of changes in the freshwater budget of the upper water column with emphasis on the history of river run-off, meltwater events from decaying ice sheets, and Atlantic Water inflow. Reconstruction and mapping of surface water salinities, as recorded by oxygen isotope values of planktic foraminifers *N. pachyderma* (sin.), are attempted for specific time slices.

2. METHODS

2.1 Core material

For the present study 20 large volume box cores from the central and eastern Arctic Ocean were selected (Table 1, Fig. 6). The cores were obtained during the Arctic'91 expedition (ARK-VIII/3) of RV *Polarstern* along transects from the Nansen Basin, across the Gakkel Ridge, the Amundsen Basin, the Lomonosov Ridge to the Makarov Basin and from the North Pole southwards across the Amundsen Basin to the Morris Jesup Rise, the Gakkel Ridge and to the Yermak Plateau (Fütterer, 1992). The standard core descriptions are found in Fütterer (1992). The cores have been studied for stratigraphic and sedimentologic parameters such as: grain size, stable isotopes ($\delta^{18}O$, $\delta^{13}C$), coarse fraction composition, amount and composition of ice rafted debris (IRD), calcium carbonate and total organic carbon (TOC) content (Appendix A). On the basis of stable isotope records and foraminifer content eight cores were selected for AMS-^{14}C dating.

Table 1. Site locations, water depths, and core lengths of box cores studied.

Core no.	Length (cm)	Area	Water depth (m)	Latitude	Longitude
PS2161-4	39	Nansen Basin	4005	85° 26.3' N	44° 18.2' E
PS2164-4	37	Gakkel Ridge	2030	86° 20.1' N	59° 16.0' E
PS2166-2	40	Gakkel Ridge	3636	86° 51.6' N	59° 45.9' E
PS2172-1	41	Amundsen Basin	4391	87° 15.4' N	68° 22.7' E
PS2176-4	39	Amundsen Basin	4364	87° 46.6' N	108° 10.0' E
PS2177-1	45	Lomonosov Ridge	1388	88° 02.2' N	134° 55.1' E
PS2178-2	46	Makarov Basin	4009	88° 00.2' N	159° 14.0' E
PS2179-1	39	Lomonosov Ridge	1230	87° 44.8' N	138° 01.7' E
PS2180-1	54	Makarov Basin	4005	87° 37.6' N	156° 40.5' E
PS2184-1	30	Lomonosov Ridge	1640	87° 36.7' N	148° 08.4' E
PS2185-3	38	Lomonosov Ridge	1051	87° 31.9' N	144° 22.9' E
PS2186-5	43	Lomonosov Ridge	2036	88° 30.9' N	140° 29.4' E
PS2187-1	46	Lomonosov Ridge	3813	88° 44.1' N	126° 54.8' E
PS2190-3	42	Amundsen Basin	4240	89° 59.0' N	84° 44.7' W
PS2192-1	50	Amundsen Basin	4375	88° 15.7' N	09° 52.7' E
PS2193-2	40	Amundsen Basin	4337	87° 31.1' N	11° 15.5' E
PS2195-4	45	Amundsen Basin	3873	86° 13.7' N	09° 35.6' E
PS2196-2	32	Amundsen Basin	3958	85° 57.1' N	00° 06.9' E
PS2200-2	35	Morris Jesup Rise	1074	85° 19.6' N	14° 00.0' W
PS2212-5	45	Yermak Plateau	2485	82° 04.0' N	15° 46.0' E

2.2 Sample processing

On board a standard core description, including photographing, x-ray, and sampling of undisturbed surface and subsurface levels for preliminary studies was carried out (Fütterer, 1992). PVC-core liners with a diameter of 12 cm were pressed vertically down into the box cores (50x50x60 cm), sealed and stored at 4°C. In the home lab the core liners were split into an archive and a working half (Fig. 7). The working half was sampled in 1 cm slices (~50 cm^3) which were freeze-dried. Subsamples for determination of bulk carbonate and organic carbon content were taken and the remaining sample was weighed and rinsed through a 63 µm mesh to separate the sand and gravel fraction from the silt and clay fraction. The final rinse process was done with distilled water. After drying >48 hours at 40-60°C, the coarse fraction was weighed and sonic sieved in separate subfractions (63-125 µm, 125-250 µm, 250-500 µm, 500-1000µm, and >1000µm). Samples with an insignificant content of coarse fraction were not sieved. The grain-size distribution data are listed in Appendix D.

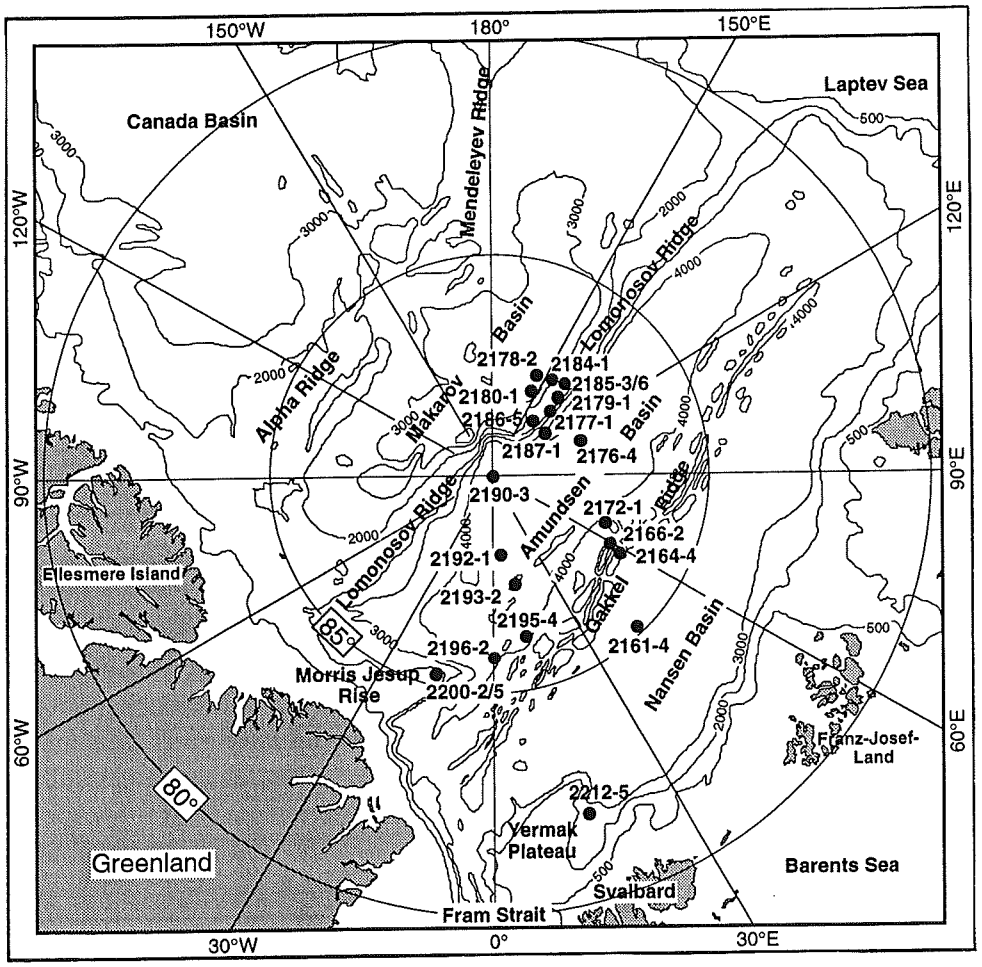

Fig. 6. Map of study area and core sites. All core identification numbers with RV *Polarstern* (PS-) prefix.

2.3 Oxygen and carbon isotope measurements

Oxygen and carbon isotope ratios ($\delta^{18}O$, $\delta^{13}C$) were measured on tests of planktic foraminifers *Neogloboquadrina pachyderma* (sinistral). 25 tests of equally sized, 4 chambered foraminifers were picked from the 125-250 µm fraction of each sample. In cases of extremely low foraminifer content, 10-20 foraminifer tests were occasionally used. Benthic foraminifers *Cibicidoides wuellerstorfi* from two cores (PS2177-1, PS2186-5) were picked from the 250-500 µm fraction for stable isotope measurements. Before measurement the tests were crushed and cleaned by ultrasonic agitation. Stable oxygen and carbon isotopes ($\delta^{18}O$, $\delta^{13}C$) were measured by standard techniques (Winn et al., 1991) on a Finnigan MAT 251 mass spectrometer at the University of Kiel Radiocarbon Laboratory. Results are expressed in the delta notation referring to the PDB standard (‰ vs. PDB) and listed in Appendix C. The external analytical reproducibility is 0.08‰ for $\delta^{18}O$ and 0.04‰ for $\delta^{13}C$ (H. Erlenkeuser, pers. comm.).

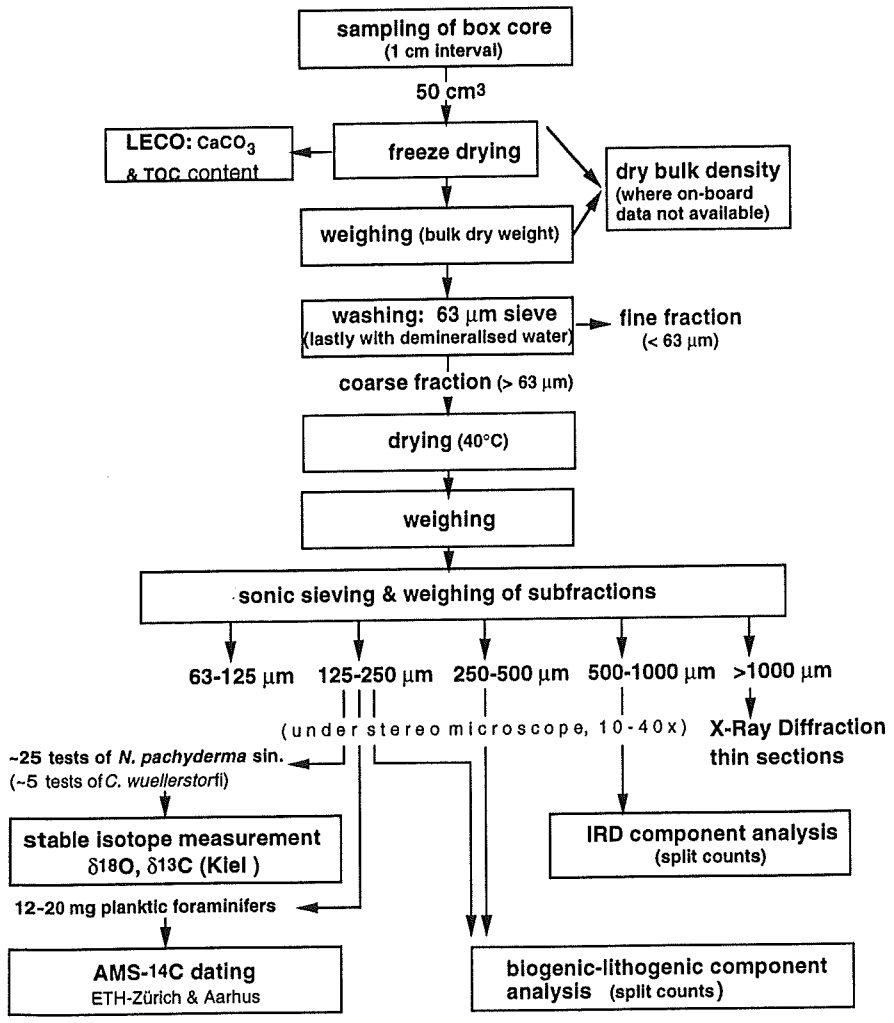

Fig. 7. Outline of analyses carried out.

2.4 AMS-^{14}C dating and age calibrations

On basis of the isotopic records and abundance distribution of planktic foraminifers, samples distributed in eight cores were selected for AMS-^{14}C dating. For each sample 1000-2000 tests of *N. pachyderma* were picked from the 125-250 µm fraction. One set of samples was prepared at the Heidelberg Academy of Sciences and measured at the ETH-Zürich Tandem Accelerator Facility. The other set was prepared and measured at the AMS-^{14}C Laboratory, Institute of Physics, University of Aarhus, Denmark. Ages were determined after $^{13}C/^{12}C$ normalization to -25‰. The dating results are given as an age in radiocarbon years before 1950. A standard reservoir correction of 400 years has been subtracted to give a 'true' ^{14}C age. Conventional radicarbon years were converted to calendar years (calibrated yr BP; A.D. 1950 = 0 cal yr BP) by using a linear approximation of Bard et al. (1990, 1993) for the period 3000-18,000 ^{14}C yr and an extended second-order fit (E. Bard, pers. comm. 1994) for the period 18,000-45,000 ^{14}C yr:

$$3\text{-}18\ ^{14}C\ ka: \ Cal.\ age = 1.24\ (^{14}C\ age) - 840$$

$$18\text{-}45\ ^{14}C\ ka: \ Cal.\ age = -5.85\ 10^{-6}\ (^{14}C\ age)^2 + 1.39\ (^{14}C\ age) - 1807$$

In Appendix B all AMS-^{14}C datings are listed with reservoir correction and calibrated calender age.

With respect to the reservoir age, different estimates have been suggested for high northern latitudes. Stuiver et al. (1986) suggested a reservoir correction of 440 years for the Fram Strait and the Arctic Ocean. For the region influenced by the East Greenland Current, Tauber & Funder (1975) suggested a correction of 550 years. Direct AMS radiocarbon dating of the present Arctic Ocean deep sea waters varies from 250 years for the Nansen Basin, 400 years for the Makarov Basin (Schlosser et al., 1990), and 430 years for the Canada Basin (Jones et al., 1994). The original estimate of Macdonald & Carmack (1991) close to 1000 years has later been revised to 500 years (Macdonald et al., 1993). These relative young ages are explained by the advection of 'young' saline waters from the continental shelves of the Arctic. The studies above imply that the deep waters of the Arctic are not relict and subsequently a 'normal' reservoir correction of 400 years has been used in the present study. For glacial periods as e.g. the Last Glacial Maximum or the Younger Dryas, different oceanographic conditions can be expected due to lowered sea level, higher degree of sea ice cover (but possibly less sea ice production), and reduced advection of surface waters from the North Atlantic (Bard et al., 1994). For this reason it is quite possible that older relict waters could have increased the reservoir age of the Arctic Ocean in glacial times thereby making the apparent ^{14}C datings slightly to old.

2.5 Coarse fraction component analyses

The biogenic part of the coarse fraction, mainly consisting of planktic foraminifers, is varying from 0 to >90 grain%. Thus, any interpretation of the grain size distribution in terms of ice rafting, planktic and benthic in situ bioproduction, carbonate dissolution, and bottom current activity demands a quantification of the lithogenic versus biogenic content. For coarse fraction analyses the 125-500μm fraction can be considered representative for the total coarse fraction (cf. Sarnthein, 1971; Henrich, 1989). In the present study the fractions 125-250 μm and 250-500 μm were studied separately. Sample splits of about 400 grains were counted under a binocular microscope and the following nine categories were identified (Appendix E):

1. *Lithic grains*
2. *Planktic foraminifers*
3. *Calcareous benthic foraminifers*
4. *Fragments of planktic foraminifers*
5. *Fragments of calcareous benthic foraminifers*
6. *Agglutinated benthic foraminifers*
7. *Ostracodes*
8. *Sponge spicules*
9. *Other biogenic remains (fragments of bivalves, echinoderms, worm tubes, etc.)*

The percentual distribution of the dominant categories: lithic grains, planktic foraminifers and calcareous benthic foraminifers, and the sum of the rest was calculated (grain-%). Moreover, the absolute abundance of respective planktic foraminifers and benthic foraminifers (125-500 μm) per g bulk sediment was calculated. As it can be expected that the amount of foraminifer fragments is higher than the amount of specimens that have disintegrated, the number of fragments counted are divided by 2 in the formula for the calculation of the total estimated abundance (Fa) of planktic or benthic foraminifers:

$$F_a = (F+Ff/2)\ S/W_b$$

where
F = *number of planktic or benthic foraminifers in sample split*
Ff = *number of fragments of planktic or benthic foraminifers in sample split*
S = *split factor* (2^n), *where n is the number of splits*
W_b = *Bulk dry sample weight (g)*

In cases of extreme low coarse fraction contents, no subfractioning was done and hencely the percentual distribution in the specific size classes could not be quantified. In such cases only the number of planktic foraminifers in the size range 125-500μm was counted for the calculation of the absolute planktic foraminifer abundance.

2.6 Ice rafted debris (IRD) analyses

The composition of the coarse sand fraction, with focus on the ice-rafted terrigenic component, was analysed under a binocular microscope. The 500-1000 µm fraction was chosen based on experience because this size range is the best compromise between a sufficient number of grains and large enough grains to allow lithological identification of most rock parameters. This size class was also used for earlier IRD studies in the eastern Arctic Ocean (Kubisch, 1992) and the Fram Strait (Spielhagen, 1991). Supplementary microscope study of the fraction >1000 µm (occasionally including granule to pebble-sized dropstones) has been helpful for the lithological identification of the specific rock types. Additionally thin section analysis of larger dropstones and x-ray diffraction were applied for the identification and mineralogical characterisation of detrital carbonate rocks (Appendix H). Three groups of components are identified: terrigenic grains (considered as IRD), authigenic grains (in situ precipitation/cementation products) and biogenic grains (Table 2).

Table 2. Coarse fraction components identified (500-1000µm).

Main IRD Group	***Rock or Mineral Type***
Monocrystalline:	*Quartz* *Feldspar* *Mafic mineral*
Polycrystalline:	*Felsic igneous (light)* *Mafic igneous (dark)*
Metamorphic:	*Schist* *Phyllite* *Quartzite* *Chert*
Sedimentary: *(siliciclastic incl. coal)*	*Sandstone* *Siltstone* *Mudstone* *Shale* *Coal*
Detrital carbonate:	*Light (white, yellowish, pink)* *Dark (grey, black)*
Other:	*Not classified IRD component*
Authigenic grains: *(in situ precipitation/ cementation)*	*Sandy ironhydroxide aggregates* *Muddy ironhydroxide aggregates* *Pyrite* *Iron-manganese micronodules* *Calcium carbonate precipitates*
Biogenic grains:	*Calcareous benthic foraminifers* *Agglutinated benthic foraminifers* *Sponge spicules* *Undifferentiated biogenic remains*

2.7 Calcium carbonate and TOC measurements

The content of calcium carbonate in bulk sediment samples was determined in eight selected cores with a LECO CS-125 infrared analyser. The freeze-dried samples were homogenised in a ball mill and dried at 40°C. For the first set of measurements, 20-30 mg sediment were weighed and baked in the high-frequency induction oven. The combustion gas was measured in a carbon infrared cell, and the carbon content relative to the sample weight was converted into weight-%. For measurement of the total organic content (TOC), a second set of samples was measured after dissolution of the inorganic carbonate with 0.25 n hydrochloric acid, degasing, and drying. The calcium carbonate content (weight-% of bulk sample) was calculated as:

$$CaCO_3 = (TC\text{-}TOC)\ 8.333$$

where
TC = total carbon weight-%
TOC = total organic carbon weight-%
8.333 = stoichiometric conversion factor

By this standard method it is assumed that all carbonate is calcite. Consequently, the presence of dolomitic carbonate, which is a common IRD component in the Arctic Ocean, causes a slight underestimation of the actual carbonate content. The content of calcite ($CaCO_3$) versus dolomite ($CaMg(CO_3)_2$) has been determined in single detrital carbonate dropstones and assemblages of characteristic detrital carbonate sand grains by x-ray diffractometry (in cooperation with C. Vogt, Alfred-Wegener-Institut für Polar und Meeresforschung, Bremerhaven). The calcium carbonate and TOC data are listed in Appendix G, and the results of the x-ray diffractometry analyses are listed in Appendix H.

2.8 Dry bulk density determination

Dry bulk density data have been provided by Dr. H. Kassens, GEOMAR (see Fütterer (1992) for detailed description). Additionally, dry bulk densities have been determined on selected cores where no on-board data existed by measurement of volume and dry weight of the sample slices in the splitted core liner halfs. By this method, dry bulk density in principle has been determined for every 1 cm sample slice. In order to compensate for indispensable deviations in sample volume (due to not perfect half-cylindrical form of individual sample slices), 3-point running mean values for calculated down-core dry bulk densities have been used. The validity of this method compared to the traditional method using pressed-down sample cylinders (10 cm^3) has been proven by direct comparison of dry bulk density values determined in the same cores. The dry bulk density (DBD) data used are listed in Appendix I together with age models and accumulation rate estimates for selected cores.

3. RESULTS

In the following section basic isotopic and lithostratigraphic data are presented along core transects. The established stratigraphy is based on AMS-^{14}C dating, oxygen and carbon isotope measurements on planktic and benthic foraminifers, coarse fraction analysis (biogenic and lithogenic components, IRD composition), and bulk carbonate content. Supplementary data on coccolith biostratigraphy (Gard, 1993) have been taken into consideration. Moreover, stratigraphic correlation of the box cores with long kastenlot cores on the Lomonosov Ridge, the Morris Jesup Rise and the Gakkel Ridge (Spielhagen et al., subm.; Bohrmann, 1991; Nowaczyk & Baumann, 1992) has been attempted in order to develop a long time scale stratigraphy for these sites.

3.1 Stratigraphy

Oxygen isotope stratigraphy on foraminifers from deep sea sediments provides a time series record of globally synchronous events with a resolution of a few thousand years for the Quaternary (Jansen, 1989). The global $\delta^{18}O$ signal is related to the waxing and waning of continental ice sheets (storage of light ^{16}O) associated with glacial-interglacial climate cycles. In spite of regional and temporal differences in the appearance of oxygen isotope records, caused by differences in water temperature, oceanic current patterns, freshwater influx, and bioturbation, the superimposed global signal with an amplitude of about 1.2-1.3‰ (Fairbanks, 1989; Jansen, 1989) generally allows the recognition of individual oxygen isotope stages and substages. This makes it an invaluable tool for stratigraphic dating, inter-core correlation and paleoceanographic reconstructions. Stacked records of many high-resolution oxygen isotope records from lower latitudes (Pisias et al., 1984), dated by orbital tuning techniques (e.g. Imbrie et al., 1984; Martinson et al., 1987) thus serve as a global chronostratigraphic reference. On Fig. 8 the oxygen isotope record of Martinson et al. (1987) is shown with oxygen isotope stages (5-1) and selected identifiable features (6.0-2.0) of the record, defined by Pisias et al. (1984). Also shown in Fig. 8 is the oxygen and carbon isotope record of core M23259 from the Bear Island Fan (Weinelt, 1993), which shows prominent isotopic features (meltwater events that can be traced over most of the Norwegian-Greenland Sea) superimposed on the global signal. It can be expected that associated events, in relation to deglaciations of circum-Arctic ice sheets, can be traced also in Arctic Ocean records.

Stable isotope stratigraphy in the Arctic Ocean is hampered by the overprint from the large freshwater component, by generally low sedimentation rates, and the locally poor preservation of calcium carbonate. In the present Arctic Ocean a high amount of riverine freshwater in the central Arctic Ocean surface mixed layer (about 10%), compared to the

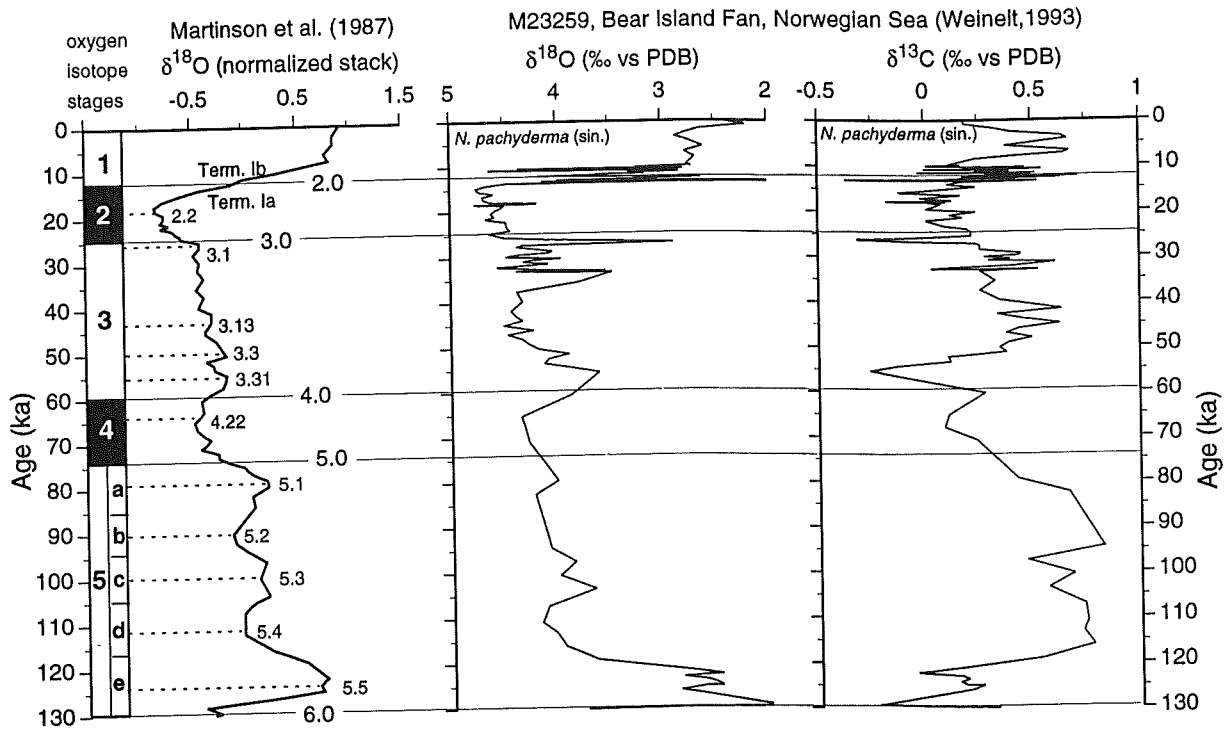

Fig. 8. Stacked oxygen isotope record of Pisias et al. (1984) with the orbitally based chronology of Martinson et al. (1987) as a time base (SPECMAP stack). Numbered horizontal lines indicate stage boundaries (6.0-2.0) and identifiable substage features of the record, defined by Pisias et al. (1984). Next to the 'global' stack are shown the $\delta^{18}O$ and $\delta^{13}C$ records (*N. pachyderma* s.) of core M23259 from the Bear Island Fan in the Norwegian Sea (Weinelt, 1993). Superimposed on the global pattern, prominent isotopic excursions in M23259 indicate major meltwater events which can be traced over most of the Norwegian-Greenland Sea (Weinelt, 1993).

southern part of the Eurasian Basin (about 2%), is causing a 3-4 ‰ difference in oxygen isotope composition of the surface waters (cf. Bauch, 1995). This isotopic range is reflected also in the $\delta^{18}O$ values of *N. pachyderma* (sin.) from Arctic Ocean surface sediment samples (Spielhagen & Erlenkeuser, 1994). Temporal changes of riverine or glacial meltwater influx may thus create $\delta^{18}O$ excursions that bias the global signal seriously and occasionally prevent positive identification of oxygen isotope stages and substage events (Jansen, 1989). It can, however, be expected that dramatic changes in the regional salinity and $\delta^{18}O$ composition of surface waters, as traced by planktic foraminifers, are related to glacial-interglacial changes in circum-Arctic glaciations, deglacial meltwater influx, amount of precipitation, and exchange of water masses with the North Alantic and the Pacific. High resolution oxygen isotope records from the Norwegian-Greenland Sea (e.g. Vogelsang,

1991; Weinelt, 1993) and the Fram Strait (e.g. Jones and Keigwin, 1988; Köhler, 1992; Dokken, 1995), reflecting paleoceanographic changes in the high northern latitude environment, become thereby valuable for stratigraphic correlation with Arctic Ocean records (cf. Fig. 8).

From earlier isotope studies in the Arctic and subarctic realm and the present work it is a general experience that the carbon isotope records are very useful too for chronology and correlation (Labeyrie & Duplessy, 1985; Jansen, 1989). Strong $\delta^{13}C$ transitions at the isotope stage boundaries may serve as correlation points and major meltwater events can typically be identified by low $\delta^{13}C$ values accompanying low $\delta^{18}O$ values (e.g. Duplessy et al., 1988; Weinelt, 1993; Stein et al., 1994c; Dokken, 1995).

The sedimentation rate and degree of bioturbation are important factors for the appearance of the isotope signals and resolution of paleoceanographic events. In the Arctic where pelagic sedimentation rates in general are low and the abundance of foraminifers in glacial and deglacial deposits can be expected to be very low, bioturbation mixing can seriously affect isotope records and radiocarbon datings. In some cases careful sampling can prevent severe bioturbation effects. Another strategy is to sample several cores from the same region to extract regional isotopic features from local deviations. In the deep basins, pelagic units comparable to sediments of elevated sites often are interlayered with very fine-grained foraminifer barren units (distal turbidites?). The character of the true basin sediments in general makes them less suitable for paleoceanographic interpretations. Apart from the uppermost 5 to 10 cm Holocene sediments, dissolution of foraminifer shells and dilution/reworking of the pelagic record often obscure signals.

Analyses of coccolith assemblages in smear slides (5 cm interval) from box cores included in the present study and associated longer gravity and piston cores have been performed by Gard (1993). As a marked difference in species composition of Holocene sediments (dominated by *Emiliania huxley* and *Coccolithus pelagicus*) compared to oxygen isotope stage 5 sediments (dominated by *Gephyrocapsa* species) has been documented in high latitude records, a rough stratigraphic subdivision is possible (e.g. Gard, 1986, 1993, pers. comm. 1995; Baumann, 1990). The coccolith stratigraphy has thus been used supplementary to oxygen isotope stratigraphy and environmental indicators as planktic foraminifer abundance data, for stratigraphic subdivision beyond the range of ^{14}C datings.

In the following, basic stratigraphic parameters plotted versus depth in core are presented along three transects (A-C) roughly following the cruise track. Interpreted oxygen isotope

stages and the extent of the last deglaciation (Termination I) are shown on all records (Figs. 9-15).

Transect A: Yermak Plateau - Nansen Basin - Gakkel Ridge (60°E) - Amundsen Basin

Transect B: Lomonosov Ridge - Makarov Basin

Transect C: Morris Jesup Rise - Gakkel Ridge (10°E) - Amundsen Basin (North Pole)

3.2 AMS-^{14}C datings

On the basis of stable isotope and abundance records of *Neogloquadrina pachyderma* (sin.) suitable levels in eight sediment cores were selected for AMS-^{14}C dating. The dating results are presented in Table 3 and shown on the stable isotope records and the foraminifer abundance records as reservoir corrected ^{14}C ages. In Chapter 4, age models have been developed for selected radiocarbon dated cores which according to correlation of oxygen and carbon isotope records and basic sedimentologic parameters are considered representative for the pelagic and ice-rafted sediment record in regional areas.

3.3 δ^{18}O and δ^{13}C records

The stable isotope stage designation is based on the oxygen isotope stratigraphy of Martinson et al. (1987) (Fig. 8), supported by Norwegian-Greenland Sea δ^{18}O and δ^{13}C records of Vogelsang (1990) and Weinelt (1993), and Fram Strait and Yermak Plateau records of Köhler (1992) and Dokken (1995).

The δ^{18}O records of *Neogloquadrina pachyderma* (sin.) show amplitudes between 1 and 2‰. From the southern Eurasian Basin to the central Arctic a clear tendency toward lower δ^{18}O values can be observed in the surface samples and the subsurface records (Fig. 9-11). A considerable variability from record to record can be observed. However, well-correlatable downcore patterns are found in regions with good core coverage. This is the case in the Gakkel Ridge area around 60°E (e.g. cores PS2166-2 and PS2172-1), on the Lomonosov Ridge (cores PS2177-1, PS2179-1, PS2184-1, PS2185-3 and PS2186-5), the Makarov Basin (cores PS2178-2 and PS2180-1), and the cores from the southwestern part of the Amundsen Basin and the adjacent Gakkel Ridge sites (cores PS2193-2, PS2195-4 and PS2196-2). The latter cores correlate well with other radiocarbon dated stable isotope records of box cores from the Gakkel Ridge (Köhler, 1992; Mienert et al., 1990).

In general the last glacial-interglacial transition, Termination I, can be well defined by one or two characteristic low-δ^{18}O excursions marking Termination Ia and a general δ^{18}O decrease during Termination Ib to Holocene levels. Prominent δ^{13}C minima parallel the low-δ^{18}O excursions. The last glacial maximum (LGM: about 18 ^{14}C ka) can be defined by relative high δ^{18}O values immediately before the beginning of Termination I. A decrease of δ^{18}O of

Table 3. Results of AMS-^{14}C datings on shells of planktic foraminifers. Uncorrected ^{14}C ages, +/-1 standard deviation, reservoir corrected ^{14}C ages (-400 years), and calibrated calendar ages are given.

Core no.	Depth (cm)	AMS-^{14}C Age (^{14}C -year BP)	St. Dev. (+/- years)	Res. Corr. ^{14}C-Age	Cal. Age (year BP)	AMS-lab. sample no.
PS2185-3	0	3080	65	2680	2680	ETH-9868
PS2185-3	1.5	3505	65	3105	3010	ETH-9869
PS2185-3	2.5	4955	60	4555	4808	ETH-10576
PS2185-3	4.5	5690	60	5290	5720	ETH-10313
PS2185-3	6.5	7140	75	6740	7518	ETH-10574
PS2185-3	7.5	8375	75	7975	9049	ETH-10573
PS2185-3	8.5	8770	85	8370	9539	ETH-9870
PS2185-3	9.5	10710	85	10310	11944	ETH-10575
PS2185-3	10.5	17130	150	16730	19905	ETH-9871
PS2185-3	10.5	16530	140	16130	19161	AAR-1717
PS2185-3	11.5	14350	160	13950	16458	ETH-10314
PS2185-3	11.5	13650	210	13250	15590	ARR-1718
PS2185-3	12.5	15960	110	15560	18454	AAR-1719
PS2185-3	13.5	18510	190	18110	21616	AAR-1720
PS2185-3	14.5	23650	230	23250	27348	AAR-1721
PS2185-3	15.5	25900	250	25500	29834	AAR-1722
PS2185-3	16.5	30780	530	30380	35022	ETH-9873
PS2185-3	19.5	34070	550	33670	38362	ETH-10315
PS2185-3	20.5	(?>)39950	1450	-	-	ETH-9874
PS2185-3	22.5	(?>)37350	690	-	-	ETH-10577
PS2185-3	24.5	(?>)35820	670	-	-	ETH-10316
PS2185-3	26.5	(?>)32570	660	-	-	ETH-10317
PS2185-3	28.5	(?>)38540	1240	-	-	ETH-9875
PS2177-1	0	2470	110	2070	2070	AAR-2415
PS2177-1	4.5	6060	60	5660	6178	ETH-10901
PS2177-1	9.5	7030	65	6630	7381	ETH-10902
PS2177-1	14.5	13290	90	12890	15144	ETH-10903
PS2177-1	16.5	20310	230	19910	23848	AAR-2093
PS2177-1	19.5	17470	130	17070	20327	ETH-11209
PS2177-1	21.5	35100	820	34700	39382	AAR-2094
PS2177-1	23.5	>39000	-	-	-	AAR-2095
PS2177-1	25.5	>34130	-	-	-	ETH-11210
PS2200-2	0	5615	60	5215	5441	ETH-11212
PS2200-2	3.5	11450	85	11050	12676	ETH-11213
PS2200-2	6.5	20120	150	19720	23155	ETH-11214
PS2200-2	8.5	27020	280	26620	30887	ETH-11215
PS2200-2	10.5	32460	460	32060	36591	ETH-11216
PS2200-2	14.5	>34870	-	-	-	ETH-11217
PS2200-2	16.5	? 28270	300	-	-	ETH-11218
PS2212-5	6.5	2900	55	2500	2500	ETH-10896
PS2212-5	13.5	6165	60	5765	6309	ETH-10897
PS2212-5	15.5	6405	60	6005	6606	ETH-10898
PS2212-5	18.5	9780	75	9380	10791	ETH-10899
PS2212-5	26-29	? 5535	60	-	-	ETH-10900
PS2195-4	0	3190	80	2790	2790	AAR-1723
PS2195-4	6.5	11750	100	11350	13234	AAR-1724
PS2195-4	9.5	23450	440	23050	27124	AAR-1725
PS2195-4	11.5	28500	490	28100	32633	AAR-1726
PS2195-4	15.5	>37000	-	-	-	AAR-1727
PS2195-4	21.5	30160	530	29760	34378	AAR-1728
PS2195-4	23.5	(?>)40000	1000	-	-	AAR-1782
PS2195-4	26.5	>42000	-	-	-	AAR-1783
PS2166-2	0	2795	65	2395	2395	AAR-1729
PS2166-2	8.5	7530	80	7130	8001	AAR-1730
PS2166-2	13.5	14010	130	13610	16036	AAR-1731
PS2166-2	15.5	12890	140	12490	14648	AAR-1732
PS2166-2	19.5	34200	1500	33800	38492	AAR-1733
PS2166-2	22.5	38800	760	38400	42943	AAR-1734
PS2166-2	25.5	>42000	-	-	-	AAR-1735
PS2180-1	0	2420	70	2020	2020	AAR-1737
PS2180-1	4.5	7260	130	6860	7666	AAR-1738
PS2180-1	8.5	16230	150	15830	18789	AAR-1739
PS2180-1	12.5	35020	800	34620	39303	AAR-1740
PS2180-1	14.5	37350	970	36950	41566	AAR-1741
PS2192-1	0	980	110	580	580	AAR-2416
PS2192-1	20.5	5675	65	5275	5701	AAR-2096

about 1-2 ‰ from the LGM to the Holocene can be observed in most oxygen isotope records, with decreasing amplitude toward the central Arctic. Very low average sedimentation rates during oxygen isotope stage 2, confirmed by AMS-^{14}C datings, and low planktic foraminifer abundances, however, indicate that the LGM signal in some cores might have been smoothed by bioturbation.

The δ^{13}C values of *N. pachyderma* (sin.) vary between 0 and 1‰. The relatively high and homogeneous values (0.7-1.0‰) in the surface sediment samples are evidence for well-ventilated and homogene surface waters without major gradients of biological activity (Spielhagen & Erlenkeuser, 1994). When comparing the δ^{18}O and δ^{13}C records of the present study with comparable other studies in the Arctic Ocean (Köhler, 1992; Stein et al, 1994c), it is a general impression that the δ^{13}C records are more straight forward to correlate than the corresponding δ^{18}O records. This may be due to the influx of low-δ^{18}O melt- or riverine water which not directly influences the carbon isotope composition of the sea water. On the other hand, parallel excursions of the δ^{18}O and δ^{13}C records to major deglacial events clearly can be observed.

a) δ^{18}O and δ^{13}C records: Yermak Plateau - Nansen Basin - Gakkel Ridge (60°E) - Amundsen Basin

Variable sedimentation rates and stratigraphic resolution lead to the different character of the isotope records in transect A (Fig. 9). The box cores from the Yermak Plateau, Nansen Basin and the Amundsen Basin are suggested to cover the last deglaciation and the Holocene. The Gakkel Ridge deep valley sites (PS2166-2 and PS2172-1) may document the sedimentation from at least oxygen isotope stage 4. Core PS2164-4 from the crest of the Gakkel Ridge presumably is more condensed and may extend well down into oxygen isotope stage 5.

Box core PS2212-5 from the Yermak Plateau records the Termination I and the Holocene. The Termination I interval is characterised by a low abundance of planktic foraminifers showing signs of carbonate dissolution. Hence, AMS-^{14}C dating was possible only down to 18.5 cm corresponding to 9.4 ^{14}C ka. Low δ^{18}O values associated with low δ^{13}C values at about 40-38 cm are suggested to represent a deglacial event in connection to Termination Ia. The lithic coarse fraction peak at 42-40 cm may thus be equivalent to a similar peak in cores from the Nansen Basin and the Gakkel Ridge (Fig. 12) which has been dated to about 14-12 ^{14}C ka. The interval at 20-15 cm, corresponding to Termination Ib, is characterised by decreasing δ^{18}O values associated with a δ^{13}C minimum dated to about 9.4 ^{14}C ka. The Holocene record shows very uniform stable isotope values. In the long kastenlot core PS2212-3 and gravity core PS1533-3 from the Yermak Plateau, combined stable isotope

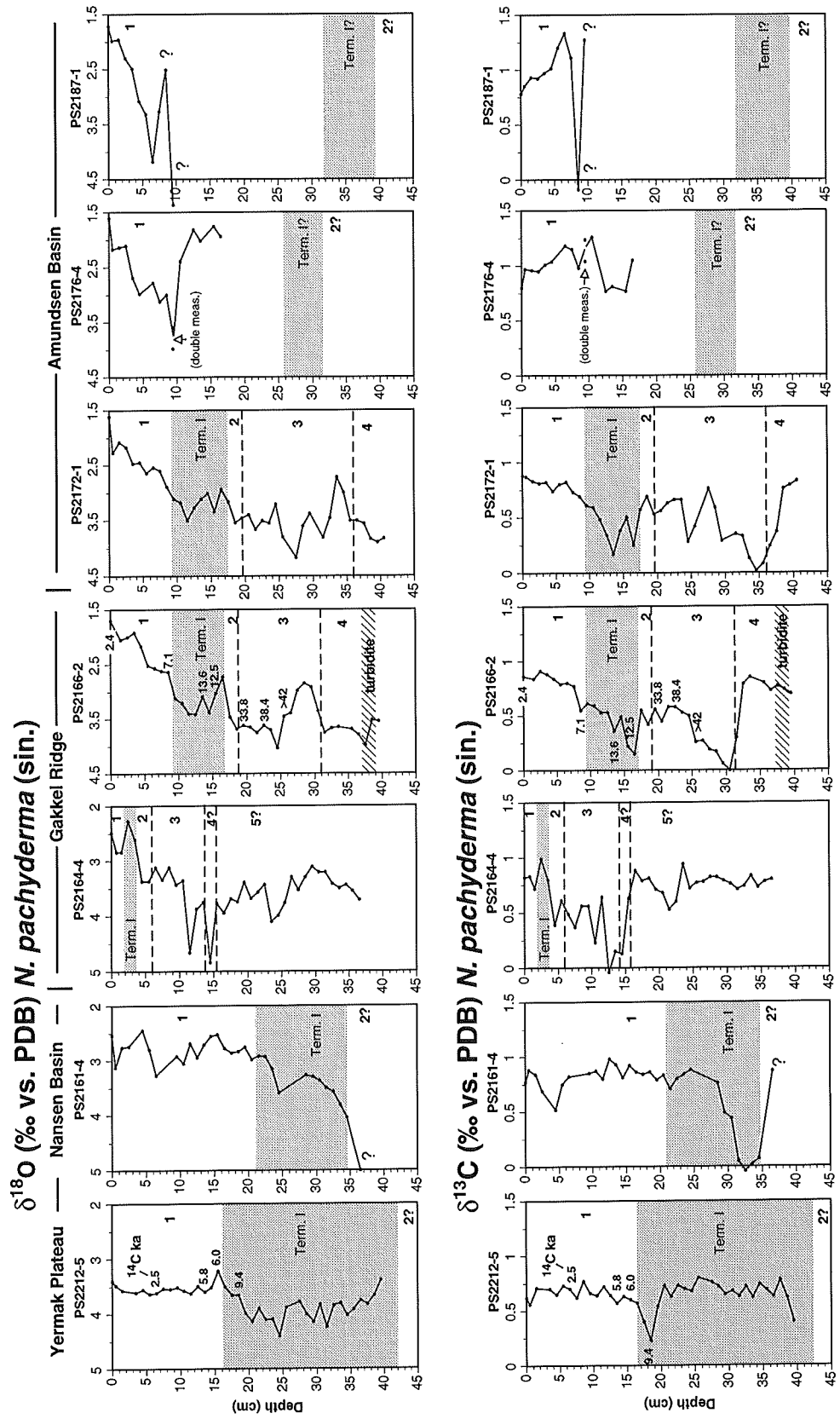

Fig. 9. $\delta^{18}O$ and $\delta^{13}C$ records of *N. pachyderma* (sin) with reservoir corrected AMS-^{14}C ages (ka) indicated at the sample levels concerned (transect A). The extent of proposed oxygen isotope stages (1-5) and Termination I (shaded bar) is given.

stratigraphy, magnetostratigraphy, and nannofossil biostratigraphy suggest that isotope stage 2 deposits are found at 110-40 cm (cf. Nowaczyk & Baumann, 1992; Nowaczyk et al, 1994; Köhler, 1992; Vogt et al., in prep.) confirming that the stage boundary 2/1 can be placed in the lowermost part of box core PS2212-5.

In core PS2161-4 from the Nansen Basin, Termination I is suggested to be found at 35-19 cm marked by a $\delta^{18}O$ decrease from about 5 to 3‰ associated with a distinct $\delta^{13}C$ minimum reaching 0‰ in the interval 35-30 cm. It is unlikely, however, that the high $\delta^{18}O$ value (5‰) and high $\delta^{13}C$ value (0.8‰) obtained at 36.5 cm are realistic for stage 2 in that region. Mapping of the $\delta^{18}O$ distribution for the Last Glacial Maximumin in the Eurasian Basin and the Fram Strait (section 5.5) indicates that maximal $\delta^{18}O$ values that can be expected for the LGM are about 4.0-4.6‰. The single high value represent possibly a measurement error.

Cores PS2166-2 (AMS-^{14}C dated) and PS2172-1 from Gakkel Ridge valley sites show well correlatable isotope records. Two low-$\delta^{18}O$ excursions at 17-9 cm, associated with $\delta^{13}C$ minima (0.2-0.3‰) showing ^{14}C ages of 14-12 ka, are ascribed to Termination Ia. A short return to relative high $\delta^{18}O$ values (3.5‰, Younger Dryas?) is followed by abrupt decreasing $\delta^{18}O$ values and increasing $\delta^{13}C$ values interpreted as Termination Ib. AMS-^{14}C dating of core PS2166-2 indicates that stage 2 is at maximum two cm thick with $\delta^{18}O$ values of about 3.5-3.7‰ and $\delta^{13}C$ values of 0.4-0.6‰. The stage 4/3 boundary is suggested to be located in the lower part of core PS2166-2 and PS2172-1 at the very prominent $\delta^{13}C$ minimum (0‰) associated with decreasing $\delta^{18}O$ values. By comparison with high resolution records from the Fram Strait (Dokken, 1995) and the Norwegian-Greenland Sea (Duplessy et al., 1988; Vogelsang, 1990; Weinelt, 1993), the low $\delta^{18}O$ values immediately following (at 29.5 cm in PS2166-2; at 33.5 cm in PS2172-1) could represent event 3.31 (55.45 ka: Martinson et al., 1987). Supporting evidence for the above stratigraphy and resulting calculated average sedimentation rates at site PS2166-2 are coccolith data of Gard (1993) which in the long piston core and trigger weight core at site PS2166-3 tentatively indicate stage 5 deposits at 60-50 cm and 41-29 cm respectively.

The coarse-grained nature and unusually high IRD content of core PS2164-4 (Figs. 12, 14) from the Gakkel Ridge crest suggets that the stratigraphic record is quite condensed, probably due to winnowing of fines. The relative high $\delta^{18}O$ value of the surface sample (2.5‰) compared to core PS2166-2 (1.7‰) suggests that the upper Holocene part is missing. Oxygen isotope stage 2 is tentatively placed at 5 to 4 cm. Stage 4 is suggested to be located in the interval at 16-14 cm where a characteristic decrease of $\delta^{13}C$ is found associated with a high $\delta^{18}O$ value (4.8‰). Below, moderate low $\delta^{18}O$ values and relative high $\delta^{13}C$ values characterise the depth interval 32-17 cm which is suggested to represent stage 5.

Abundant planktic and benthic foraminifers including, *C. wuellerstorfi,* are found in this interval (Fig. 13a). The lower part of the core, however, appears disturbed.

In core PS2176-4 from the central part of the Amundsen basin and core PS2187-1 from the lowermost rim of the Lomonosov Ridge, the isotope records only cover the uppermost 15 cm due to the complete absence of planktic foraminifers below. Surprisingly high $\delta^{18}O$ values exceeding 3.5‰ are found in both cores between 5 and 10 cm in the planktic foraminifer low abundance tail. At this level there is an extensive occurrence of fragmentary and pitted shells indicating severe carbonate dissolution (Fig. 13a). The anomalous $\delta^{13}C$ trend downcore to values of about 1.2-1.3‰ (considerably higher than the core top), however, indicates that the high $\delta^{18}O$ values hardly can represent isotope stage 2. There is no resemblance to the Termination I isotopic pattern unambiguously observed in cores from the Gakkel Ridge and the Lomonosov Ridge. Also cores PS2190-1 and PS2192-1 from the Amundsen Basin (transect C) show strikingly high $\delta^{18}O$ values associated with relative high $\delta^{13}C$ values in an interval where an AMS-^{14}C dating indicates a Holocene age. One possibility is that reworking of former glacial deposits and deposition in the form of fine-grained turbidites may obscure parts of the basinal records. Moreover, the IRD component analyses (Fig. 15a) reveal characteristic IRD peaks ascribed to Termination I in the lower part of the cores.

b) $\delta^{18}O$ and $\delta^{13}C$ records: Lomonosov Ridge - Makarov Basin

The stratigraphic record of the lithostratigraphic well-correlatable box cores from the crest of the Lomonosov Ridge is suggested to represent oxygen isotope stages 1-4 and may in cores PS2185-3 and PS2184-1 extend into late stage 5 (Fig. 10). The AMS-^{14}C datings and stable isotope records verify that the uppermost 10-15 cm of the Lomonosov Ridge sediment cover represent Termination I and the Holocene. Surprisingly, in the Makarov Basin sites nearby, the glacial stage 2 to Holocene record is more condensed than the Lomonosov Ridge record as evidenced by radiocarbon datings in core PS2180-1.

The Holocene sediments have $\delta^{18}O$ values scattered around 2‰ and $\delta^{13}C$ values of about 0.7-1.0‰. The Termination I can be identified as low-$\delta^{18}O$ excursions (1.5-2.0‰), at 15-10 cm, accompanied by a very distinct $\delta^{13}C$ minimum (0.0-0.5‰). Oxygen isotope stage 2 is represented by a fine-grained interval only 3-5 cm thick as evidenced by AMS-^{14}C datings in cores PS2177-1 and PS2185-3. Apparent Last Glacial Maximum $\delta^{18}O$ values are in the range of 2.5-2.9‰. $\delta^{13}C$ values in stage 2 show a drastic decrease from high values exceeding 1‰ at the stage 3/2 transition to low values (0.0-0.5‰) associated with the very beginning of Termination I.

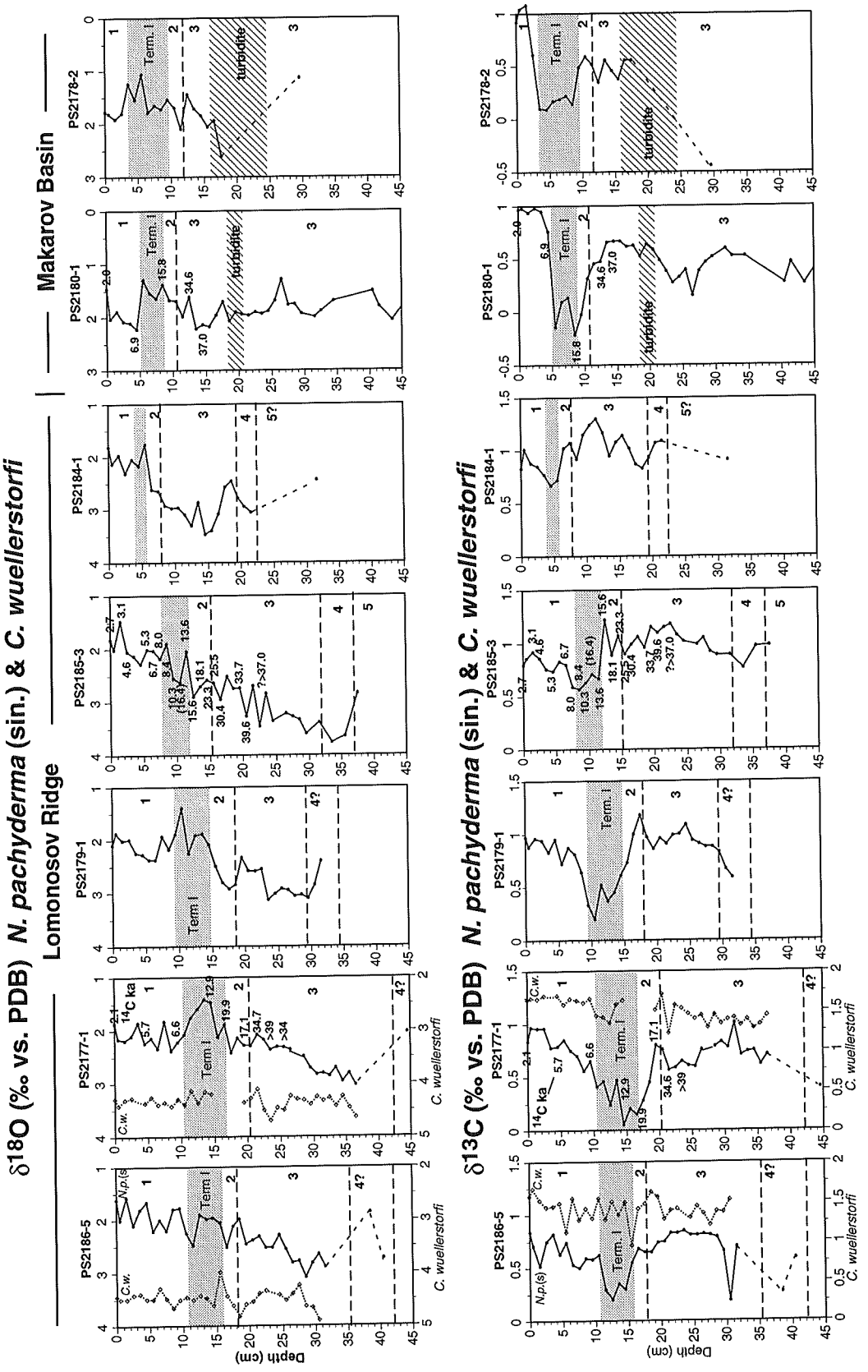

Fig. 10. $\delta^{18}O$ and $\delta^{13}C$ records of *N. pachyderma* (sin) with reservoir corrected AMS-^{14}C ages (ka) indicated at the sample levels concerned (transect B). The extent of proposed oxygen isotope stages (1-5) and Termination I (shaded bar) is given.

The pattern of finite and infinite ^{14}C datings performed on the planktic foraminifer-rich interval at 30-20 cm suggests that this may represent the middle stage 3 period, which also in cores from the Gakkel Ridge (e.g. PS2166-2, PS2195-4, PS2196-2) show a similar planktic foraminifer maximum. The lowermost part of the box core sections from the Lomonosov Ridge shows characteristic peaks of lithic sandy material (30-35%) and is almost barren of planktic and benthic foraminifers. The continuous $\delta^{18}O$ and $\delta^{13}C$ record from site PS2185-3/6 (combined box core and kastenlot record of Spielhagen & Stein (unpubl. data), shown in Fig. 19, indicate that glacial stage 4 sediment may be represented by the high $\delta^{18}O$ values at 36-32 cm. The sandy peak accordingly may represent the stage 4/3 transition and/or deglacial event 3.31. The latter interpretation is supported by the isotope record of core PS2184-1 which shows low $\delta^{18}O$ values associated with the sandy peak, very similar to records from the Gakkel Ridge (PS2166-2 and PS2172-1) and the Morris Jesup Rise (PS2200-2). In PS2185-3/6 (Fig. 19) the isotope record shows at 36-39 cm an abrupt transition downcore to considerably lower $\delta^{18}O$ values and moderately high $\delta^{13}C$ values, suggested to document the stage 5/4 transition.

The two box cores from the Makarov Basin show, in the uppermost 15 cm, stable isotope records similar to the Lomonosov Ridge cores with pronounced Termination I excursions. Radiocarbon datings of core PS2180-1 confirm that the sedimentation rate at this site, during stage 2 and 1, was even lower than the modest rates observed on the Lomonosov Ridge. A sandy turbidite is found at 20 cm in both cores and the very fine-grained and partly fine laminated lower part (distal turbidites?), which are almost barren of planktic foraminifers, may represent stage 3.

In core PS2177-1 (depth: 1388 m) and core PS2186-5 (depth: 2036 m) oxygen and carbon isotopes were additionally measured on the epibenthic species *Cibicidoides wuellerstorfi*. The benthic stable isotope records are shown in Fig. 10 next to the *N. pachyderma* (sin.) records but plotted on different scales. The *C. wuellerstorfi* $\delta^{18}O$ records show low amplitudes and values between 4.0‰ and 4.9‰. The Holocene values are in the range of 4.3-4.5‰. In the Termination I interval, signals characterised by low $\delta^{18}O$ values associated with low $\delta^{13}C$ values may corrrespond to major surface water deglacial episodes. This can be observed in core PS2186-5 in the earliest part of Termination I and in core PS2177-1 in the younger part of the deglacial interval. In core PS2177-1 no specimens of *C. wuellerstorfi* were found in the interval corresponding to the last glacial maximum and the earliest part of the deglaciation. In comparison, in the Norwegian Sea, *C. wuellerstorfi* first appeared after stage 2 about 13 ^{14}C ka (Streeter et al., 1982; Vogelsang, 1990). In the Lomonosov Ridge cores the benthic $\delta^{18}O$ values in the middle part of stage 3, where the abundance of benthic and planktic foraminifers are relative high (Fig. 13b), are about the Holocene level (4.3-

4.5‰). The lower part of the cores, suggested to represent late stage 5 to the early part of stage 3, is almost barren of benthic and planktic foraminifers.

c) $\delta^{18}O$ and $\delta^{13}C$ records: Morris Jesup Rise - Gakkel Ridge (10° E) - Amundsen Basin (North Pole)

Cores PS2200-2, PS2196-2, and PS2195-4 from the Morris Jesup Rise toward the lower rim of the Gakkel Ridge, presumably show isotope records extending well down into oxygen isotope stage 5 (Fig. 11). The higher sedimentation rate records from the central Amundsen Basin (PS2193-2, PS2192-1 and PS2190), influenced by turbidites, are suggested to extend down to glacial stage 2 and/or late stage 3. At these sites incorporation of mass flows and/or distal turbidites may bias the stable isotope records by reworking and displacement of sediments.

Core PS2200-2 from the Morris Jesup Rise has a very condensed upper section. The relative old (5.2 ^{14}C ka) and high core top $\delta^{18}O$ value suggests that winnowing or erosion of the upper Holocene have taken place. Oxygen isotope stage 2 (8-6 cm) and Termination I can be well identified by the isotope signature supported by ^{14}C datings. An infinite age >35 ka is reached at about 14.5 cm. The relative low $\delta^{18}O$ values associated with a pronounced $\delta^{13}C$ minimum (≈0‰) at 23-21 cm are suggested to represent the stage 4/3 transition and/or event 3.31. Stage 4 is placed in the interval 27-24 cm associated with a high $\delta^{18}O$ value (4.1‰). The box core record below, interpreted as stage 5, is barren of foraminifers and the isotope values shown (Figs. 11, 19) are taken from kastenlot core PS2200-5 from the same site (R. Spielhagen & C. Vogt, unpubl. data.).

Cores PS2196-2, PS2195-4 and PS2193-2 from the lower rim of the Gakkel Ridge (0-10°E) toward the central Amundsen Basin show a pronounced $\delta^{18}O$ decrease (2.0‰) from the Last Glacial Maximum to the Holocene. The Termination I interval displays only minor bends or low-$\delta^{18}O$ excursions associated with moderate low $\delta^{13}C$ values. The reason for this is likely bioturbation smoothening of the condensed core sections. Radiocarbon datings of core PS2195-4 confirm that stage 2 comprises an only 2-3 cm thick fine-grained unit. Infinite ^{14}C ages are reached at about 15 cm at a characteristic foraminifer abundance maximum. Stage 4 is suggested to be associated with the pronounced bend in the $\delta^{13}C$ record at 25-20 cm in core PS2195-4 similar to the $\delta^{13}C$ records of cores PS2196-2, PS2200-2, PS2166-2 and PS2172-1. The third foraminifer-rich unit from above (35-25 cm in PS2195-4), with moderately high $\delta^{18}O$ values and high $\delta^{13}C$ values, is designated to late

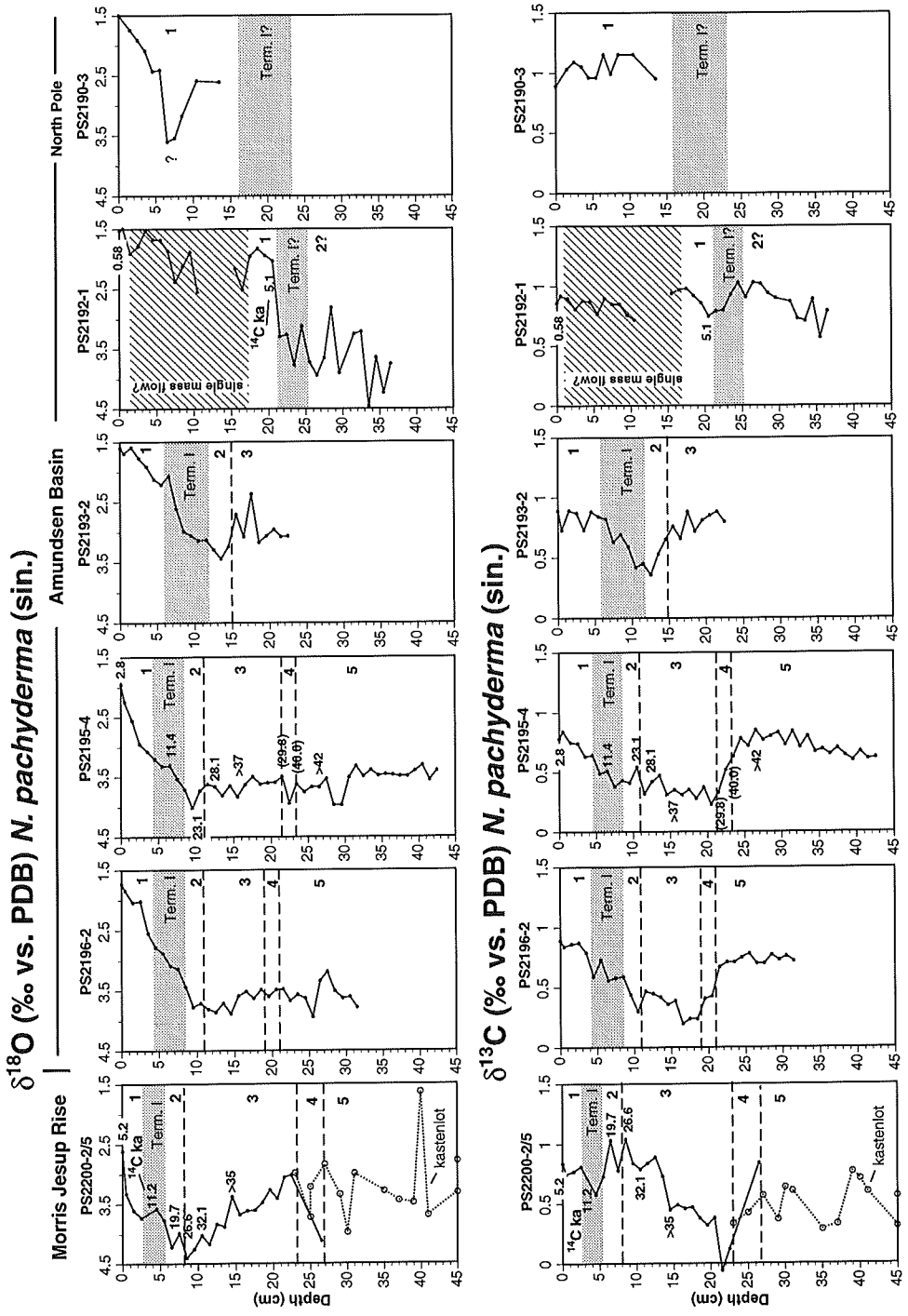

Fig. 11. $\delta^{18}O$ and $\delta^{13}C$ records of *N. pachyderma* (sin) with reservoir corrected AMS-^{14}C ages (ka) indicated at the sample levels concerned (transect C). The extent of proposed oxygen isotope stages (1-5) and Termination I (shaded bar) is given.

stage 5. Supporting evidence herefore is the coccolith assemblage in the interval 30-25 cm which, according to Gard (1993; pers. comm. 1995), is dominated by *Gephyrocapsa mullerae* typical of Stage 5 in high latitude sections. The $\delta^{18}O$ values within the suggested stage 5 are quite high (2.6-3.5‰) compared to the Holocene. Higher $\delta^{18}O$ values in the middle part (4.0‰) coincide with an IRD peak. This event is tentatively suggested to represent substage 5b. In the lowermost part of core PS2195-4 there is a prominent coarse fraction peak, which is almost barren of foraminifers (Fig. 13c). Cores PS2195-4, PS2196-2 and PS2193-2 show in general the same isotope record, similar to cores PS1527-10, PS1528-7 and PS1524-1 from the Gakkel Ridge nearby (Köhler, 1992).

Core PS2192-1 from the central Amundsen Basin shows a Holocene section with a very young $CaCO_3$-rich mass flow unit (17-1 cm) intercalated. The 1 cm thick brown-colored surface layer overlying the mass flow unit, has an AMS-^{14}C age of only 580 yr. This is the youngest core top age ever reported from Arctic Ocean deep sea sediments. The brown-colored foraminifer-rich unit at 21-17 cm, with relative low $\delta^{18}O$ values (2.0-1.8‰), has an AMS-^{14}C age of 5.1 ka. Below, an abrupt transition downward to high $\delta^{18}O$ values may correspond to the glacial-interglacial transition. This is supported by the occurrence of detrital carbonate IRD at 25-21 cm associated with Termination I in other Amundsen Basin and Lomonosov Ridge-Makarov Basin sites (Fig. 14). The scattered but consistently high $\delta^{18}O$ values (4.0-3.0‰) found below 21 cm in core PS2192-1 may thus document an expanded glacial stage 2 section. The corresponding $\delta^{13}C$ record, however, show relative high $\delta^{13}C$ values (0.6 to 1.0‰). This is quite atypical for the stage 2/Termination I interval in that region, which tends to show considerably lower $\delta^{13}C$ values. It therefore cannot be ruled out that the oxygen isotope signals observed are influenced by an allochthonous assemblage of planktic foraminifers deposited by distal mass flows. Stratified fine-grained sediments are thus found from about 29 cm to the core base. The unique depositional conditions at site PS2192-1 may excellently demonstrate the effect of bioturbation in Arctic Ocean deep sea sediments. The sharp lower boundary and the massive character of the mass flow unit (17-1 cm) suggest that it was deposited during a single late Holocene depositional event. Planktic foraminifers found only in the upper 10 cm of the mass flow unit (Fig. 13c) have supposedly been mixed downward by bioturbation.

Core PS2190-3 from at the North Pole shows a short stable isotope record suggested also to represent Holocene sediments, influenced by resedimentation comparable to core PS2176-4 and PS2187-1 from the Amundsen Basin. An interval at 9-6 cm, characterised by high $\delta^{18}O$ values (≈3.5‰) and high $\delta^{13}C$ values, is thus interpreted as an allochtonous unit. Based on correlation of IRD content (Fig. 14) the Termination I interval is placed at 28-16 cm.

3.4 Grain size distribution and coarse fraction composition

The amount and composition of the coarse fraction reflect the sedimentation mode, flux of ice-rafted debris, planktic and benthic productivity as well as modification of surface sediments by bottom currents, calcium carbonate dissolution and precipitation of authigenic minerals (e.g. iron-manganese micronodules). Fig. 12 shows the amount of coarse fraction (>63μm and >500 μm) and the relative content of lithic grains, planktic foraminifers, benthic foraminifers and other biogenic remains respectively in the grain size fraction 125-250 μm. Other biogenic components encompass ostracodes, sponge spicules and fragments of bivalves, echinoderms, worm tubes, etc.

On ridges, plateaus and local highs, ice-rafted debris and planktic foraminifers make up major constituents of the bulk sediment. The coarse fraction >63 μm varies between 5% and 40%, and the grain-size curves are locally well-correlatable between cores (e.g. the Lomonosov Ridge transect). Sediments in a few generally coarser-grained cores (e.g. PS2184-1, PS2200-2 and PS2164-4) have obviously been subject to winnowing of fine material. In surface sediments and some subsurface intervals planktic foraminifers make up the dominant part of the coarse fraction. In the deep basins equivalent pelagic units are often diluted or interlayered with foraminifer-barren, very fine-grained sediments (distal turbidites). Occasionally graded and well-sorted sandy turbidites with up to 80% coarse fraction are found in the deep basin cores (e.g. box core PS2178-2).

The Holocene sediments have between 5% and 10% coarse fraction, mainly consisting of planktic foraminifers. Sediments below representing the last deglaciation and oxygen isotope stage 2 are in general very fine-grained (2-5%) due to relative low foraminifer contents. Only cores from the eastern Gakkel Ridge transect (PS2166-2, PS2172-1), the Nansen Basin (PS2161-4), and the Yermak Plateau (PS2212-5), show a characteristic peak of lithic material (15-30% >63 μm) corresponding to the early part of the deglaciation. Stage 3 sediments have 5-15% coarse fraction also mainly reflecting the planktic foraminifer content. On the Lomonosov Ridge the stage 4/3 transition is suggested to be associated with a conspicuous peak of lithic coarse fraction (30-35%). Records suggested to span stage 5 and 4 reveal some larger regional differences. Processes as locally enhanced sediment ice rafting, winnowing, and depth-dependent carbonate dissolution are all considered important for grain size characteristics and sedimentation rates observed.

Fig. 12. Coarse fraction records (weight-% >63μm and >500μm). The percentage of lithic grains, planktic foraminifers, benthic foraminifers and other biogenic remains in the grain size fraction 125-250μm is shown. Where 'no data' is indicated subdivision of the coarse fraction has not been done (>63μm ≈0%). The extent of proposed oxygen isotope stages (1-5) and Termination I is given. a) Transect A, b) Transect B, and c) Transect C.

12. a)

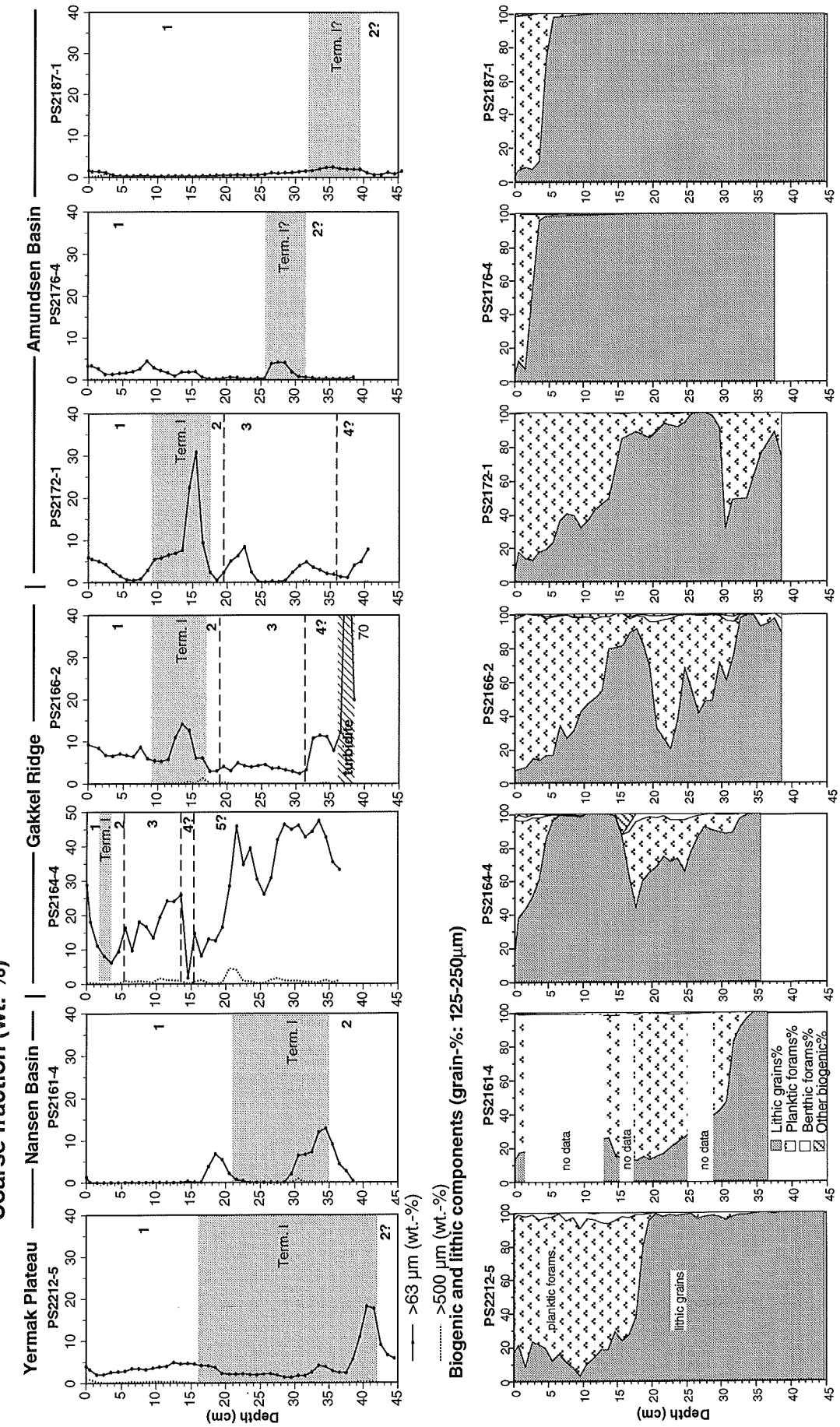
Coarse fraction (wt.-%)
Yermak Plateau
Nansen Basin
Gakkel Ridge
Amundsen Basin
PS2212-5
PS2161-4
PS2164-4
PS2166-2
PS2172-1
PS2176-4
PS2187-1
Depth (cm)
Term. I
Term. I?
Turbidite
>63 µm (wt.-%)
>500 µm (wt.-%)
Biogenic and lithic components (grain-%: 125-250µm)
planktic forams.
lithic grains
no data
Lithic grains%
Planktic forams%
Benthic forams%
Other biogenic%

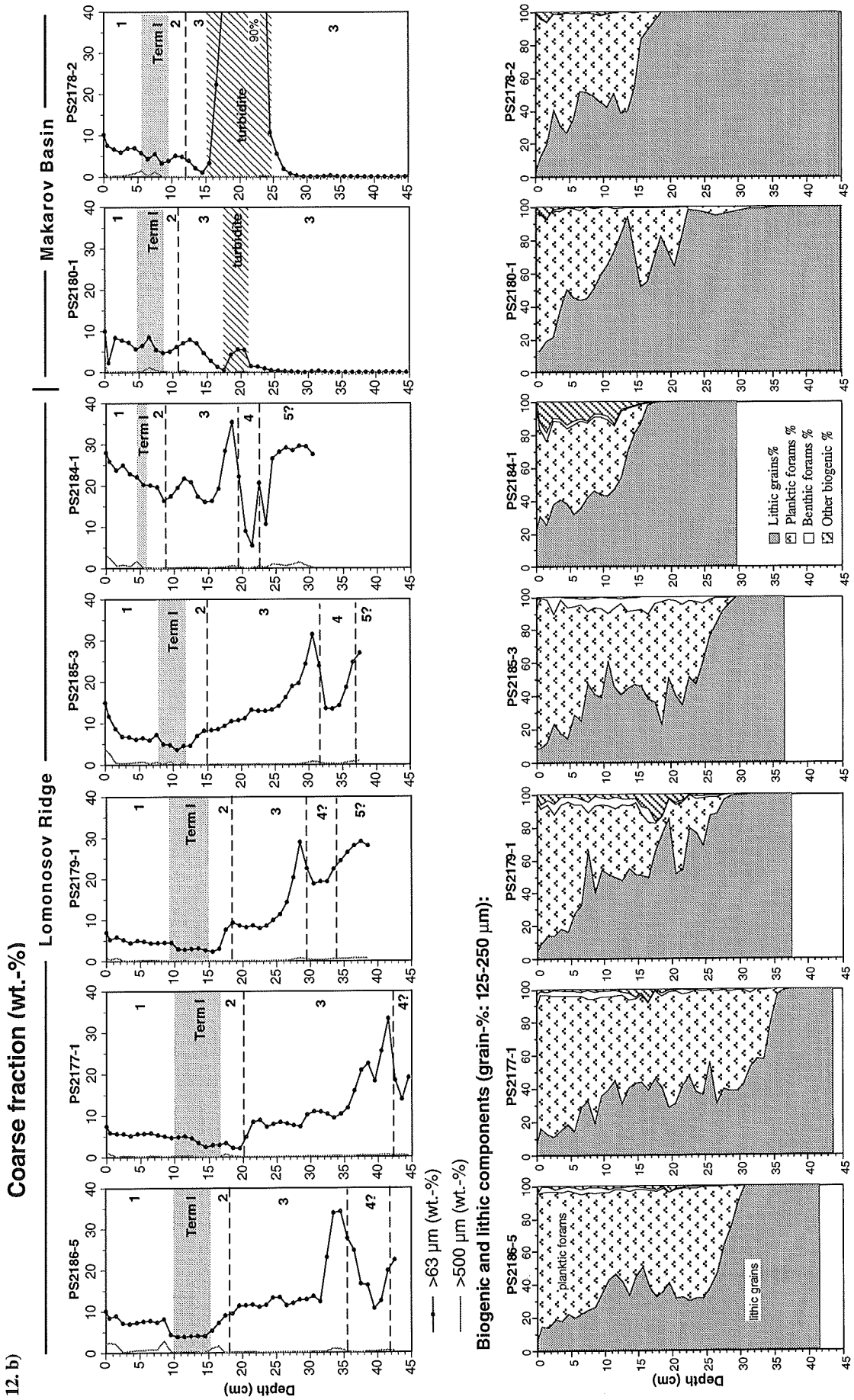
12. b)
Coarse fraction (wt.-%)
Lomonosov Ridge
Makarov Basin
PS2186-5
PS2177-1
PS2179-1
PS2185-3
PS2184-1
PS2180-1
PS2178-2
Term I
turbidite
90%
>63 µm (wt.-%)
>500 µm (wt.-%)
Depth (cm)
Biogenic and lithic components (grain-%: 125-250 µm):
planktic forams
lithic grains
Lithic grains%
Planktic forams %
Benthic forams %
Other biogenic %

12. c)

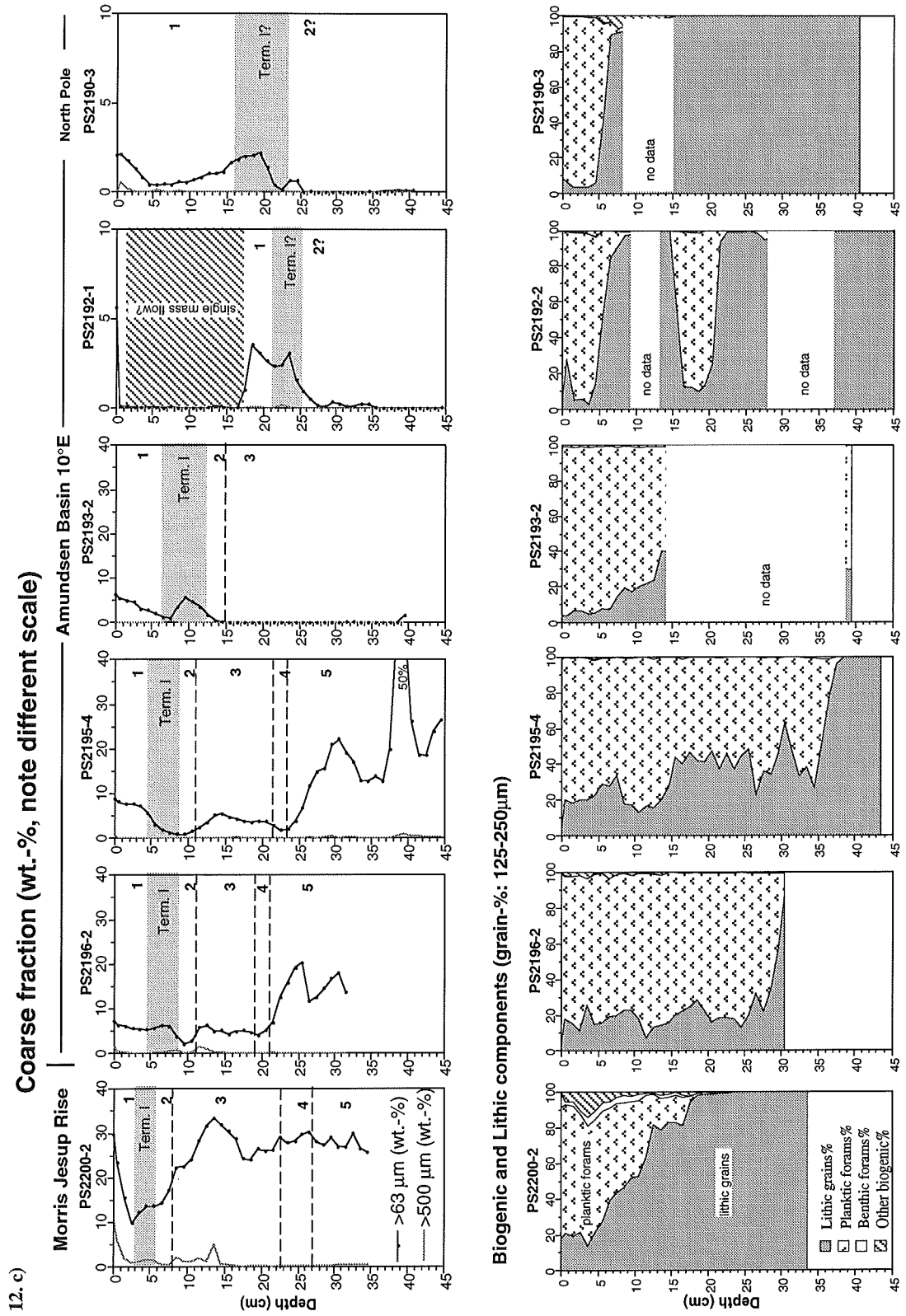
Coarse fraction (wt.-%, note different scale)
Morris Jesup Rise
Amundsen Basin 10°E
North Pole
PS2200-2
PS2196-2
PS2195-4
PS2193-2
PS2192-1
PS2190-3
Term. I
Term. I?
2?
single mass flow?
50%
>63 µm (wt.-%)
>500 µm (wt.-%)
Depth (cm)
Biogenic and Lithic components (grain-%: 125-250µm)
planktic forams
lithic grains
no data
Lithic grains%
Planktic forams%
Benthic forams%
Other biogenic%

The Lomonosov Ridge and Morris Jesup Rise box cores show sections spanning late stage 5 to early stage 3 characterised by a high coarse fraction content, almost devoid of planktic foraminifers. These sites are suggested to have been influenced by severe carbonate dissolution. Some records from deeper turbidite-protected sites in the Amundsen Basin, however, show foraminifers throughout this interval. In core PS2195-4 e.g. the stage 5 section have peaks of lithic coarse fraction (IRD) intercalated with finer-grained intervals showing high abundances of planktic foraminifers. Also core PS2164-4 from the Gakkel Ridge at a depth of 2030 m shows coarse-grained sediments with abundant planktic foraminifers in the interval interpreted as stage 5.

The fraction >500 µm additionally is shown in the coarse fraction plots. Many works have considered coarse terrigenic material in high latitude marine sediments to be the result of ice-berg rafting if other transport mechanisms can be ruled out (e.g. Molnia, 1972; Clark and Hanson, 1983; Heinrich, 1988; Bischof et al., 1990; Spielhagen, 1991; Bond et al., 1992). The amount of coarse fraction >500 µm shows an important difference in distribution compared to the >63 µm fraction. In many cores, the stage 2 and Termination I interval, representing >63 µm minima, contain relatively high amounts of the >500µm fraction. The abundance of IRD (grains/g sediment) in the fraction 500-1000 µm has been quantified (see section 3.6).

3.5 Abundance and preservation of planktic and benthic foraminifers

The abundance of planktic and benthic (calcareous) foraminifers reflects the biogenic production, the flux of lithogenic material (dillution), bioturbation mixing, and degree of calcium carbonate dissolution. The present study confirms that left-coiled *N. pachyderma* totally dominate the planktic foraminifer assemblage in the Arctic Ocean. In Fig. 13 the abundance of planktic and benthic foraminifers (fraction 125-500 µm) per gram sediment is shown for all core sections. Indicated are also intervals totally barren of planktic foraminifers as well as intervals with evidence of severe carbonate dissolution (pitted and fragmentary thin shells). The percentages of fragmentary shells are additionally shown.

Three major abundance maxima of planktic and benthic foraminifers can be ascribed to late oxygen isotope stage 5, middle stage 3 and the mid- to late Holocene. In these intervals maximum abundances reach 5,000 -10,000 planktic foraminifers/g sediment and 100-500 benthic foraminifers/g sediment. Pronounced foraminifer minima are found in stage 4, early stage 3 and stage 2. In general the planktic and benthic foraminifer abundance records parallel each other. There seems to be no obvious difference between the abundance records of planktic foraminifers from the Gakkel Ridge sites to the Lomonosov Ridge. Core PS2200-2 from the Morris Jesup Rise, however, is more unique in having high abundances

of planktic and benthic foraminifers in the stage 2 interval. One explanation could be that bioturbation mixing of stage 3 and stage 1 foraminifer maxima has blurred out the record in the condensed core section. This is contradicted, however, by the planktic $\delta^{18}O$ record, which in the stage 2 interval shows quite high $\delta^{18}O$ values (4.2-4.4‰) close to the stage 2 values reported from the higher-sedimentation rate FRAM-I/4 site not far away (Markussen et al., 1985; Zahn et al., 1985).

Following the abundance minimum in glacial stage 2, an increase in foraminifer abundance associated with Termination Ia can be observed. This seems to be most pronounced in the Gakkel Ridge cores and less pronounced in the Lomonosov Ridge record. A stagnation, possibly related to the Younger Dryas-Termination Ib period, is followed in the early Holocene by a drastic increase in planktic foraminifer abundance. On the ridges, Holocene sediments contain 5,000-10,000 planktic foraminifers/g sediment making up 80-90% of the 125-250 μm coarse fraction.

By the comparison of stratigraphic records, foraminifer abundance data, percentage of fragmentary shells, and the preservational state of the foraminifer shells, the influence of dissolution on individual core sections can be evaluated. Planktic and benthic calcareous foraminifers are in general well-preserved on the sea floor surface of the Arctic Ocean. However, sediments from the deep Amundsen Basin only a few cm below surface, are typically characterised by rare, thin-shelled and fragmentary planktic foraminifers with dissolution holes. This can be observed in cores PS2176-4 and PS2190-3 (water depth 4364 m and 4240 m, respectively). For that reason, stratigraphic division by means of stable isotopes and AMS-^{14}C datings are not possible in many deep core sites. In several cores there is evidence that the carbonate dissolution may be confined to certain time and depth intervals. The quite identical isotopic records and sedimentation rates of core PS2166-2 (depth: 3636 m) and the deeper core PS2172-1 (depth: 4479 m) make them suitable for a comparison of the dissolution effect. In core PS2172-1 there is signs of carbonate dissolution during the mid-Holocene where the abundance of planktic foraminifers shows a distinct minimum. In the neighbouring ^{14}C dated core PS2166-2 the equivalent interval shows very well-preserved foraminifers and displays actually an abundance maximum. A similar situation probably can explain why the planktic foraminifer maximum in core PS2166-2 dated to about 40 ka is missing in core PS2172-1 (interval here characterised by a relative high percentage of fragmentary shells, Fig. 13a). Apparently the lysocline in the Amundsen Basin during these periods was situated somewhere between 4400 and 3700 m. In a study of Gakkel Ridge cores from water depths in the range 2913-3972 m, Pagels (1992) documented a high planktic and benthic foraminifer abundance in the periods 80-70 ka, 60-40 ka and 20-0 ka and limited carbonate dissolution for the last 80 ky.

In the Makarov Basin cores PS2178-2 and PS2180-1 from water depths of about 4000 m there is no evidence of carbonate dissolution in the rather condensed sections encompassing the last 40 ka. In the Nansen Basin only core PS2161-4 from about 4000 m is included in this study. The planktic foraminifers in PS2161-4 encompassing the Termination I and the Holocene are in general well-preserved. The concentration of foraminifers in a few core intervals apparently reflects the effect of dilution by fine-grained turbidites rather than carbonate dissolution. Pagels (1992) found that carbonate dissolution in Nansen Basin cores in general is low to medium and may be the cause of foraminifer barren horizons in the time intervals 70-50 ka, 40-35 ka and 18-5 ka.

In core PS2212-5 taken at 2485 m from the eastern lower flank of the Yermak Plateau the foraminifer-barren character of the Termination I interval may be ascribed to generally poor carbonate preservation. Markussen (1986) found that poor carbonate preservation prevails along the continental margin north of Svalbard. Carbonate poor sediments are found above 1000 m at the Eurasian Basin continental margin where seasonal mixing of low salinity surface and Arctic Atlantic Water dissolves the carbonate (Aagaard et al., 1985).

The lowermost coarse-grained part of the cores from the Lomonosov Ridge and the Morris Jesup Rise taken at water depths between 1000 and 2000 m are more or less barren of planktic foraminifers. The poor preservational state of planktic and benthic foraminifers and the high percentage of fragmentary planktic foraminifers from the lowermost part of the abundance maxima corresponding to the early stage 3 (Figs. 13b, 13c) may suggest that carbonate dissolution to this time was prevailing in relative shallow water depths in the central Arctic Ocean. Also sediments assigned to stage 4 and stage 5 are almost barren of planktic foraminifers and show extremely low bulk carbonate contents.

Fig. 13. Down-core abundance records of planktic and calcareous benthic foraminifers (shells/g sediment) in the size fraction (125-500 μm). Note the scale difference between planktics (x1000) and benthics (x100). For planktic foraminifers, barren levels with rare (+) or no (-) shells are indicated. The percentage of fragmentary planktic foraminifer shells is shown by the dotted line. Reservoir corrected ^{14}C ages (ka) and the extent of proposed oxygen isotope stages (1-5) and Termination I are given. a) Transect A, b) Transect B, and c) Transect C.

Abundance of planktic (x10³) and benthic (x10²) foraminifers/ g sediment

13. a)

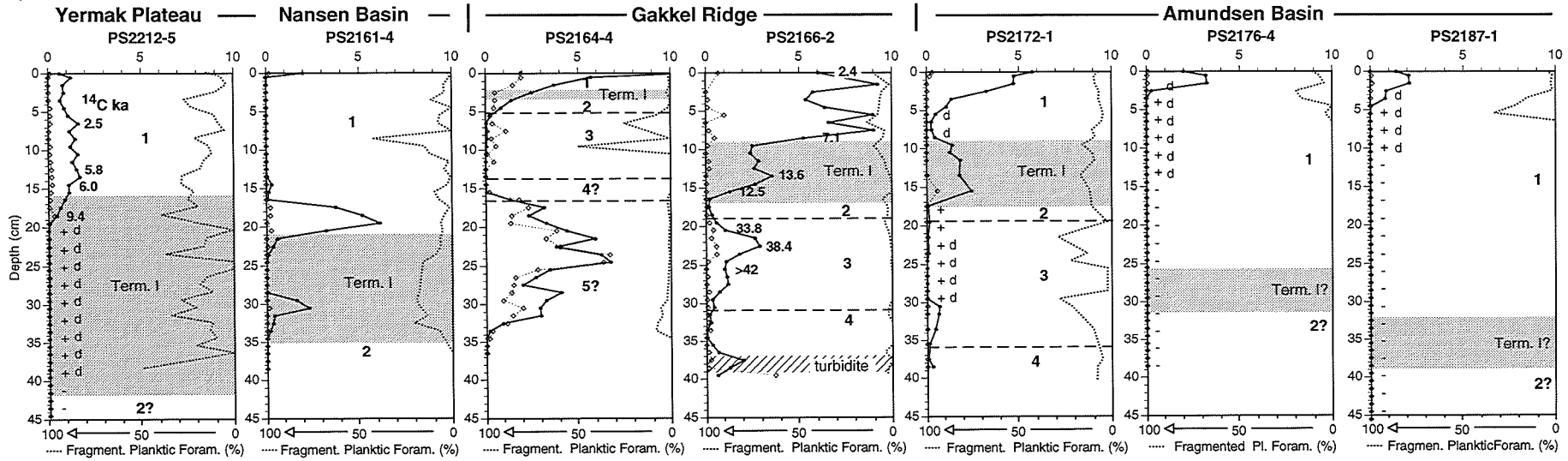

13. b)

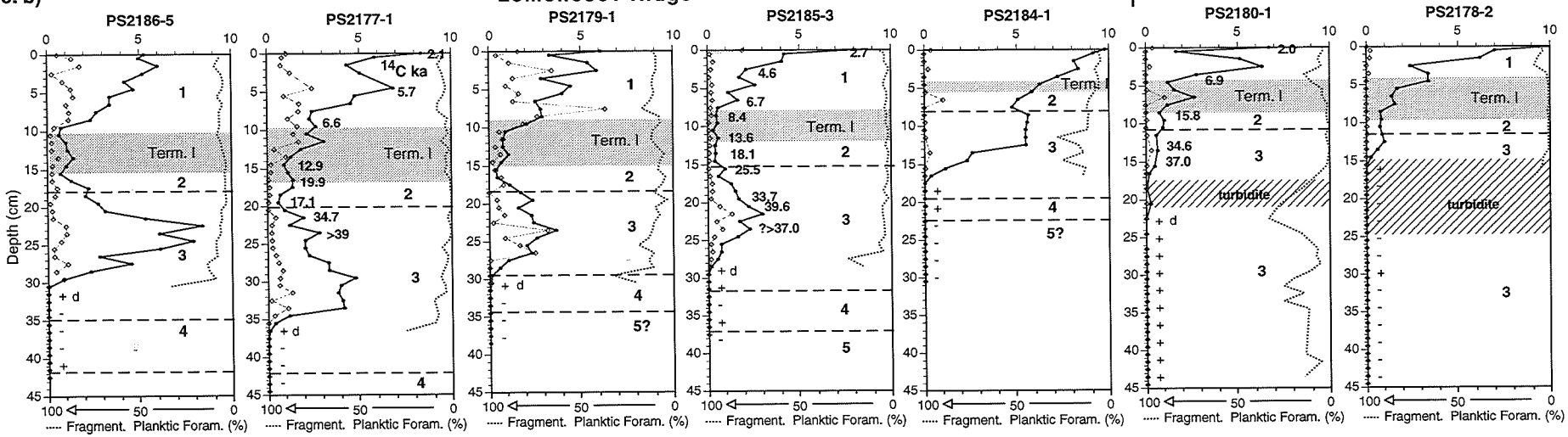

— Planktic foraminifers 10^3/g sed.
◇ Benthic foraminifers 10^2/g sed.

\+ rare planktic foraminifers in sample
\- no planktic foraminifers in sample
d dissolution (pitted, fragmentary shells)

13. c)

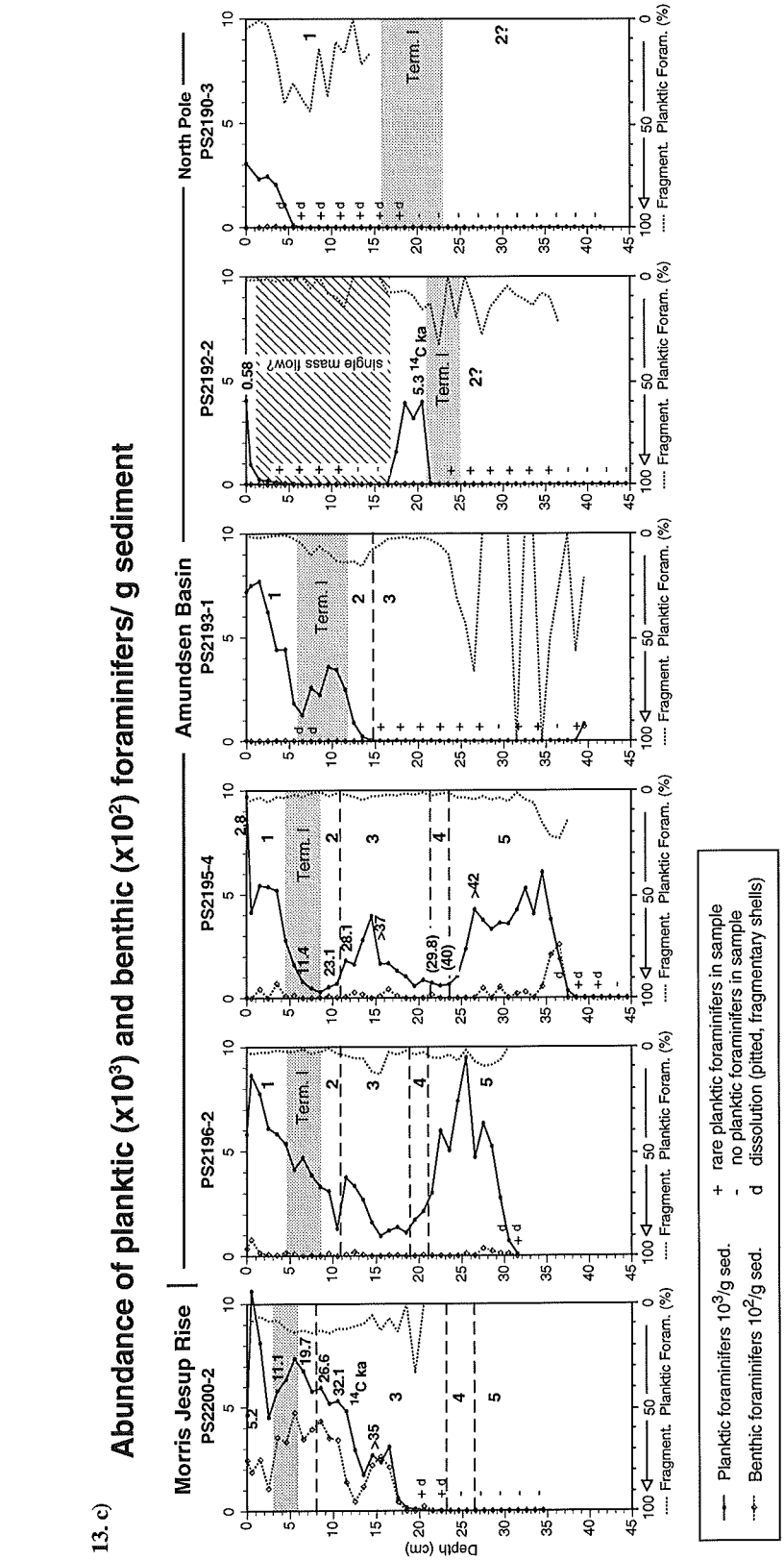
Abundance of planktic (x10³) and benthic (x10²) foraminifers/ g sediment
Morris Jesup Rise
Amundsen Basin
North Pole
PS2200-2
PS2196-2
PS2195-4
PS2193-1
PS2192-2
PS2190-3
Depth (cm)
Fragment. Planktic Foram. (%)
Term. I
single mass flow?
14C ka
Planktic foraminifers 10³/g sed.
Benthic foraminifers 10²/g sed.
+ rare planktic foraminifers in sample
- no planktic foraminifers in sample
d dissolution (pitted, fragmentary shells)

3.6 Ice-rafted debris (IRD) abundance and composition

The abundance and petrographic composition of ice-rafted debris can be used to make inferences about provenance and ice-drift patterns in relation to the circum-Arctic glaciation/deglaciation history. The downcore total abundance of IRD (grains per g sediment, 500-1000µm) are shown in Fig. 14. The abundance of the five major IRD components are shown in Fig. 15 including an additional plot of the siliciclastic sedimentary and detrital carbonate components which seem to indicate different provenance regions. Relative percentage plots have been avoided as major parts of the core sections yield a sparse IRD content.

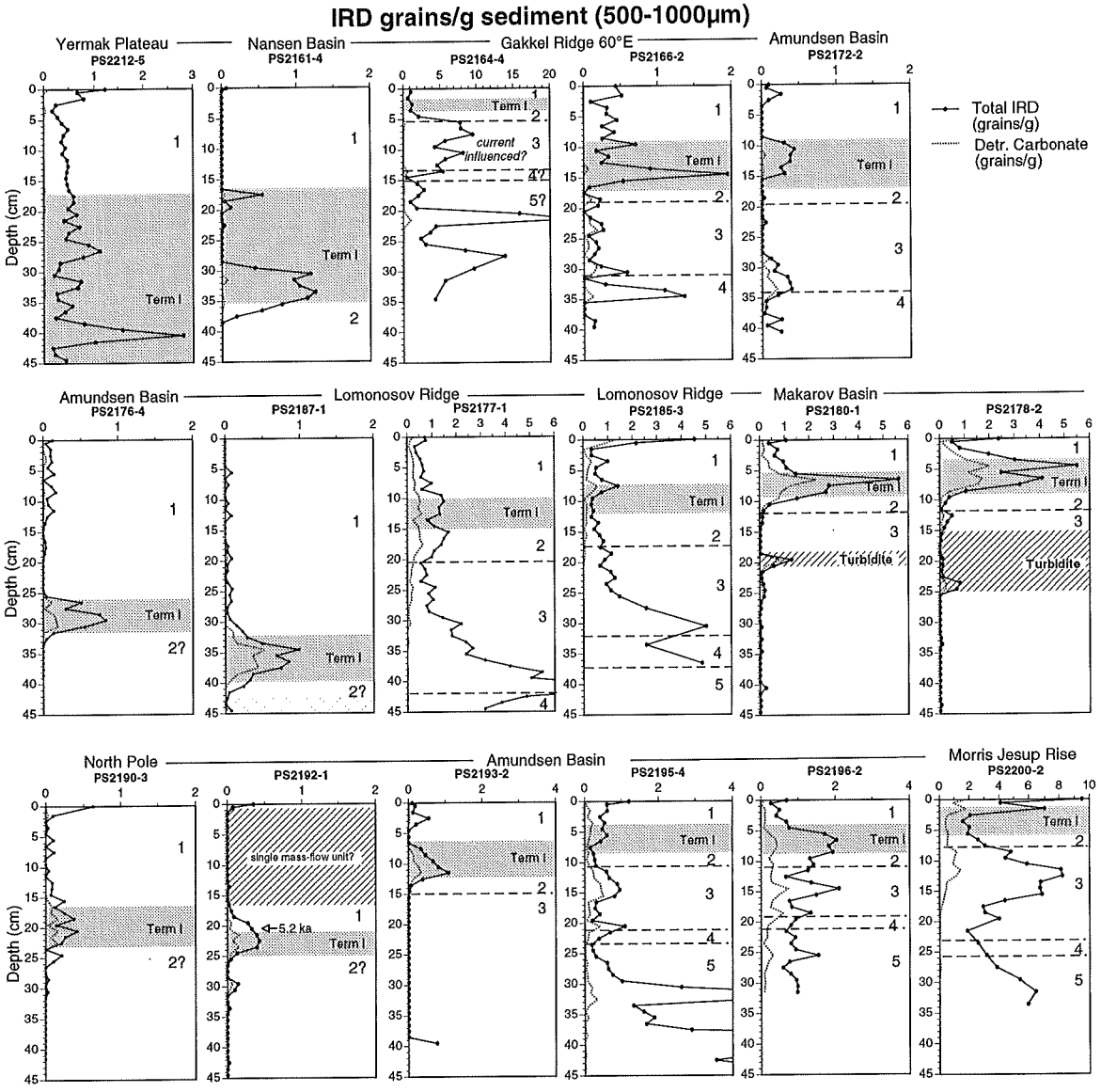

Fig. 14. Ice-rafted debris (IRD) abundance and amount of detrital carbonate. The fraction 500-1000µm was investigated. Note different scales.

Several factors tend to modify the downcore IRD content observed. First of all variable bulk sedimentation rates dilute the IRD 'rain' to a varying degree. Bioturbation may obliterate fine changes of IRD deposition patterns. In the deep basins rapid deposition of fines by turbidites or nepheloid layers may explain horizons practically devoid of IRD. Abnormal high IRD abundances in some cores from ridge crest sites (e.g. PS2164-4, PS2200-2), on the other hand, may indicate very low bulk sedimentation rates eventually associated with winnoving of fines. As ice-rafting is the only likely process which can transport coarse terrigenic sand and gravel out onto deep ocean ridges and highs, the IRD content there may be used as a rough measure for sedimentation rates and depositional processes.

Peaks of IRD abundance apparently are related to the period of the last deglaciation. This is evident in core sections from turbidite-protected ridges and highs and may also be observed in cores from the deep basins (Fig. 14) where the IRD content may be used as a tool for stratigraphic subdivision of sections barren of planktic foraminifers. A prominent IRD peak related to Termination Ia is observed in cores from the Yermak Plateau, the Nansen Basin, and the Gakkel ridge. Datings of the IRD peak in the Gakkel Ridge core PS2166-2 gave ages in the range 13.5-12.3 ^{14}C ka (associated with an age reversal). The IRD peak is remakably rich in siliciclastic sedimentary fragments and shows very few grains of detrital carbonate. The late part of the deglaciation, i.e. Termination Ib, reveals only a minor IRD peak in cores PS2161-4 and PS2166-2. In cores PS2166-2 and PS2172-1 stage 2 and stage 3 sediments are characterised by a low IRD content. Higher abundances are seen at the stage 4/3 transition and the lowermost part of stage 3, where detrital carbonates may amount to 50% of the total IRD grains. Core PS2164-4 from the Gakkel Ridge crest shows abnormal high IRD abundances which probably cannot be explained by the condensed character alone. E.g. the stage 3 interval (14-5 cm) in core PS2164-4 shows IRD abundances of 5-10 grains/g, whereas the equivalent interval in core PS2166-2 shows IRD abundances not exceeding 0.5 grains/g. Current activity and/or mass flows may have accumulated coarse material at the PS2164-4 site and interpretation based on this core is avoided.

The Lomonosov Ridge cores show in the lower more sandy part a pronounced peak of IRD rich in quartz. This peak is suggested to mark the stage 4/3 transition and may include deglacial event 3.31 (cf. Chapter 4). In the upper half of the core sections, corresponding to late stage 3, stage 2, and stage 1, the total IRD abundance is lower but shows an increasing content of detrital carbonate fragments reaching its maximum in the Termination I interval. In cores PS2180-1 and PS2178-1 from the nearby Makarov Basin, the Termination I interval is characterised by peaks of IRD exceeding the abundance observed on the Lomonosov Ridge. Detrital carbonate makes up to 50% of the total assemblage. The thin glacial stage 2 interval shows in contrary a very low IRD content. The lower part of the box cores from the

Makarov Basin (stage 3?), characterised by very fine-grained, mostly laminated sediments with turbidite intercalations, is almost devoid of IRD.

In the Amundsen Basin cores, an about 5-10 cm thick unit with a markedly higher abundance of IRD stands out from sediments having a very limited amount of IRD (Fig. 14). In cores PS2176-4, PS2187-1, and PS2190 stratigraphical subdivision by means of stable isotopes is hampered by the absence of planktic foraminifers below 10 cm. Stable isotopic records of cores PS2193-2 and PS2192-1, however, indicate that the IRD peak observed in all cores may be associated with the Termination I. The high content of detrital carbonate IRD in the cores near to the Lomonosov Ridge (PS2187-1, PS2176-4, PS2190-1) and in the western part of the Amundsen Basin (PS2192-1, PS2193-2), support the correlation of the IRD-rich unit with the radiocarbon-dated Lomonosov Ridge and Makarov Basin records. Additional lithostratigraphic data document stratified fine-grained turbidites below the IRD-rich interval in the Amundsen Basin. These turbidites were likely deposited during the last glacial sea-level low stand. Coarse sand grains are only rarely found in this turbidite sequence.

The cores from the continental margin off northern Greenland (Morris Jesup Rise: PS2200-2) into the southwestern part of the Amundsen Basin (PS2196-2 and PS2195-4) show a marked decrease in the down-core abundance of IRD with increasing distance to North Greenland. The composition of the ice rafted material, which is relatively rich in detrital carbonate (20-40%), and the general pattern of IRD abundance peaks, seem at least for upper stage 5 - stage 1 deposits rather uniform in the three cores. Peaks of IRD are found in the late part of stage 5, in the early and late part of stage 3 and the (late?) part of Termination I.

The IRD rich lower part of cores PS2200-2 and PS2195-4 (early stage 5?) contains abundant quartz and shows in core PS2200-2 also abundant fragments of greenish phyllite and schist. This part is practically devoid of detrital carbonate IRD and also show very low bulk carbonate contents.

Fig. 15. Abundance of main IRD components in the grain size fraction 500-1000µm. Below the content of siliciclastic sedimentary IRD and detrital carbonate IRD is shown on reverse scales to illustrate regional differences. The extent of proposed oxygen isotope stages (1-5) and Termination I is given. Note different scales. a) Transect A, b) Transect B, and c) Transect C.

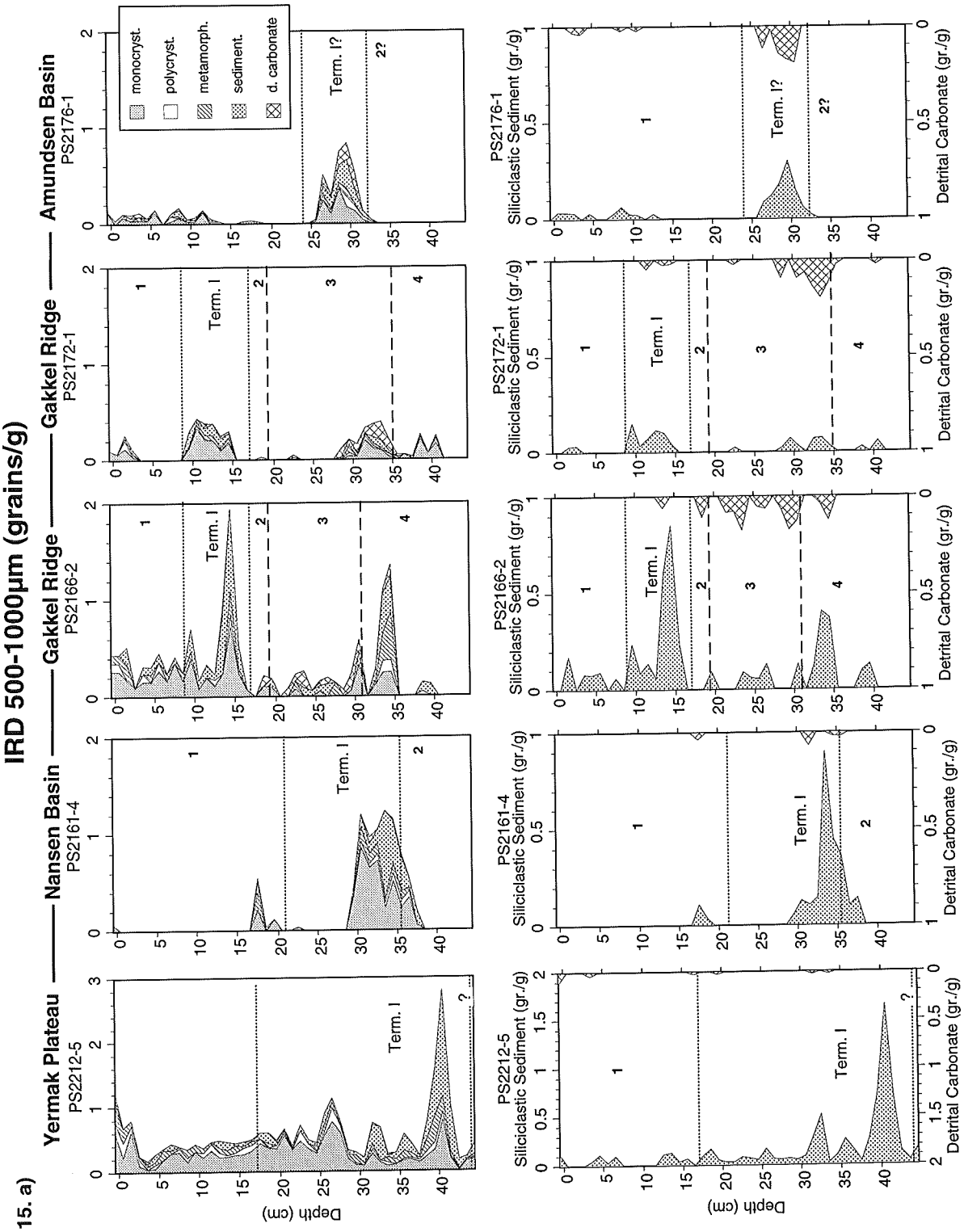
15. a)
IRD 500-1000µm (grains/g)
Yermak Plateau
Nansen Basin
Gakkel Ridge
Gakkel Ridge
Amundsen Basin
PS2212-5
PS2161-4
PS2166-2
PS2172-1
PS2176-1
monocryst.
polycryst.
metamorph.
sediment.
d. carbonate
Term. I
Term. I?
2?
Depth (cm)
Siliciclastic Sediment (gr./g)
Detrital Carbonate (gr./g)

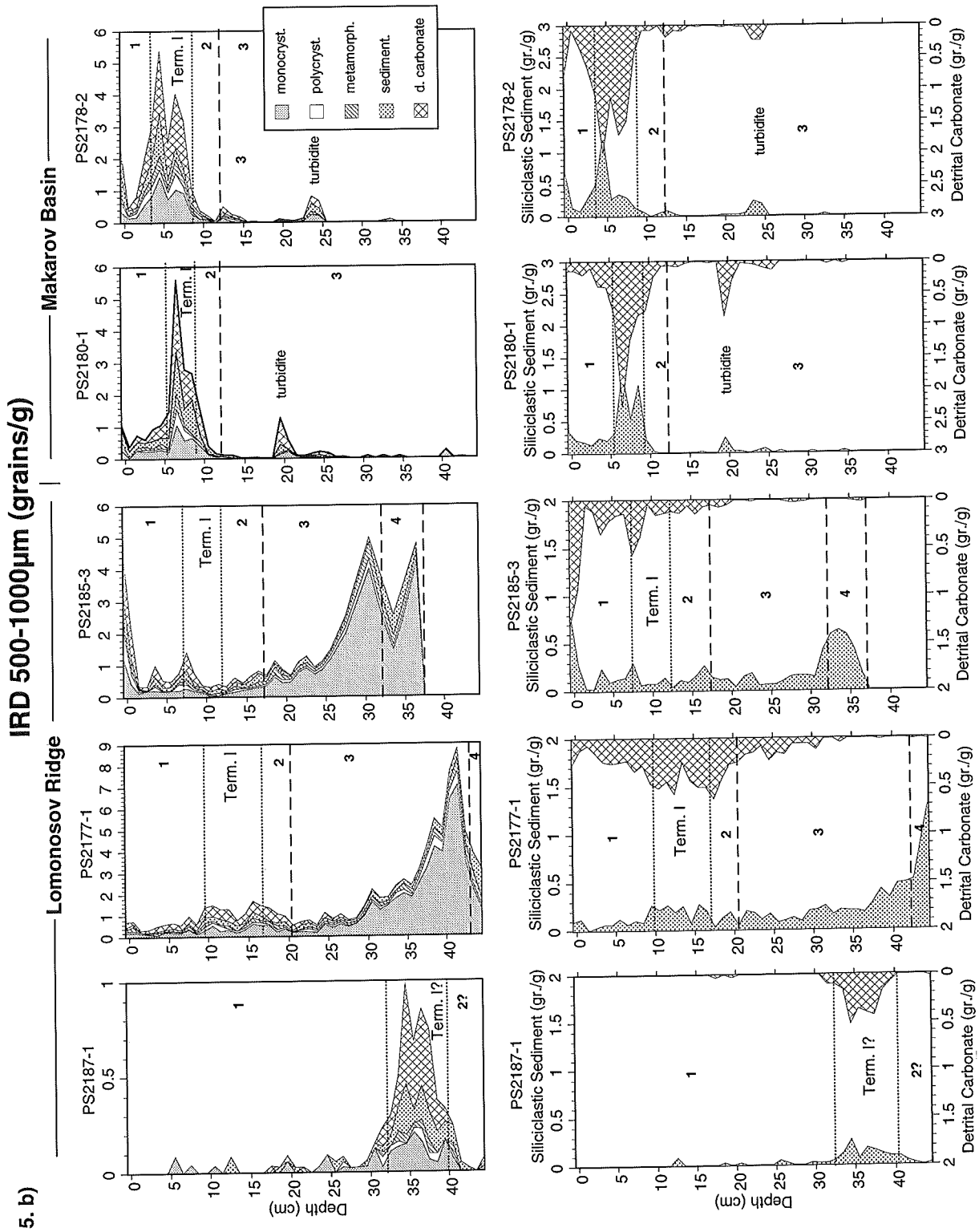
15. b)
IRD 500-1000µm (grains/g)
Lomonosov Ridge
Makarov Basin
PS2187-1
PS2177-1
PS2185-3
PS2180-1
PS2178-2
Term. I
Term. I?
turbidite
monocryst.
polycryst.
metamorph.
sediment.
d. carbonate
Depth (cm)
Siliciclastic Sediment (gr./g)
Detrital Carbonate (gr./g)

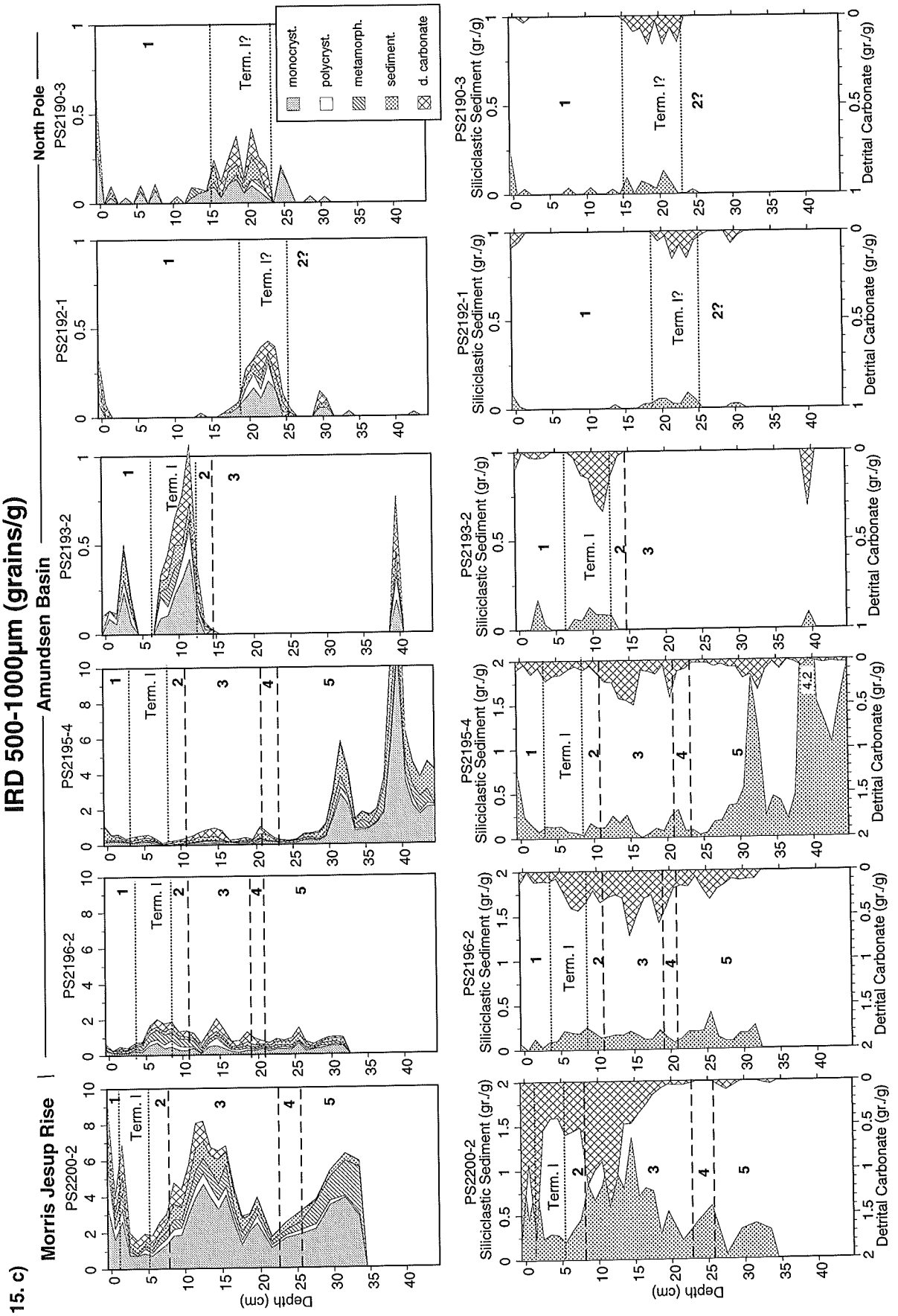
15. c)
IRD 500-1000µm (grains/g)
Morris Jesup Rise
Amundsen Basin
North Pole
PS2200-2
PS2196-2
PS2195-4
PS2193-2
PS2192-1
PS2190-3
Term. I
Term. I?
2?
monocryst.
polycryst.
metamorph.
sediment.
d. carbonate
Depth (cm)
Siliciclastic Sediment (gr./g)
Detrital Carbonate (gr./g)

The areal distribution pattern of detrital carbonate IRD has at least since the beginning of the last deglaciation been rather similar. Detrital carbonates occur abundantly in the Makarov Basin, on the Lomonosov Ridge, in the central and western part of the Amundsen Basin, on the Morris Jesup Rise and the western part of the Gakkel Ridge. On the contrary, almost no detrital carbonates are found in post-stage 2 sediments on the Gakkel Ridge further eastward (60°E) and in the Nansen Basin and the Yermak Plateau records. At these sites, under the Siberian Branch of the Transpolar Drift close to the Eurasian continental margin, siliciclastic sedimentary rocks make up a higher share. In late stage 5, stage 4, and stage 3 the distribution of detrital carbonates is ubiquitous and also reached the Gakkel Ridge at 60°E.

Calculated fluxes of IRD in the fraction 500-1000μm have been mapped out for three periods (Fig. 16): 8-0 cal. ka (mid- to late Holocene), 17-8 cal. ka (Termination I), and 27-17 cal. ka (incl. the Last Glacial Maximum). Although a local high scatter can be observed (due to statistical variance and influence of bioturbation mixing), the IRD flux patterns reveal significant differences. For all three periods, it is evident that the fluxes of IRD over the Gakkel Ridge and the Amundsen Basin were minimal and increased significantly toward the northern Greenland, the Barents Sea and the Lomomonosov Ridge/ Makarov Basin regions (Fig. 16a). This may be related to the origin and melting of icebergs from continental ice sheets and glaciers of the Eurasian continental margin and from northern Greenland and the northern Canadian achipelago (Beaufort Gyre transport). The average IRD flux for the LGM is estimated to have been about half of the Holocene level, whereas the average IRD flux for the Termination I period is estimated to have been about double so high as the Holocene level. For the Termination I, the mapped-out flux of detrital carbonate and siliciclastic sediment particles, reveals different source regions and transport routes (Fig. 16e-f). A 5-10 fold increase in the flux of detrital carbonate IRD apparently took place from the Amundsen Basin, across the Lomonosov Ridge toward the Makarov Basin. This may indicate that a relatively higher amount of IRD were released from a Beaufort Gyre-like ice drift (icebergs from the Canadian archipelago?) compared to the amount released over the central Eurasian Basin. From the western part of the Gakkel Ridge toward the Morris Jesup Rise, a considerable increase in the flux of detrital carbonate can be inferred too for the Termination I period (Fig. 16f), suggesting a northern Greenland and/or Ellesmere Island provenance of icebergs. With respect to the flux of siliciclastic sediment IRD, which show highest values in the Nansen Basin/ Yermak Plateau region (Fig. 17e), it is likely that the Barents Sea Continental Margin was the main iceberg source region during the Termination I (cf. Elverhøi et al., 1995).

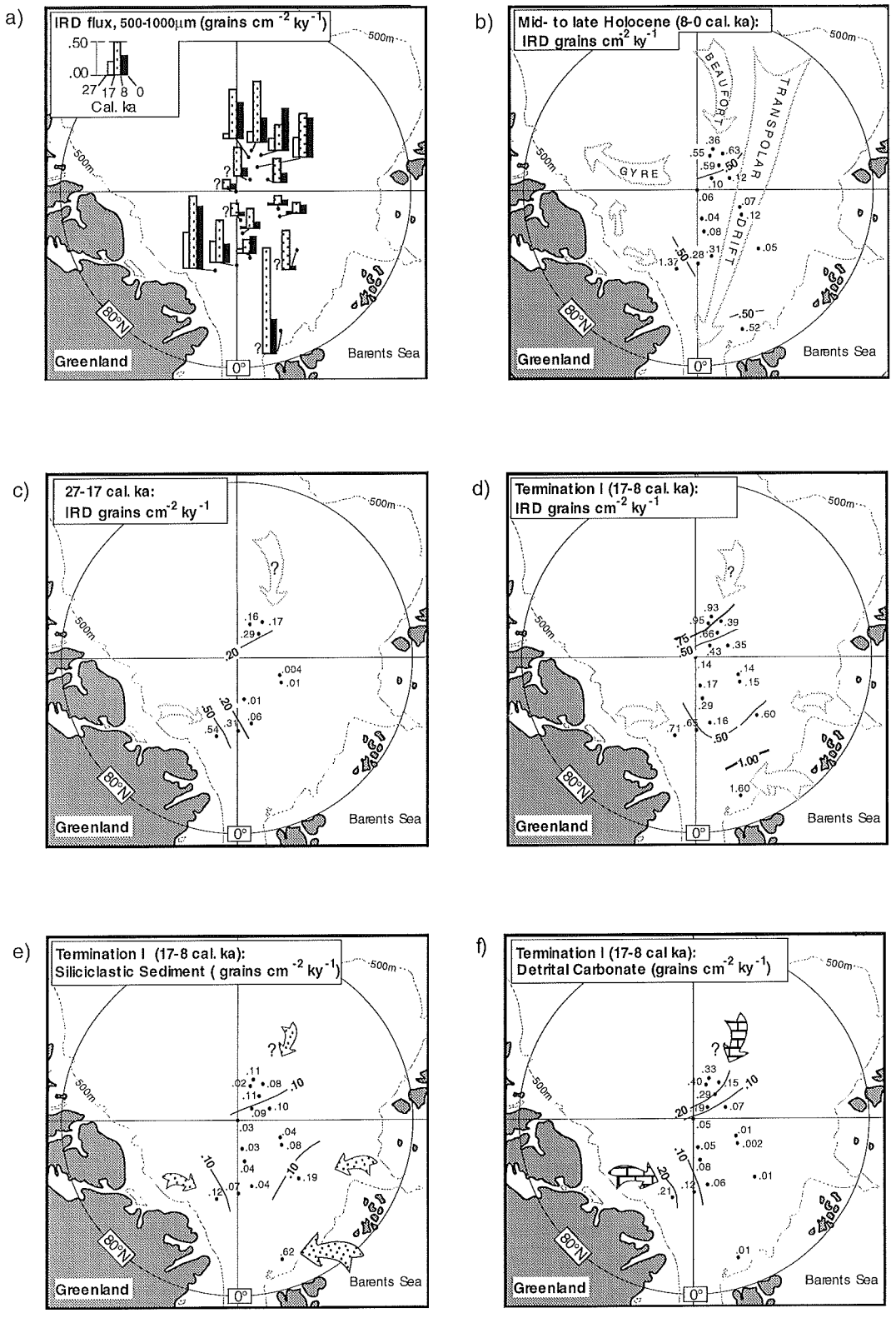

Fig. 16. Average flux of IRD (500-1000μm) displayed for three time periods from the last glacial to the Holocene. In a) Bar diagrams for each core site (small dots) show IRD flux levels for the time periods 27-17, 17-8, and 8-0 cal. ka. In b), c), and d), the estimated IRD flux values for each time slice have been mapped out and used for tentative reconstructions of ice drift patterns (arrows). In e) and f) the flux estimates of siliciclastic sediment and detrital carbonate grains have been mapped out separately for the Termination I.

3.7 Calcium carbonate and TOC records

In eight of the cores investigated, calcium carbonate content and total organic carbon (TOC) have been measured. The calcium carbonate content reflects the flux of carbonate-shelled organisms (mostly planktic and benthic foraminifer and nannoplankton), the flux of ice-rafted detrital carbonate, the dilution by non-carbonatic sediments and the degree of carbonate dissolution.

Downcore calcium carbonate records reveal characteristic variations that can be correlated between the cores (Fig. 17). Although peak values are different from core to core, highest calcium carbonate contents (5-9%) were measured in the mid- to late stage 3, stage 2 and the late Holocene. A pronounced minimum can be observed in early stage 3. Whereas several of the cores from elevated sites show extremely low carbonate contents (<1%) in stage 4 and 5 sediments, the Amundsen Basin core PS2195-4 shows two characteristic maxima of up to 7% calcium carbonate in mid-(?) to late stage 5 sediments.

With exception of the stratigraphic interval of oxygen isotope stage 2, bulk carbonate contents in general parallel the abundance curves of planktic foraminifers (Fig. 13). In stage 2, however, a characteristic peak reaching maximum values of 6-9% can be observed where the abundance of foraminifers is at a minimum. This may be ascribed to a high flux of detrital carbonate most of which may be in the clay to silt fraction. Moreover, this stratigraphic level is, in some of the cores, rich in authigenic calcium carbonate precipitates (e.g. PS2166-2 and PS2200-2). The transition downward to early stage 3 and 4 in core PS2177-1, PS2185-3, PS2200-2 and PS2195-4 is characterised by a sharp decline in carbonate content paralleling the abundance curves of planktic and benthic foraminifers (Fig. 13) and the decline in detrital carbonate IRD (Figs. 14, 15).

Very high values of bulk carbonate in the range 15-30% are found in core PS2200-2 from the Morris Jesup Rise close to North Greenland which is supposed to be one of the major source areas for detrital carbonate. Moreover, in the deep Amundsen Basin core PS2192-1, there is a light coloured, calcium carbonate-rich (14-15%) clayey unit (17-1 cm) dated as younger than 5 ^{14}C ka BP. This unit is suggested to represent a single Holocene mass flow event derived from the North Greenland continental margin. A comparable unit with about 14% carbonate has been reported from multicore PS2171-2 from the Amundsen Basin further to the east (Schubert, 1995). In core PS2176-4 further to the northeast in the Amundsen Basin, very low calcium carbonate values (0-2 %) are found, probably due to the combined effect of carbonate dissolution and dilution by distal low-carbonate turbidites. Small calcium carbonate peaks in the foraminifer-barren Termination I interval in core PS2192-1 and PS2176-4 correlate with peaks of detrital carbonate IRD (Fig. 15). Moreover,

in core PS2180-1 from the Makarov Basin a characteristic bulk carbonate peak in Termination I clearly parallels the conspicuous peak of detrital carbonate IRD (Fig. 15b). A second calcium carbonate peak in core PS2180-1 at 20 cm marks a turbidite unit with some detrital carbonate grains.

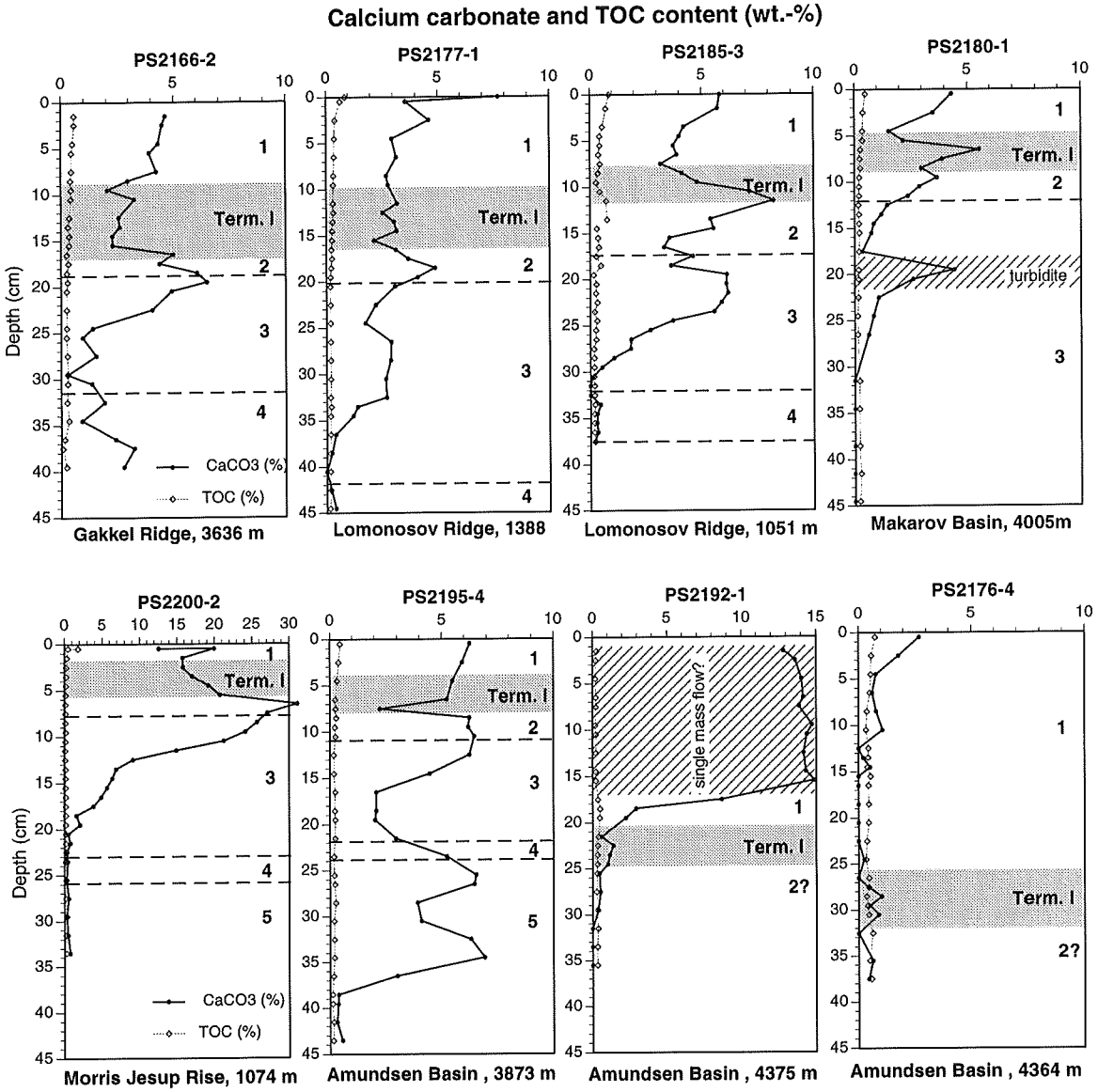

Fig. 17. Calcium carbonate and total organic carbon (TOC) content determined on selected cores. The extent of proposed oxygen isotope stages (1-5) and Termination I is given. Note different scale for core PS2200-2.

On single detrital carbonate dropstones and assemblages of detrital carbonate sand grains the dolomite/calcite ratio has been determined by x-ray diffraction (Appendix H). These measurements show that dolomite is the dominant carbonate mineral in the coarse IRD (Fig. 18). The dolomite contents of detrital carbonate dropstones are typically in the range 85-95%.

The quantification of bulk calcium carbonate content, foraminifer abundance and detrital carbonate IRD, has revealed that both biogenic production and detrital carbonate IRD flux are important for the actual calcium carbonate content in Arctic Ocean deep sea sediments. Where detrital carbonate IRD is absent, the calcium carbonate records normally parallel the foraminifer content. However, independently of the foraminifer content, units with a high detrital carbonate IRD content show a high bulk carbonate content. Determination of mineralogical constituents in bulk sediment samples by Vogt (in prep.) in cores PS2185-3 and PS2200-5 shows that calcite is dominant in the intervals having maxima of planktic foraminifer, whereas dolomite dominates over or equals the calcite content in periods characterised by enhanced detrital carbonate deposition.

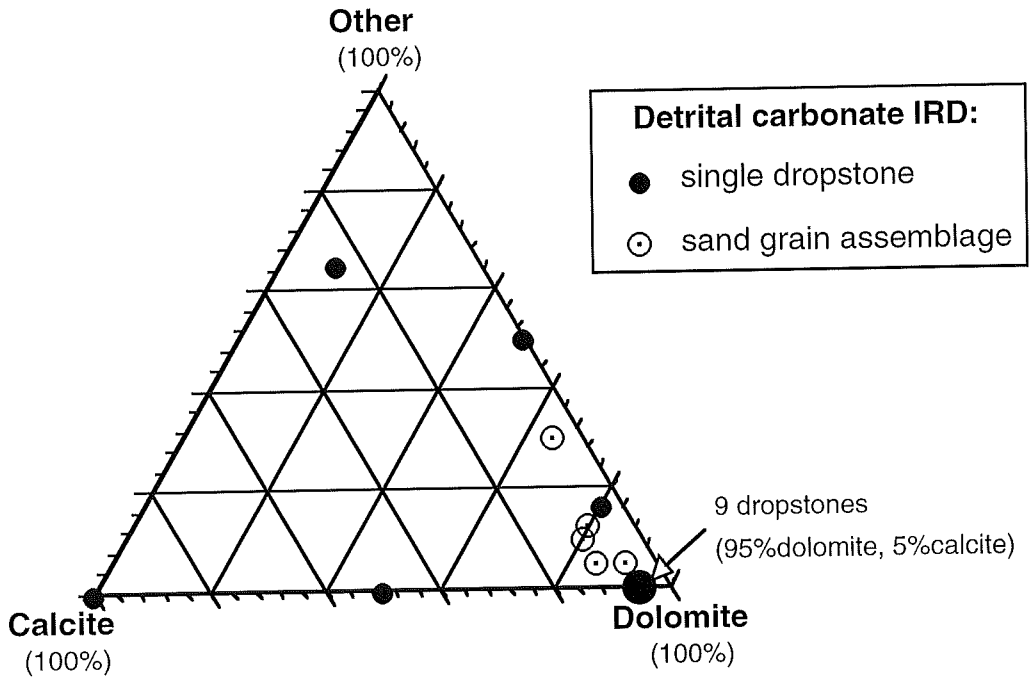

Fig. 18. Composition of detrital carbonate IRD (sand grains and larger dropstones) from the Lomonosov Ridge and Morris Jesup Rise cores determined by x-ray diffraction. Note that 9 single dropstones have roughly the same composition (95% dolomite, 5% calcite).

As a standard method, total organic carbon (TOC) has been measured in the process of bulk $CaCO_3$ measurements. TOC contents are shown together with carbonate contents in Fig. 17. In general the TOC values are very low (0.1-1.0%) and show a low down-core variability, making them less suitable for correlation and paleoceanographic interpretation. A steep downward decline in values observed in the uppermost few cm can be explained by normal surface-near biodegradational processes. Earlier organochemical studies of Arctic Ocean sediments have established that extreme low marine bioproductivity in combination with terrigenic sediment dilution can explain the low TOC values (Markussen, 1986; Pagels, 1992; Schubert, 1995). Determination of organic carbon hydrogen index (HI) and carbon/nitrogen ratio (C/N) indicates that organic carbon in Arctic Ocean sediments mainly is composed of terrigenic material (Schubert, 1995).

4. AGE MODELS FOR SELECTED KEY CORES

Age models have been developed for 5 cores which are considered representative for the hemipelagic and ice-rafted sedimentation in regional areas during the last glacial-interglacial cycle (i.e. PS2166-2 from the Gakkel Ridge valley, PS2195-4 from the Amundsen Basin, PS2200-2/5 from the Morris Jesup Rise, PS2177-1 and PS2185-3/6 from the Lomonosov Ridge). The age models are the basis for the calculation of bulk accumulation rates and the flux of the different components.

4.1 Age model construction and accumulation rates

Absolute age control is available from AMS-^{14}C dates (converted into calendar years) of the younger parts of the sediment cores. Beyond the range of ^{14}C datings correlation with the standard oxygen isotope record (SPECMAP time scale) of Martinson et al. (1987) has been attempted (Fig. 19). Supplementary data like δ^{13}C records, foraminifer abundance, nannoplankton stratigraphy (Gard, 1993), magnetostratigraphy (Frederichs, 1995), ^{230}Th , ^{10}Be, electron spin resonance (ESR) and aminoacid dating (Schäper, 1994; Molnar, 1995) have been used in order to verify specific stratigraphic subdivisions. Age determinations for the calculation of sedimentation rates and the timing of the paleoclimatic events are, however, limited by the sample resolution and/or gaps in the oxygen isotope records. Between age fix points linear interpolation has been applied.

The age models are the basis for a more detailed evaluation of flux rates for different sediment components. Bulk accumulation rates in g cm^{-2} ky^{-1} have been calculated from linear sedimentation rates (cm ky^{-1}) and dry bulk density data (g cm^{-3}); Appendix H. In Fig. 20 age versus depth models have been plotted together with the respective bulk accumulation rate estimates. The accumulation rate of single parameters, like the flux of the >63 µm fraction (g cm^{-2} ky^{-1}), planktic foraminifers (shells cm^{-2} ky^{-1}), IRD (grains cm^{-2} ky^{-1}), and $CaCO_3$ (g cm^{-2} ky^{-1}) can subsequently be calculated (Appendix H). Hereby a picture of temporal changes of the hemipelagic sediment flux appears. In Fig. 21 stable isotope records versus age and the respective flux estimates of single parameters are presented. In Chapter 6 these key records of environmetal proxies are used for a chronostratigraphic presentation and discussion of Arctic Ocean paleoceanography during the last glacial-interglacial cycle.

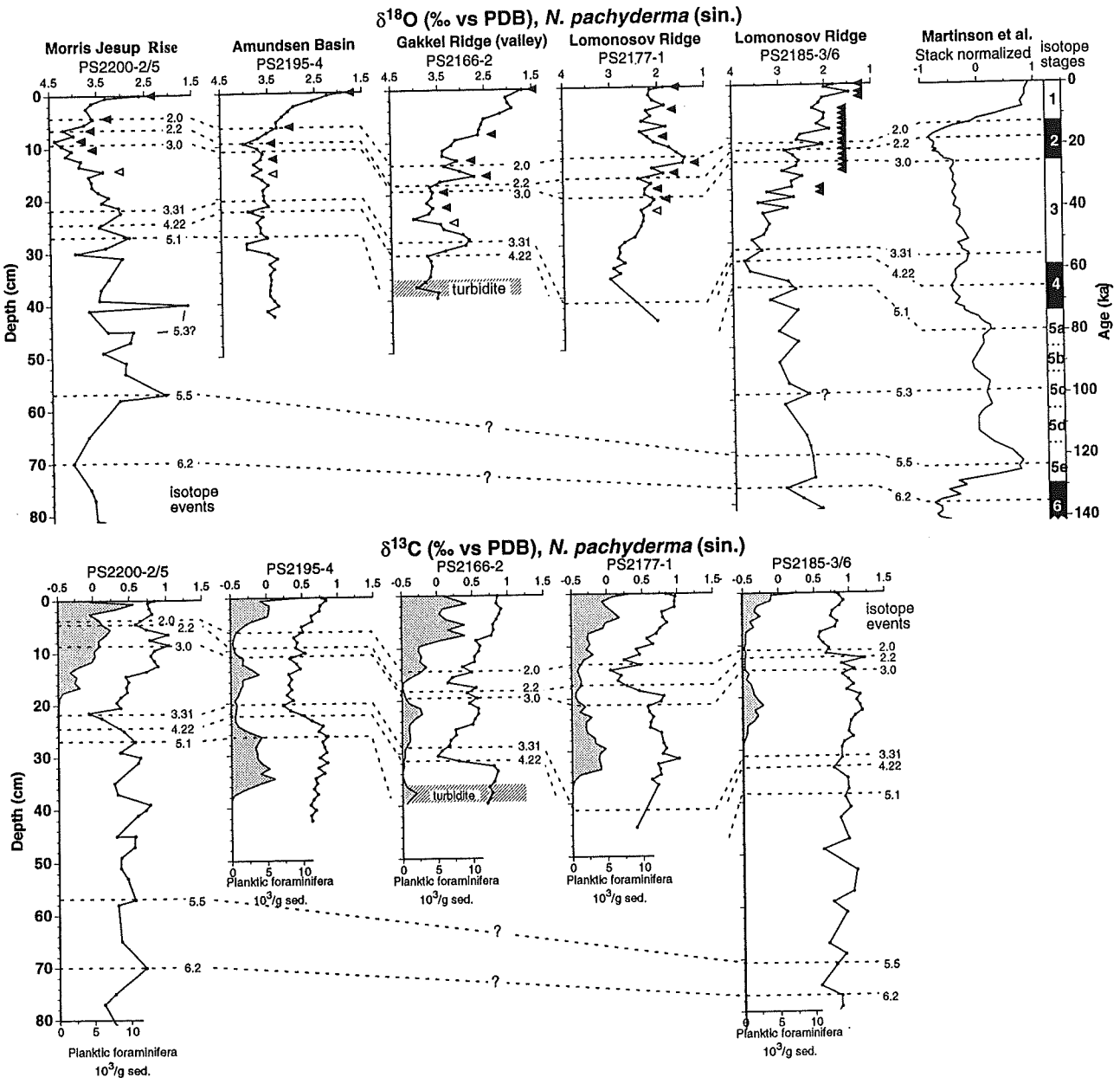

Fig. 19. Stable isotope records for five AMS-^{14}C dated cores. Radiocarbon datings are marked at the sample level concerned (black arrows) and listed in Table 3. White arrows denote infinite ^{14}C ages (>35-42 ka). Specific oxygen isotope events (sensu Pisias et al., 1984) are tentatively correlated to the normalized stack of Martinson et al. (1987). For cores PS2200-5/2 and PS2185-3/6 the combined records of box cores and long kastenlot cores (Spielhagen & Stein, unpubl. data) are shown. The abundances of planktic foraminifers are shown parallel to the δ^{13}C records.

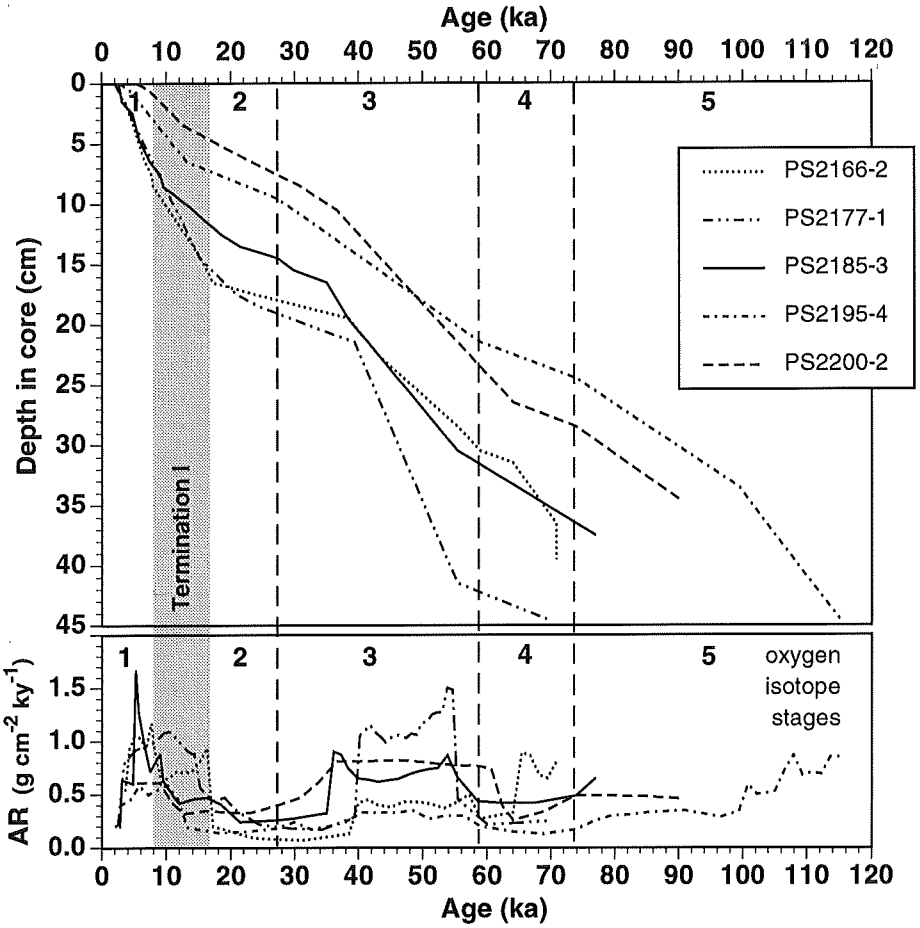

Fig. 20. Age-depth models for five selected key cores. The corresponding bulk accumulation rates (AR) versus age are shown below. Core PS2166-2 (Gakkel Ridge valley, 60°E), PS2195-4 (Amundsen Basin), PS2200-2 (Morris Jesup Rise), and PS2185-3 and PS2177-1 (Lomonosov Ridge crest).

a) Core PS2166-2 (Gakkel Ridge valley)

Cores PS2166-2 is suggested to include sediments from oxygen isotope stage 4 to 1 (Fig. 21a). The extent of Termination Ia and Ib can be determined by the characteristic course of the isotope record supported by AMS-^{14}C datings. The minor age reversal observed within Termination Ia (13.5 ^{14}C ka at 13.5 cm, and 12.3 ^{14}C ka at 15.5 cm) has been dealed with by asigning an average age of 12.9 ^{14}C ka to the level 14.5 cm. The ^{14}C age of 33.6 ka at 19.5 cm indicates that the stage 2 record is only about two cm thick. The planktic foraminifer maximum at 22.5 cm was dated to 38.4 ^{14}C ka and at 25.5 cm an infinite age (>42 ka) was reached.

The stage 4/3 boundary is suggested to be located in the lower part of core PS2166-2 at the very prominent $\delta^{13}C$ minimum (0‰) associated with decreasing $\delta^{18}O$ values. By comparison with high resolution records from the Fram Strait (e.g. Dokken, 1995) and the Norwegian-Greenland Sea (Duplessy et al., 1988; Vogelsang, 1990; Weinelt, 1993), the low-$\delta^{18}O$ spike immediately following is interpreted as isotopic event 3.31 (55.54 ka: Martinson et al., 1987). A sandy turbidite is found in the lowermost cm of the core. The high $\delta^{18}O$ values immediately above, associated with high $\delta^{13}C$ values, are suggested to represent early stage 4. Coccolith data of Gard (1993) support in general the above stratigraphy and calculated average sedimentation rates at site PS2166-2. In the long piston core and trigger weight core at site PS2166-3, Gard (1993) tentatively indicated the position of stage 5 at 50-60 cm and 29-41 cm respectively.

a) Core PS2195-4 (Amundsen Basin)

Core PS2195-4 from the Amundsen Basin-Gakkel Ridge transition about 200 km northeast of the Morris Jesup Rise is suggested to represent a section down to the lower to middle part of oxygen isotope stage 5 (?5c or 5d) (Fig. 21b).

Radiocarbon datings verify that the glacial stage 2 and Holocene record is quite condensed. A ^{14}C dating at 11.5 cm gave an age of 28.1 ka and ^{14}C datings of planktic foraminifer maxima at 15.5 cm and 26.5 cm gave infinite ages (>37 ka and >42 ka respectively). The two datings at 21.5 cm (29.8 ^{14}C ka) and 23.5 cm (40 ^{14}C ka) from a foraminifer minimum have been rejected and probably represent material bioturbated downwards from the foraminifer maximum above. The characteristic sharp bend of the $\delta^{13}C$ curve in the interval 24-21 cm, from high values (0.7-0.8‰) to low values (0.25‰), is suggested to represent glacial stage 4 in accordance with a similar shape of the $\delta^{13}C$ record in core PS1524 from the Gakkel Ridge (Köhler, 1992) and a large suite of well-dated cores from the Fram Strait and the Norwegian-Greenland Sea (Dokken, 1995; Duplessy et al., 1988; Vogelsang, 1990; Weinelt, 1993). The same phenomenon can be observed in the record of core PS2196-2 nearby and in cores PS2166-2 and PS2172-1 from the Gakkel Ridge-Amundsen Basin further eastward. Supporting evidence for the stage 5 designation to the interval 39 to 24 cm, characterised by high $\delta^{13}C$ values, comes from the work of Gard (1993, pers. comm. 1995). In the interval 30-25 cm a characteristic stage 5 (substage 5a?) coccolith assemblage dominated by *Gephyrocapsa* species was documented by Gard (1993). The identification of single stage 5 substages below is more uncertain because there is only limited variation in the stable isotopic values measured. It is suggested that the higher $\delta^{18}O$ values observed around 30 cm may represent substage 5b. Around 35 cm maximum abundances of planktic and benthic foraminifers may indicate substage 5c. The distinct peak of lithic sandy sediment in the interval 38-40 cm is suggested to mark substage 5d. As the sandy peak and the

lowermost part of the box core is almost barren of planktic foraminifers, the isotopic signals from the few *N. pachyderma* (sin.) present likely originate from younger specimens from above. In piston core PS2195-3 from the same site, a sandy and silty unit rich in mud clasts is found in the interval 90-45 cm (Fütterer, 1992). This fits into the general pattern of sandy stage 6 sediments with numerous mud clasts as observed in well-dated records from the Gakkel Ridge, the Yermak Plateau, and the Fram Strait (cf. Spielhagen & Thiede, 1994). A recent paleomagnetic study by Schneider et al. (1996) reveals positive inclination throughout the 9.5 m long PS2195-3, implying that the record does not extent beyond the Brunhes Chron (average sedimentation rates thereby >1.2 cm ky^{-1}). However, as the lower 3-4 m of the core contains many sandy turbidites (Fütterer, 1992), it is likely that average sedimentation rates for the more surface near sediment record (correlatable to box core PS2195-4) were considerably lower.

c) Core PS2200-2 (Morris Jesup Rise)

The box core PS2200-2 is suggested to cover the interval from late oxygen isotope stage 5 to the Holocene (Fig. 21c). Combining the record of kastenlot core PS2200-5 (Spielhagen & Stein, unpubl. data) with the box core record makes it possible to construct an age model for this site encompassing the last interglacial-glacial cycle.

The Holocene section on site PS2200 is only about 4 cm thick, relative coarse-grained, and shows a core top age of 5.2 ^{14}C ka. Winnoving supposedly has taken place. The glacial stage 2 is found at 9-4 cm as documented by the high oxygen isotope values and ^{14}C datings (6.5 cm: 20.1 ^{14}C ka; 8.5 cm: 27.0 ^{14}C ka) . At 10.5 cm 32 ^{14}C ka is measured and at 14.5 cm an infinite age >35 ka is reached. The interval 23-9 cm is interpreted to represent stage 3. At 21 cm the minimum $\delta^{13}C$ value (0‰) associated with a low $\delta^{18}O$ value may correspond to the deglacial event 3.31 (55.54 ka: Martinson et al., 1987) in accordance with similar patterns in cores nearby (e.g. PS2195-4, PS2196-2, PS1524 and PS2166). Stage 4 is designated to the interval 26-23 cm associated with high $\delta^{18}O$ values and the characteristic upward transition from high to low $\delta^{13}C$ values. In the combined box core and kastenlot record from site PS2200 (Fig. 19) the interval 58-26 cm is interpreted as isotope stage 5. The abrupt transition downcore to higher $\delta^{18}O$ values around 60 cm may likely correspond to the stage 6/5 transition.

d) Cores PS2177-1 and PS2185-3 (Lomonosov Ridge)

The stratigraphic record documented in the well-correlatable box cores from the top of the Lomonosov Ridge covers oxygen stages 4-1 and may, in core PS2185-3, extend into late oxygen isotope stage 5 (Fig. 21d). The more extended section documented in PS2177-1 allows a better time resolution of the stage 3-1 section (Fig. 21e).

AMS-^{14}C-datings and stable isotope records verify that the uppermost 10-15 cm of the Lomonosov Ridge sediment cover represents Termination I and the Holocene. In PS2177-1 the ^{14}C dating at 9.5 cm (6.6 ka) may be an artefact caused by bioturbation of a planktic foraminifer maximum above (4.5 cm dated to 5.6 ^{14}C ka). A similar rapid sedimentation rate interval, however, is recorded in PS2185-3 (Fig. 18d) and consequently it cannot be ruled out that the event reflects a period in the time span 7-5 ka with enhanced sedimentation rates. The peak accumulation rates calculated, however, may have been somewhat biased by bioturbation mixing increasing the apparent linear sedimentation rates. Oxygen isotope stage 2 is here as well as in the Makarov Basin cores PS2180-1 and PS2178-2 represented by a fine-grained interval only 3-5 cm thick. The pattern of finite and infinite ^{14}C datings performed on the foraminifer-rich interval 30-20 cm, suggests that this may represent the middle stage 3 period, 50-40 cal. ka, which also in cores from the Gakkel Ridge (e.g. PS2166-2, PS2195-4) and the Yermak Plateau (PS1533-3: Pagels, 1992) shows a similar planktic foraminifer maximum. The lowermost part of the box core sections from the Lomonosov Ridge shows characteristic peaks of lithic sandy material (30-35%) and is almost barren of planktic and benthic foraminifers. Continuous δ^{18}O and δ^{13}C records from site PS2185-3/6 (combined box core and kastenlot record) indicate that glacial stage 4 sediment may be represented by the δ^{18}O-maximum at 36-32 cm (Fig. 19) corresponding to a fine-grained interval immediately below a lithic sand peak. The sandy peak may accordingly represent the stage 4/3 transition and/or isotopic event 3.31. The latter interpretation is supported by the isotope record of PS2184-1 which at this level shows a low-δ^{18}O spike associated with a δ^{13}C minimum, quite similar to the pattern observed in cores PS2166-2 and PS2200-2. The oxygen isotope record in core PS2185-3/6 shows an abrupt transiton downward to considerably lower δ^{18}O values and moderate high δ^{13}C values suggested to represent stage 5 (Fig. 19).

Fig. 21. Key core records of stable isotopes, bulk accumulation rates, flux of planktic foraminifers, $CaCO_3$, IRD (500-1000μm) and/or lithic grains (125-500μm) plotted versus calendar age. Major deglacial 'meltwater events' 3.31 and Termination I are accentuated. a) PS2166-2, Gakkel Ridge; b) PS2195-4, Amundsen Basin; c) PS2200-2, Morris Jesup Rise; d) PS2185-3, Lomonosov Ridge; e) PS2177-1, Lomonosov Ridge.

21. a)

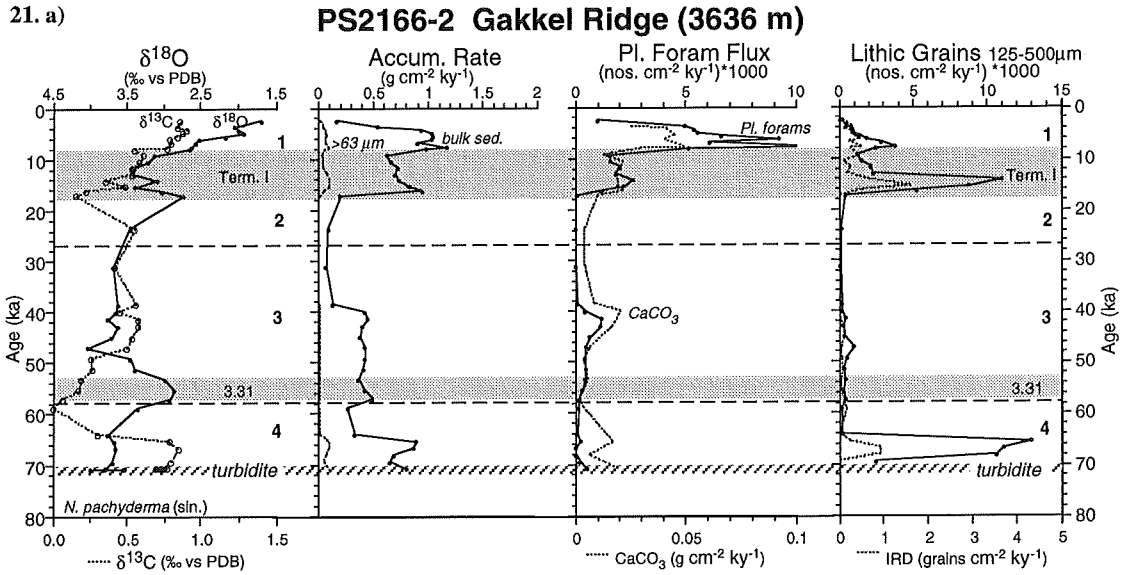
PS2166-2 Gakkel Ridge (3636 m)
δ18O (‰ vs PDB)
Accum. Rate (g cm-2 ky-1)
Pl. Foram Flux (nos. cm-2 ky-1)*1000
Lithic Grains 125-500µm (nos. cm-2 ky-1) *1000
δ13C
δ18O
>63 µm
bulk sed.
Pl. forams
CaCO3
Term. I
3.31
turbidite
N. pachyderma (sin.)
Age (ka)
δ13C (‰ vs PDB)
CaCO3 (g cm-2 ky-1)
IRD (grains cm-2 ky-1)

b)

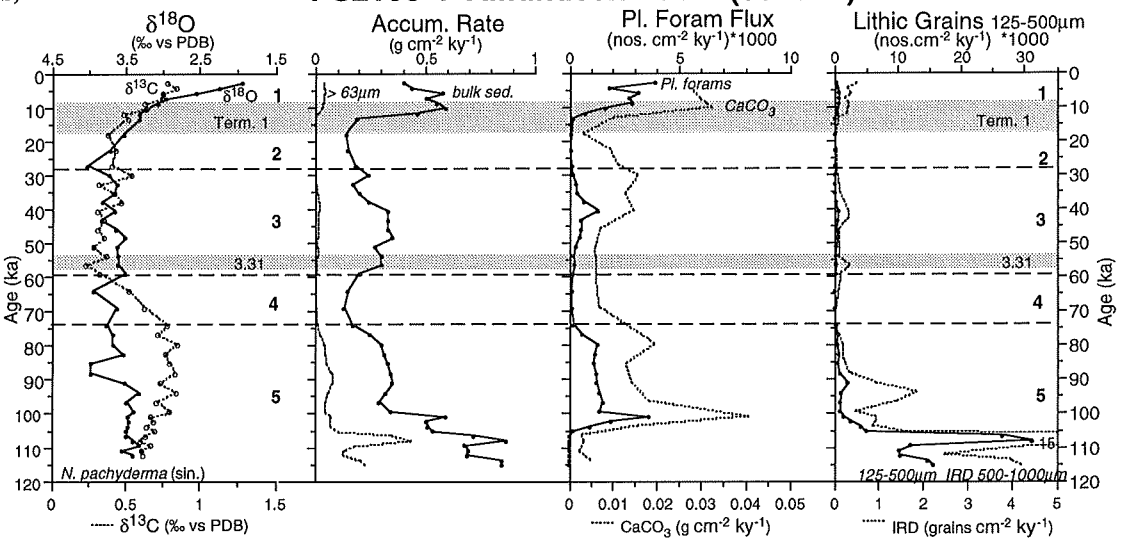
PS2195-4 Amundsen Basin (3873 m)
δ18O (‰ vs PDB)
Accum. Rate (g cm-2 ky-1)
Pl. Foram Flux (nos. cm-2 ky-1)*1000
Lithic Grains 125-500µm (nos.cm-2 ky-1) *1000
δ13C
δ18O
> 63µm
bulk sed.
Pl. forams
CaCO3
Term. 1
3.31
N. pachyderma (sin.)
125-500µm IRD 500-1000µm
Age (ka)
δ13C (‰ vs PDB)
CaCO3 (g cm-2 ky-1)
IRD (grains cm-2 ky-1)

c)

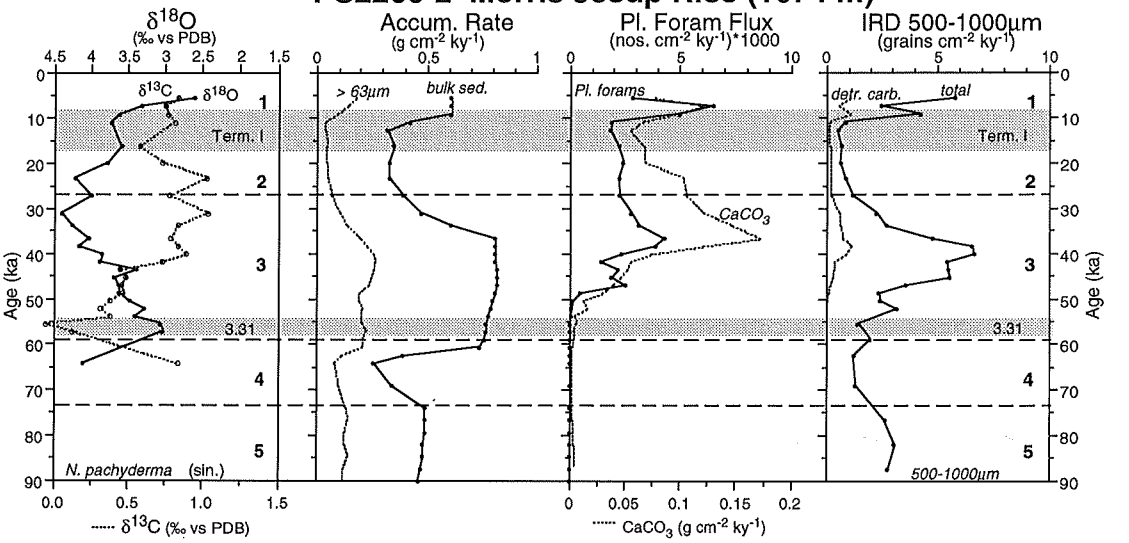
PS2200-2 Morris Jesup Rise (1074 m)
δ18O (‰ vs PDB)
Accum. Rate (g cm-2 ky-1)
Pl. Foram Flux (nos. cm-2 ky-1)*1000
IRD 500-1000µm (grains cm-2 ky-1)
δ13C
δ18O
> 63µm
bulk sed.
Pl. forams
CaCO3
detr. carb.
total
Term. I
3.31
N. pachyderma (sin.)
500-1000µm
Age (ka)
δ13C (‰ vs PDB)
CaCO3 (g cm-2 ky-1)

21. d)

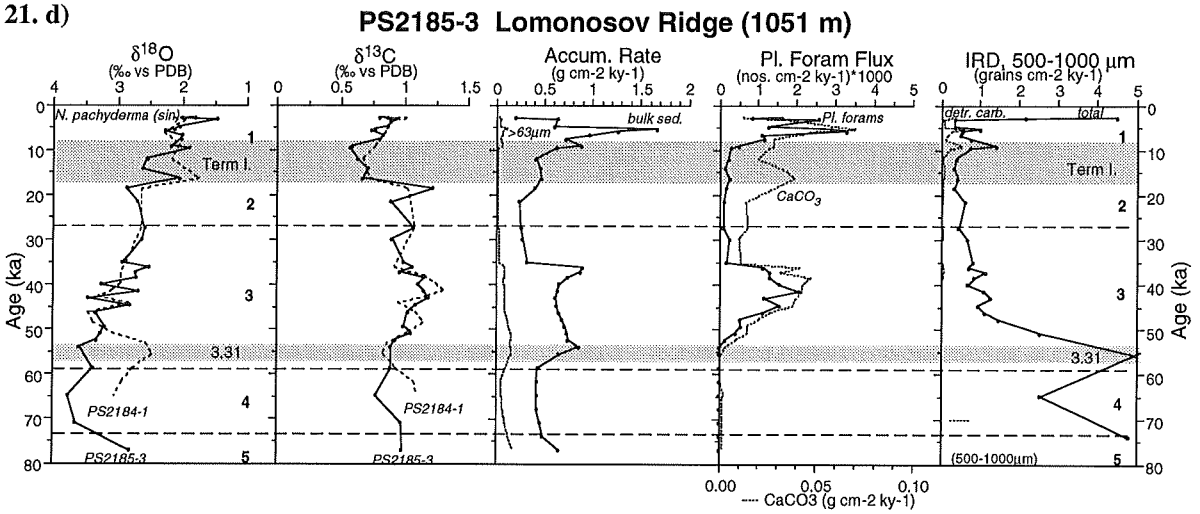
PS2185-3 Lomonosov Ridge (1051 m)
δ18O (‰ vs PDB)
δ13C (‰ vs PDB)
Accum. Rate (g cm-2 ky-1)
Pl. Foram Flux (nos. cm-2 ky-1)*1000
IRD, 500-1000 µm (grains cm-2 ky-1)
N. pachyderma (sin)
>63µm
bulk sed.
Pl. forams
CaCO3
detr. carb.
total
Term I.
3.31
PS2184-1
PS2185-3
(500-1000µm)
Age (ka)
CaCO3 (g cm-2 ky-1)

e)

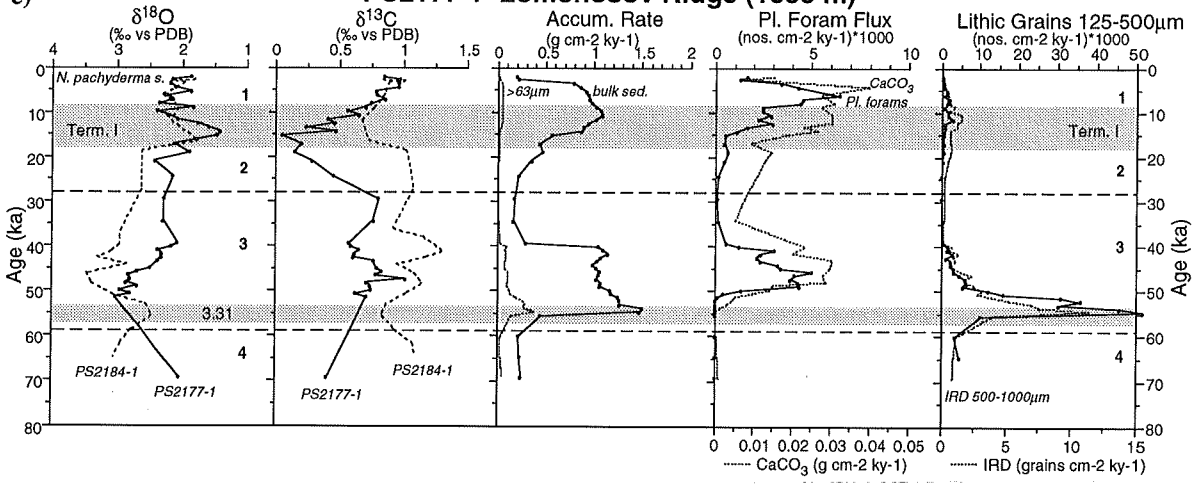
PS2177-1 Lomonosov Ridge (1388 m)
δ18O (‰ vs PDB)
δ13C (‰ vs PDB)
Accum. Rate (g cm-2 ky-1)
Pl. Foram Flux (nos. cm-2 ky-1)*1000
Lithic Grains 125-500µm (nos. cm-2 ky-1)*1000
N. pachyderma s.
>63µm
bulk sed.
CaCO3
Pl. forams
Term. I
3.31
PS2184-1
PS2177-1
IRD 500-1000µm
Age (ka)
CaCO3 (g cm-2 ky-1)
IRD (grains cm-2 ky-1)

5. TIME SLICE SALINITY RECONSTRUCTIONS

In this section it is attempted to reconstruct and map the distribution of surface water salinity in the eastern and central Arctic Ocean for selected time slices based on $\delta^{18}O$ values of planktic foraminifers *N. pachyderma* (sin.) in well-dated sediment cores. Comparable studies by e.g. Duplessy et al. (1991, 1992), Weinelt (1993), Schäfer-Neth (1994), Sarnthein et al. (1995), and Seidov et al. (1996) for the North Atlantic and the Norwegian-Greenland Sea, have focussed on reconstructing paleocirculation, density structure, melt water events, and deep water formation during the last glacial and deglacial period. In the Arctic Ocean, time slice salinity reconstructions have until now not been feasible due to the lack of widely distributed sediment cores and a poor stratigraphic framework.

The $\delta^{18}O$ ratios of calcite-shelled planktic foraminifers living in the upper water masses, can be used as a tracer of surface ocean temperature and salinity. Under the assumptions (1) that *N. pachyderma* (sin.) calcifies in equilibrium with the ambient water mass, and (2) that *N. pachyderma* (sin.) lives in the uppermost water column and thus reflects surface water conditions, the oxygen isotope ratio of the water ($\delta^{18}O_W$) can be calculated from the paleotemperature equation when the temperature T (°C) of the water mass is known (Epstein et al., 1953; Shackleton, 1974):

$$T = 16.9 - 4.38\,(\delta^{18}O_C - \delta^{18}O_W) + 0.10\,(\delta^{18}O_C - \delta^{18}O_W)^2 \qquad (5.1)$$

where
$\delta^{18}O_C$ *is the equilibrium calcite* $\delta^{18}O$ *ratio (in vs. PDB standard)*
$\delta^{18}O_W$ *is the* $\delta^{18}O$ *value of the ambient water mass (in vs. PDB standard)*

For this equation the oxygen isotope ratio of the water sample CO_2 is expressed relative to the CO_2 of the PDB standard. In order to use Standard Mean Ocean Water (SMOW) values (Craig, 1961) for the $\delta^{18}O_W$ term, it has to be corrected by a factor of about 0.22% (Erlenkeuser, pers. comm. 1995):

$$\delta^{18}O_W\,(SMOW) = 1.00022\,\delta^{18}O_W\,(PDB) + 0.22 \qquad (5.2)$$

Solving equation 5.1 with respect to $\delta^{18}O_W$ thus gives:

$$\delta^{18}O_W = -21.68 + \delta^{18}O_C + 5(12.4244 + 0.4\,T)^{1/2} \qquad (5.3)$$

with
$\delta^{18}O_C$ *expressed in vs. PDB*
$\delta^{18}O_W$ *expressed in vs. SMOW*

In lower latitude waters, surface water temperatures can be estimated from transfer functions based on microfaunal assemblages in well-dated sediment cores (e.g. Imbrie and Kipp, 1971; Molfino, 1992; Pflaumann et al., 1996). As a fairly good linear relationship exists between present day $\delta^{18}O_w$ and salinity (e.g. GEOSECS, 1987), paleosalinity can be calculated when corrections for the global ice volume effect on mean ocean $\delta^{18}O_w$ and salinity are done.

In the present 'interglacial' Arctic Ocean, surface water temperatures are close to the freezing point (-1.5 to -1.8°C), and ideally, when *N. pachyderma* (sin.) calcifies under constant temperature surface ocean conditions, changes in the $\delta^{18}O$ ratio of the carbonate shells should reflect changes in the $\delta^{18}O_w$ ratio of the surface water mass. During peak glacials, sea surface temperatures cannot have been much lower and unlikely were higher than today. Consequently, $\delta^{18}O$ values of planktic foraminifers mapped out for specific time slices may, beside the global ice volume effect, mainly record regional changes in surface water mass $\delta^{18}O_w$ distribution.

Salinity changes due to the formation and melting of sea ice remain to be a principal problem, as these processes show minor isotope fractionation only (Craig and Gordon, 1965; Jeffries et al., 1989; Melling & Moore, 1994) and cannot be quantified from planktic foraminifer isotope data. A detailed study of the present Arctic Ocean $\delta^{18}O_w$ and salinity values (Bauch, 1995) shows that sea ice formation and melting processes can displace the ideal linear relationship, by lowering or raising surface ocean salinity with up to 2‰, without a corresponding change in $\delta^{18}O_w$. The calculated paleosalinity values shall therefore be considered without this effect. Another factor, important for high latitude salinity reconstructions, is the observation that living *N. pachyderma* (sin.), at the cold end of the sea water temperature scale, apparently show a $\delta^{18}O$ offset (?vital effect) of about 1‰ compared to potential equilibrium $\delta^{18}O_c$ values calculated from the ambient water properties (Bauch et al., 1997).

Taken the above limitations and corrections into account, it is attempted to reconstruct the paleosalinity distribution for three time slices, the Last Glacial Maximum, the Termination Ia, and the modern (late Holocene), over a broad area from the Fram Strait to the central Arctic Ocean. Critical for these time slice reconstructions is that sufficient well-dated sediment cores with high enough sedimentation rates to limit severe effects of bioturbation mixing are available. The generally low sedimentation rates of Late Quaternary central Arctic Ocean sediments imply that the time slices defined comprise several thousand years. Rather than representing paleosynoptic conditions, the reconstructed salinity distributions represent average conditions for these time periods. Before going into details with the salinity

calculation method, some basic principles which can be learned from the comparison of modern Arctic Ocean properties (temperature, salinity, $\delta^{18}O_w$) with *N. pachyderma* (sin.) $\delta^{18}O$ values from core top samples and of living foraminifers from the water column shall be presented.

5.1 Habitat and calcification depth of *N. pachyderma* (sin.)

The depth habitat, faunal variation, and morphological changes of living *N. pachyderma* (sin.) and *G. quinqueloba* were documented for the upper 500 m water column in a transect from the Barents shelf northward up to the Gakkel Ridge at 86°N by Carstens & Wefer (1992). South of 83°N, the concentrations of planktic foraminifers are highest as well as the percentage of subpolar species and right-coiling individuals. Both species prefer the water below the pycnocline at about 100 m. North of 83°N, left-coiling *N. pachyderma* (sin.) totally dominates and displays maximum abundance in the upper 50-100 m, where the water is close to the freezing point and fresher than below the pycnocline. It is, however, important to note that the maximum rate of calcified individuals was observed to lie at least 100 m below the depth of maximum abundance. The stable isotopic signals preserved in planktic foraminifers sinking to the bottom, may thus be biased by halocline water properties, having a wide range of salinity and $\delta^{18}O_w$ values. During gametogenetic calcification (Hemleben et al., 1989; Bé, 1980) the wall of a foraminifer test is thickening and an additional amount of calcite is added. A weight increase of *N. pachyderma* (sin.) of about 3 to 4 times due to secondary calcification is suggested by Kohfeld et al. (1995) and Bauch et al. (1997).

5.2 $\delta^{18}O$-salinity relationship of Arctic Ocean surface water

$\delta^{18}O_w$ of the Arctic Ocean surface waters is mainly reflecting the mixing relationship of Atlantic Water ($\delta^{18}O_w$=0.3, salinity=34.9) and freshwater from river run-off and precipitation ($\delta^{18}O_w$=-21, salinity=0), cf. Bauch (1995). Pacific Water ($\delta^{18}O_w$=-1, salinity=33) is a subordinary component and as its composition lies close to the mixing line of Atlantic Water and river run-off, it can be neglected as regards the $\delta^{18}O_w$ - salinity mixing relationship. In Fig. 22 the $\delta^{18}O_w$ distribution of surface water samples from the eastern and central Arctic Ocean plotted versus salinity shows that the mixing relationship is far from the ideal linear state. This is due to sea ice formation and melting processes that influence surface water salinity without a corresponding change in oxygen isotope ratios of the ambient water mass. As the $\delta^{18}O_w$ of surface waters are reflecting the amount of fresh water (river run-off), and the fractionation due to sea ice formation is insignificant (fractionation factor = 1.0021: Melling & Moore, 1994), the respective deviation from the ideal mixing line can be taken as a measure for the positive or negative fraction of sea ice meltwater (c.f. Bauch, 1995). A "negative fraction of sea ice meltwater", obtained for the central Arctic

Ocean surface mixed layer from the mass balance study of Bauch (1995), means that sea ice formation has raised the net salinity of the ambient water mass (up to 2‰ higher salinity). In the southwestern part of the Nansen Basin sea ice melting is causing a relative lowering of salinity (Fig. 22). Neglection of the above considerations and placing a best fit line through the measure point cause an unrealistic low $\delta^{18}O_w$ value of the zero salinity fix point (-40 to -50‰) compared to average river run-off (-21‰) which is the main contributer of freshwater to the Arctic Ocean (Aagaard & Carmack, 1989).

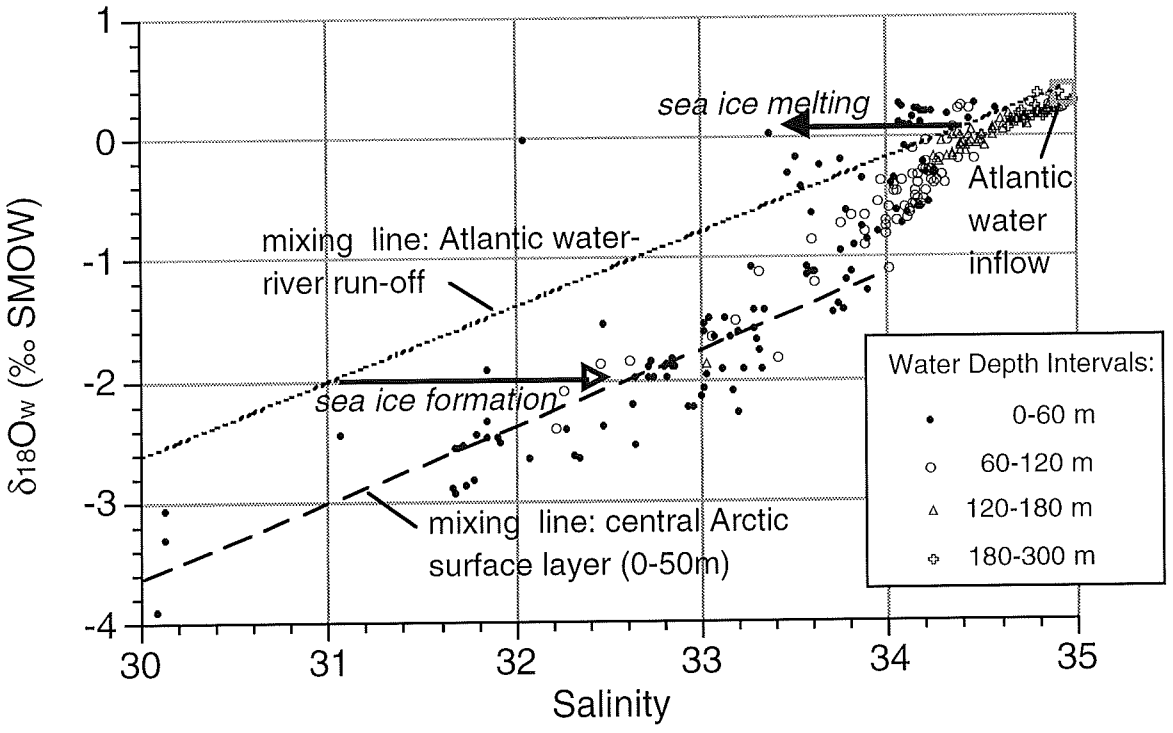

Fig. 22. Relationship between salinity and $\delta^{18}O_w$ in Arctic Ocean surface waters (0-300m). No ideal linear relationship can be expected because sea ice formation and melting influences salinity of the ambient water mass differently in different regions (Bauch, 1995). There seems to be a parallel offset between the 'ideal' mixing line of Atlantic Water - river run-off and the observed mixing line in the central Arctic Ocean (north of 83°N). Data from Bauch (1995), Östlund et al. (1987), and Donk & Mathieu (1969).

5.3 $\delta^{18}O$ of *N. pachyderma* (sin.) as a tracer of surface water mass properties

In Fig. 23 a comparison between potential equilibrium calcite $\delta^{18}O_c$ values calculated for the water column by insertion of $\delta^{18}O_w$ and temperature (from Bauch, 1995) in the paleotemperature equation and $\delta^{18}O$ values of *N. pachyderma* (sin.) in surface sediments (from Spielhagen & Erlenkeuser, 1994) is shown along two transects from the Yermak Plateau to the central Arctic Ocean. It is evident that marked horizontal gradients in potential

$\delta^{18}O_c$ (and salinity) as observed in the upper 100 m water column of the northern Nansen Basin-Gakkel Ridge area also are reflected in the corresponding core top *N. pachyderma* (sin.) values. This supports the hypothesis that the $\delta^{18}O$ signals preserved in

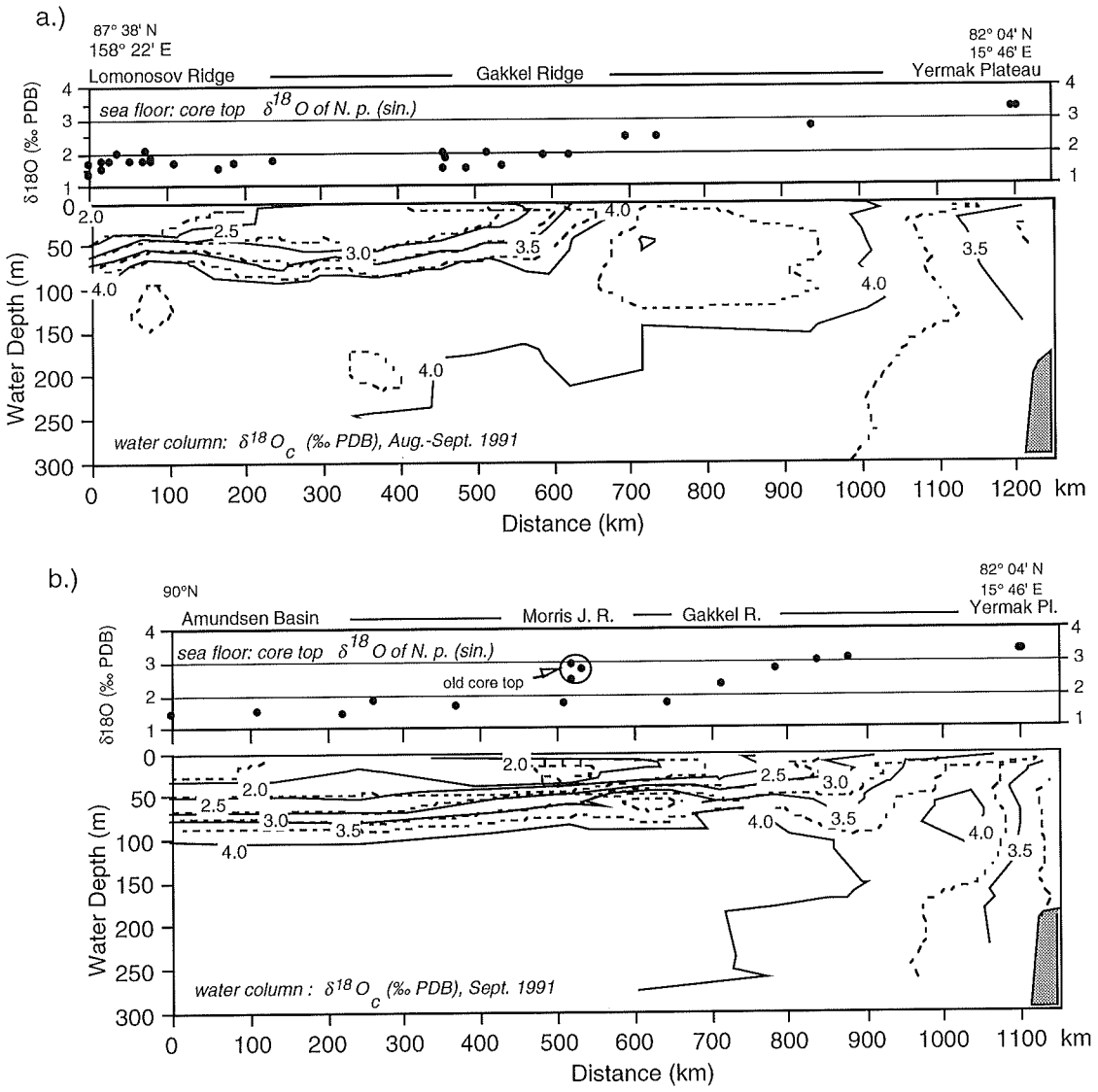

Fig. 23. Comparison between core top $\delta^{18}O$ values of *N. pachyderma* (sin.) (from Spielhagen & Erlenkeuser, 1994) and potential equlibrium calcite values ($\delta^{18}O_c$) calculated for the water column (0-300m) along two transects across the Eurasian Basin (ARCTIC '91). Temperature and $\delta^{18}O_w$ data used for the calculation of $\delta^{18}O_c$ are from Bauch (1995). Over the Gakkel Ridge a zone of marked change in $\delta^{18}O_c$ values for the upper 100 m clearly is paralleled by a corresponding change in the core top values. a) Transect from the Yermak Plateau across the Gakkel Ridge (60°E), and the Lomonosov Ridge (158°E), b) Transect from the Yermak Plateau across the Gakkel Ridge (0°E), the Morris Jesup Rise, and the Amundsen Basin.

N.pachyderma (sin.) mainly reflect conditions in the uppermost 50-100 m of the water column. If the planktic foraminifers calcified mainly below the halocline (>100 m), they should have recorded rather constant high values. In the southern Nansen Basin and the

Yermak Plateau region characterised by the core of inflowing Atlantic Water (1-4°C), the depth gradient of potential $\delta^{18}O_c$ values is almost absent due to less riverine freshwater in the surface water and a higher subsurface water temperature (Fig. 23). Predictions of habitat depth in the southern region based on comparative water column-core top studies can therefore not be recommended. Fig. 23 also reveals that most core top $\delta^{18}O$ values are about 0.5-1.0‰ too low compared to the potential $\delta^{18}O_c$ values calculated from the paleotemperature equation. An explanation could be that the water column profiles are not representative for average late Holocene conditions as recorded in core top sediments. This interpretation, however, can be rejected by a recent study in Arctic surface waters where a similar offset of about 1‰ has been found between *N. pachyderma* (sin.) in plankton tows and potential $\delta^{18}O_c$ values calculated from the ambient water column properties (Bauch et al., 1997). In Fig. 24 the isotopic differences between potential $\delta^{18}O_c$ values and $\delta^{18}O$ values of living *N. pachyderma* (sin.) from Bauch et al. (subm.) have been plotted versus temperature. The largest differences ($\delta^{18}O_c$-$\delta^{18}O_{Nps}$) are seen in the coldest temperature area (Fig. 24). In order to compensate for the apparent temperature dependant offset (vital effect?), the regression line equation derived from Fig. 24 has been used to correct *N. pachyderma* (sin.) $\delta^{18}O$ values ($\delta^{18}O_{Nps}$) used in the paleotemperature equation for the calculation of $\delta^{18}O_w$ and paleosalinity:

$$\delta^{18}O_C = \delta^{18}O_{Nps} - 0.167\,T + 0.902 \qquad (5.4)$$

substitution of $\delta^{18}O_c$ in equation 5.3 thus gives:

$$\delta^{18}O_W = -21.68 + (\delta^{18}O_{Nps} - 0.167\,T + 0.902) + 5(12.4244 + 0.4\,T)^{1/2} \qquad (5.5)$$

The temperature-dependant correction factor (-0.167 T + 0.902) is based on data from the temperature range -1.7° - +2°C (Fig. 24) and used only in that range for the time slice salinity reconstructions. Fig. 25. displays the different character of three typical hydrographic stations (0-300 m water column) from the Lomonosov Ridge, the Nansen Basin at about 83°N, and the northern Barents Sea slope. Based on $\delta^{18}O_w$ and temperature data from Bauch (1995), profiles of potential $\delta^{18}O_c$ values (calculated from equation 5.3) and potential $\delta^{18}O_{Nps}$ values (calculated from equation 5.5) have been constructed and compared to core top $\delta^{18}O$ values of *N. pachyderma* (sin.) (Fig. 25). From this it can be seen that at the Nansen Basin station the potential $\delta^{18}O_{Nps}$ values lie within the range of the core top values. At the Lomonosov Ridge station, core top values lie close to the potential $\delta^{18}O_c$ values of the surface mixed layer. Supposing that the potential $\delta^{18}O_{Nps}$ values better represent the true conditions, an apparent habitat in the upper halocline waters about 50 m is indicated.

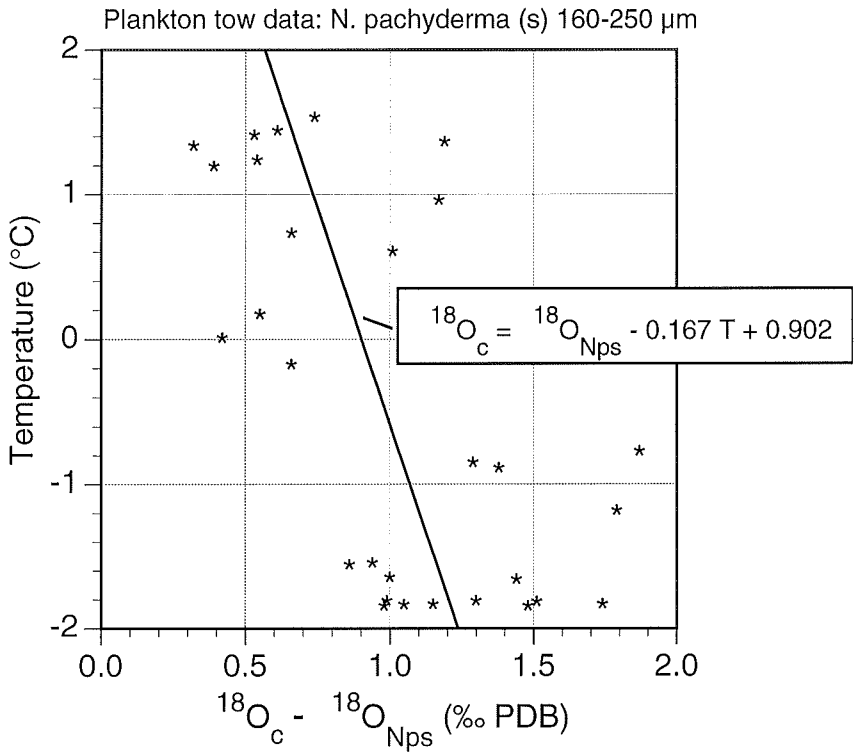

Fig. 24. Isotopic difference of equilibrium calcite $\delta^{18}O_c$ values and of $\delta^{18}O$ values of net sampled *N. pachyderma* (sin.) versus temperature in the Eurasian Basin (data from Bauch et al., 1997). The largest isotopic difference is seen below 0°C representing conditions in the central Arctic Ocean surface waters. The regression line equation has been used to correct foraminifer $\delta^{18}O$ data used in the paleotemperature equation.

It is likely that the main *N. pachyderma (sin.)* habitat in the central Arctic Ocean is in the low salinity surface mixed layer (cf. Carstens and Wefer, 1992) and that secondary gametogenetic calcification in deeper waters has modified the $\delta^{18}O$ signals preserved in the planktic foraminifers (cf. Kohfeld et al., 1995; Bauch et al., 1997). The result, an integrated $\delta^{18}O$ signal of the upper water column, limits the degree of accuracy to which surface water salinity can be reconstructed in strongly stratified waters as the Arctic Ocean. At the northern Barents Sea slope hydrographic conditions are characterised by the core of Atlantic Water inflow. Sediment surface $\delta^{18}O$ values of *N. pachyderma (sin.)* (3.4-3.8‰) are here scattered between the potential $\delta^{18}O_{Nps}$ values and the $\delta^{18}O_c$ values for a habitat depth of about 100-200 m (cf. Carstens & Wefer, 1992).

The Fram Strait and the southern Nansen basin region may, not only during the Holocene, but possibly also during parts of the Last Glacial Maximum (LGM) and the deglacial period, have been characterised by the advection of warmer Atlantic Water and seasonally open water conditions (cf. Veum et al., 1992; Hebbeln et al., 1994; Dokken, 1995). As a result of

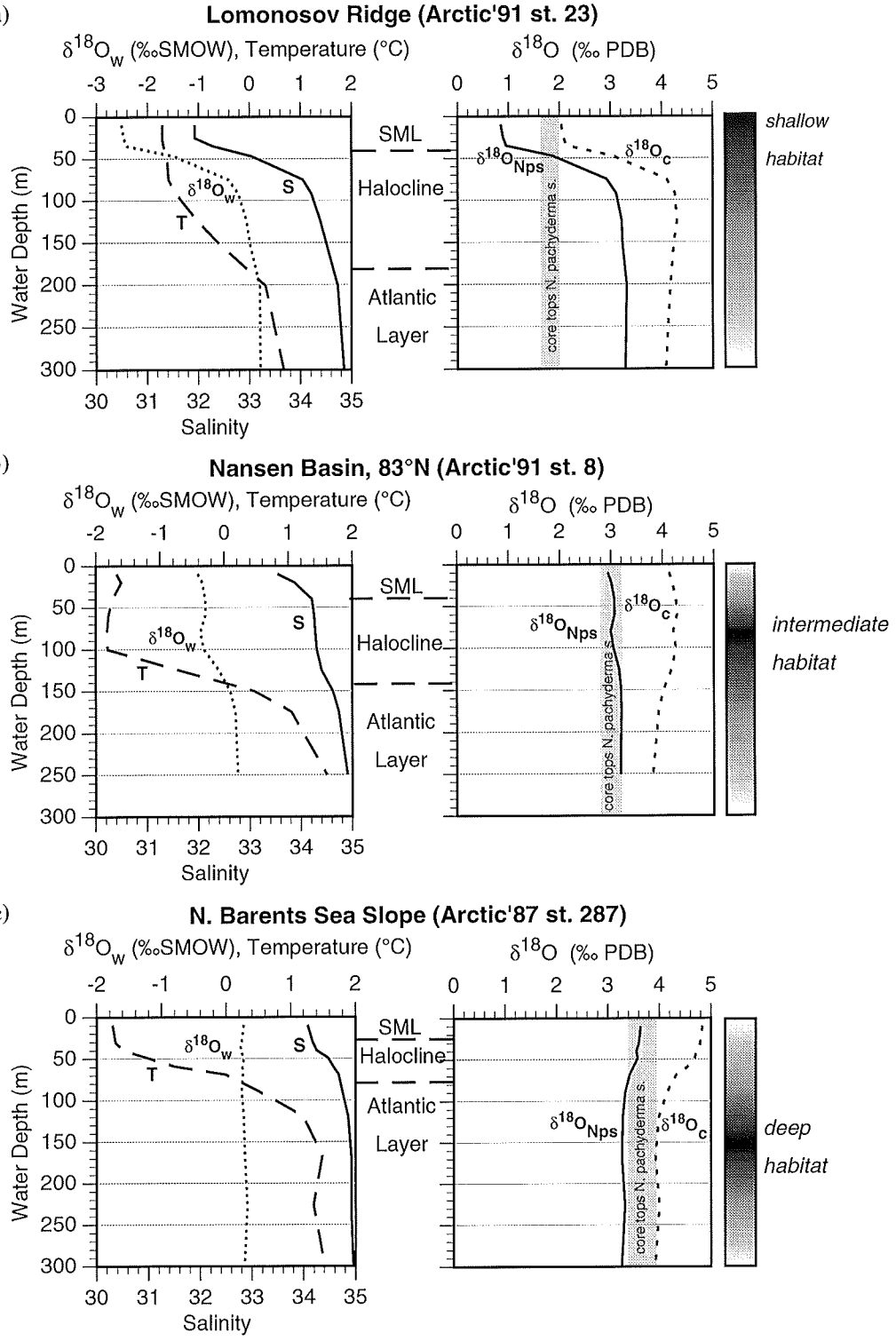

Fig. 25. Examples of surface ocean hydrographic conditions (temperature, salinity, $\delta^{18}O_w$), potential $\delta^{18}O_c$ values and core top $\delta^{18}O$ values (N. pachyderma s.) for stations typical for (a) the central Arctic (Lomonosov Ridge), (b) the central Nansen Basin region, and (c) the northern Barents Sea Slope region. Temperature, Salinity and $\delta^{18}O_w$ data are from Bauch (1995). The core top value intervals given (shaded bar) are based on data from Spielhagen & Erlenkeuser (1994). $\delta^{18}O_{Nps}$ values shown represent $\delta^{18}O_c$ values corrected for a possible low-temperature dependant vital effect observed in living N. pachyderma (sin.); cf. Fig. 24.

that, the $\delta^{18}O$ records from this region, where *N. pachyderma* (sin.) prefers a habitat of about 100-200 m (Carstens & Wefer, 1992), may not reflect surface water conditions very well. As the paleotemperature distribution is not known from this region, simplified temperature estimates have to be used for the determination of potential salinity distribution.

5.4 Salinity reconstruction method

Taken the above conditions into account, paleosalinities have been reconstructed according to the method of Schäfer-Neth (1994). In contrary to Duplessy et al. (1991, 1992) that uses modern salinity as a reference for calculation of paleosalinity anomalies, the method of Schäfer-Neth (1994) is considered to be better suited for Arctic Ocean conditions, where sea ice formation and melting bias the modern salinity distribution. Independent of the method used, this salinity modification cannot be traced by planktic foraminifers, and consequently the reconstructed salinity distribution shall be considered without this superimposed modification.

Basis for the salinity calculation are *N. pachyderma* (sin.) $\delta^{18}O$ values mapped out for specific time slices. These data are partly based on $\delta^{18}O$ records from the present study and partly on other published ^{14}C dated $\delta^{18}O$ records from the Eurasian Basin and the Fram Strait region. Core numbers and data used for the salinity calculation are listed in Appendix J and the position of cores and sediment surface samples is shown in Fig. 26.

Using the paleotemperature equation of Epstein et al. (1953) and Shackleton (1974) and incorporating the correction factor for the expected vital effect (equation 5.4) the potential surface ocean $\delta^{18}O_w$ values have been calculated (cf. equation 5.5):

$$\delta^{18}O_W = -21.68 + (\delta^{18}O_{Nps} - 0.167\,T + 0.902) + 5(12.4244 + 0.4\,T)^{1/2} \qquad (5.6)$$

For the LGM and Termination Ia time slice, a uniform temperature (T) of -1.5°C has been used in the equation. For the modern (late Holocene) time slice the temperature distribution at 100 m water depth (Gorshkov, 1983) has been used (cf. Spielhagen & Erlenkeuser, 1994) in order to comply with the deeper water (higher temperature) habitat of *N. pachyderma* (sin.) in the region south of 83°N characterised by the core of Atlantic Water. North of 83°N the temperature at the 100 m level is close to -1.5°C and surface ocean temperatures.

It is assumed that a linear mixing relationship between $\delta^{18}O_w$ and salinity exists with Atlantic Water and freshwater as end-member fix points. Apart from the effect of changes in global ice volume and sea level, the Atlantic Water $\delta^{18}O_w$ and salinity composition cannot

have varied much and are set to the modern values (cf. Schäfer-Neth, 1994). The equation for the line between the two fix points accordingly is:

$$S = S_{aw} + (S_{aw}/(\delta^{18}O_{aw} - \delta^{18}O_{fw}))(\delta^{18}O_{w} - \Delta\delta^{18}O_{ice\ vol.}) + \Delta S_{ice\ vol.} \qquad (5.7)$$

where
S_{aw} (= 34.92) is the modern salinity of least modified Atlantic Water in the Arctic Ocean,
$\delta^{18}O_{aw}$ (= 0.3) is the modern $\delta^{18}O$ value of least modified Atlantic Water,
$\delta^{18}O_{fw}$ is the estimated $\delta^{18}O$ value of fresh water (river run-off, precipitation, melt water),
$\delta^{18}O_{w}$ is the local surface ocean water $\delta^{18}O$ value determined by equation 5.5,
$\Delta\delta^{18}O_{ice\ vol.}$ is the difference in average ocean $\delta^{18}O$ compared to the Holocene level (Fairbanks, 1989),
$\Delta S_{ice\ vol.}$ is the difference in average ocean salinity compared to the Holocene level (Duplessy et al., 1991)

Unlike the Atlantic Water fix point, the freshwater $\delta^{18}O_{fw}$ value can be expected to vary considerably through time following atmospheric temperature variations and changes in distance of moisture sources for the precipitation (Dansgaard et al., 1973; Charles et al., 1994). Estimates for $\delta^{18}O_{fw}$ used in this study are based on ice core oxygen isotope records. The mean modern $\delta^{18}O_{fw}$ value of circum-Arctic river run-off is about -21‰ (Bauch, 1995). This value has been used for the modern (late Holocene) salinity reconstruction. For the Last Glacial Maximum a value of -30‰ has been used, as ice core records from Greenland and North Canada show Last Glacial Maximum values 7-13‰ lower than the Holocene level (cf. Paterson & Hammer, 1987 (table 2); Johnsen et al., 1992). For the Termination Ia, a freshwater component of -27‰ has been used as the above ice core records show values intermediate between last glacial and Holocene levels, and it can be expected that discharge of large amount of glacial meltwater (low $\delta^{18}O$ ratio) periodically caused that the average freshwater fix point was lying close to the glacial value. Using a value of e.g. -25‰ instead of -27‰ as freshwater end member, causes the salinity calculated to be maximally 0.3‰ lower.

The quantification of the global ice volume effect on mean ocean $\delta^{18}O_{w}$ and salinity is based on the $\delta^{18}O$-sea level curve for the last 18 ^{14}C ky of Fairbanks (1989). $\Delta\delta^{18}O_{ice\ vol.}$ for the LGM is set to 1.2‰ and for the Termination Ia to 1.0‰. The corresponding salinity change ($\Delta S_{ice\ vol.}$) is calculated according to Duplessy et al. (1991):

$\Delta S_{ice\ vol.}$ = mean modern salinity x Δsea level / (present m. ocean water depth - Δsea level)

consequently
$\Delta S_{ice\ vol.}$ (LGM) = 34.7 x 120 / (3900 - 120) = 1.04
$\Delta S_{ice\ vol.}$ (Termination Ia) = 34.7 x 100 / (3900 - 100) = 0.91

Table. 3. Variables used for the calculation of paleosalinity for the three time slices. [1]For the modern (Late Holocene) time slice the 100 m temperature distribution of Gorshkov (1983) was used.

	LGM	Termination Ia	Modern (L. Holocene)
Temperature (°C)	-1.5	-1.5	100m data set[1]
$\delta^{18}O_{fw}$ (‰ SMOW)	-30	-27	-21
$\Delta\delta^{18}O_{ice\ vol.}$	1.2	1.0	0
$\Delta S_{ice\ vol.}$ (sea level)	1.04 (-120m)	0.91 (-100m)	0 (0m)

Using these parametres, a calculation of salinity at selected core sites (Fig. 26) for the three time slices is possible. The results and basic parametres used are listed in Appendix J and the areal distribution of $\delta^{18}O$ and salinity is shown for separate time slices in Figs. 27-29.

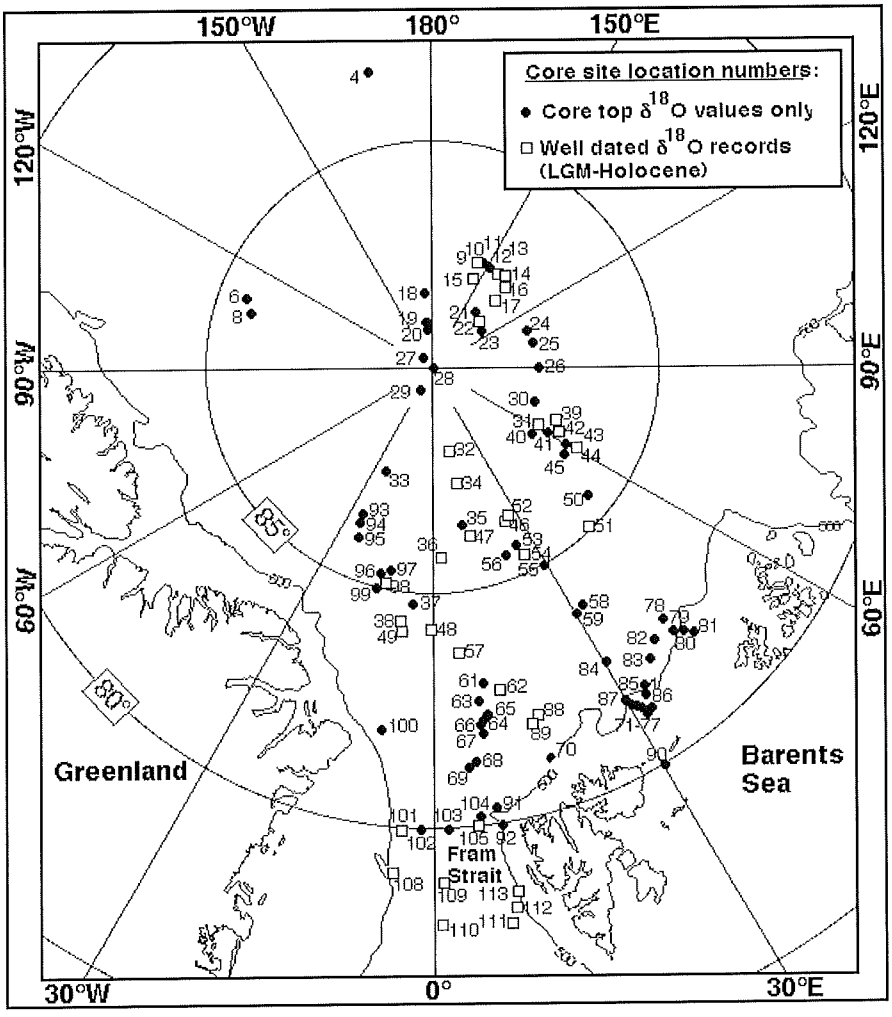

Fig. 26. Location of surface sediment samples and sediment cores used for the salinity reconstructions. $\delta^{18}O$ values of core tops were taken from Spielhagen and Erlenkeuser (1994). Selected $\delta^{18}O$ records from the present study and ^{14}C dated records from other studies are basis for the LGM and Termination Ia time-slice reconstructions. Core numbers, $\delta^{18}O$ values and references are listed in Appendix J.

5.5 Time slice reconstructions

In the following the distribution of *N. pachyderma* (sin.) $\delta^{18}O$ values and reconstructed surface ocean paleosalinity distribution for the Last Glacial maximum, the Termination Ia, and the modern late Holocene time slices will be discussed.

a) Last Glacial Maximum (LGM: 18-15 ^{14}C ka)

The *N. pachyderma* (sin.) $\delta^{18}O$ distribution for the LGM time slice shows a marked gradient from values of about 4.5‰-4.7‰ in the southwestern Nansen Basin and the Fram Strait to values between 2‰ and 3‰ on the Lomonosov Ridge and the Makarov Basin (Fig. 27). The relatively high local variability seen in the central Arctic probably reflects the influence of bioturbation on LGM sediments in combination with very low sedimentation rates. The strong gradient $\delta^{18}O$ distribution is in sharp contrast to the homogeneous Norwegian-Greenland Sea data set for the LGM, which show $\delta^{18}O$ values between 4.5‰ and 4.8‰ (e.g Vogelsang, 1990; Weinelt, 1993; Sarnthein et al., 1992, 1995).

The reconstructed salinity distribution for the LGM time slice shows values of about 36‰ in the southwestern Nansen Basin and in the Fram Strait (Fig. 27). Taken into account that the mean ocean salinity for the LGM was raised about 1‰ due to storage of freshwater in the ice sheets (cf. section 5.4), the salinity calculated for the southern region is close to the 'normal' Atlantic Water salinity which should be expected for the LGM. The LGM surface salinity reconstruction for the Norwegian-Greenland Sea by Schäfer-Neth (1994) thus infers salinities of about 35.2-35.6‰ for the 75 m water depth level. With reference to the modern situation, it is likely that planktic foraminifers in the southern Eurasian Basin region to a large extent have recorded warmer subsurface conditions rather than conditions of the surface layer. As a uniform temperature of -1.5°C has been used for the salinity calculation it cannot be ruled out that the salinity estimates for the southern Eurasian Basin region are not right. Intrusions of warm Atlantic Water up to Svalbard during the LGM has been documented by Veum et al. (1992) and Hebbeln et al. (1994). Subsurface Atlantic Water advection into the Arctic Ocean accordingly should have influenced the temperature regime under which *N. pachyderma* (sin.) calcified in the southern part of the Eurasian Basin. A salinity reconstruction for the LGM using a calcification temperature of +2°C instead of -1.5°C would lead to estimates for salinities about 0.5‰ higher.

Toward the central Arctic Ocean a marked decrease in salinity reconstructed can be observed. The salinities calculated for the central Arctic are in the range of 33-34‰ and thereby only slightly more saline than the modern 50 m salinity estimate (about 33‰) for the central Arctic (Anderson et al., 1994). The salinity gradient of about 3‰ from the Fram Strait to the Lomonosov Ridge obtained for the LGM time slice is of the same order as the modern

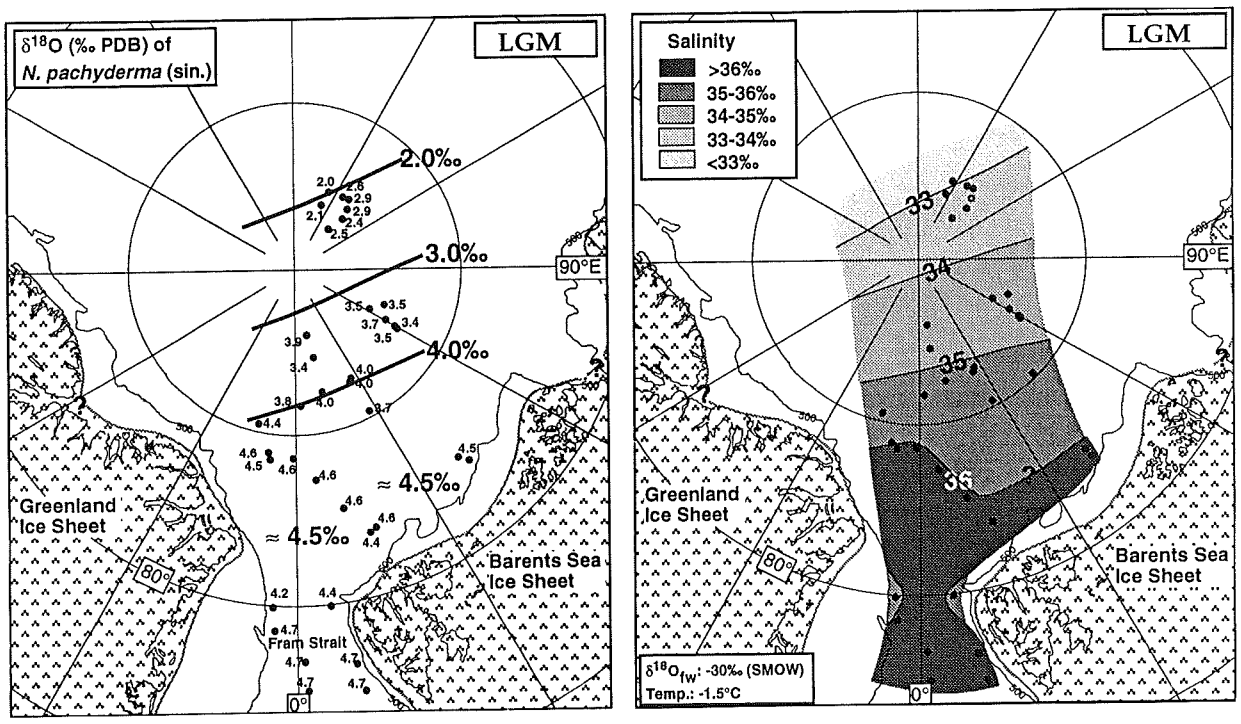

Fig. 27. $\delta^{18}O$ (*N. pachyderma* sin.) distribution and corresponding reconstructed salinity for The Last Glacial Maximum (LGM: 18-15 ^{14}C ka).

salinity gradient observed (Fig. 5). The result may either indicate a considerable freshwater influx to the Arctic Ocean during the LGM or an extended residence time of the low salinity surface mixed layer. A more isolated Arctic Ocean surface water mass is envisaged with a diminished export rate through the Fram Strait and the Canadian Archipelago and a shut-off import of Pacific Water due to a subaerially exposed Bering Strait. Evidence from ice cores indicates that high latitude precipitation was significantly reduced during the Last Glacial Maximum (Reeh, 1990; Alley et al., 1993) and the cold temperature regime may effectively have reduced melting of continental ice sheets which showed a maximal extension during that time. It is likely, that the total freshwater supply to the Arctic Ocean, through rivers and melting of glacier ice, also was significantly reduced. The main factor proposed for explaining the LGM salinity gradient is thus a longer residence time of fresh water in a stable surface water layer.

b) Termination Ia (14.5-13 ^{14}C ka)

The distribution of N. pachyderma (sin.) $\delta^{18}O$ mapped out for the early part of the last deglaciation (Termination Ia) shows values lowered by 0.5 to 1.3‰ compared to the LGM

time slice (Fig. 28). The LGM-Termination Ia difference in global ice volume effect amounts to about 0.2‰ (Fairbanks, 1989). Assuming that there had been no pronounced increase in surface water temperatures (analogous to modern conditions), the remaining part of the amplitude (0.3 to 1.1‰) should reflect a dramatic increase of low-$\delta^{18}O$ freshwater influx to the Arctic Ocean, related to the initial deglaciation of the circum-Arctic ice sheets (cf. Jones & Keigwin, 1988; Weinelt, 1993; Koc & Jansen, 1994; Stein et al, 1994b; Elverhøi et al., 1995; Dokken, 1995). In the southern part of the Eurasian Basin, including the 0-30°E Gakkel Ridge sector, and in the central Fram Strait, maximal $\delta^{18}O$ values of about 3.0-3.6‰ are recorded. The associated salinity values calculated for that region lie in the range of 34.3-34.9‰ (Fig. 28). Toward the Lomonosov Ridge and the Makarov Basin sites in the central Arctic, the $\delta^{18}O$ values decrease to 1.5 -2.0‰ corresponding to a salinity of about 32.8-32.1‰. This is slightly below the modern central Arctic 50 m salinity estimate of about 33‰ (Fig. 5).

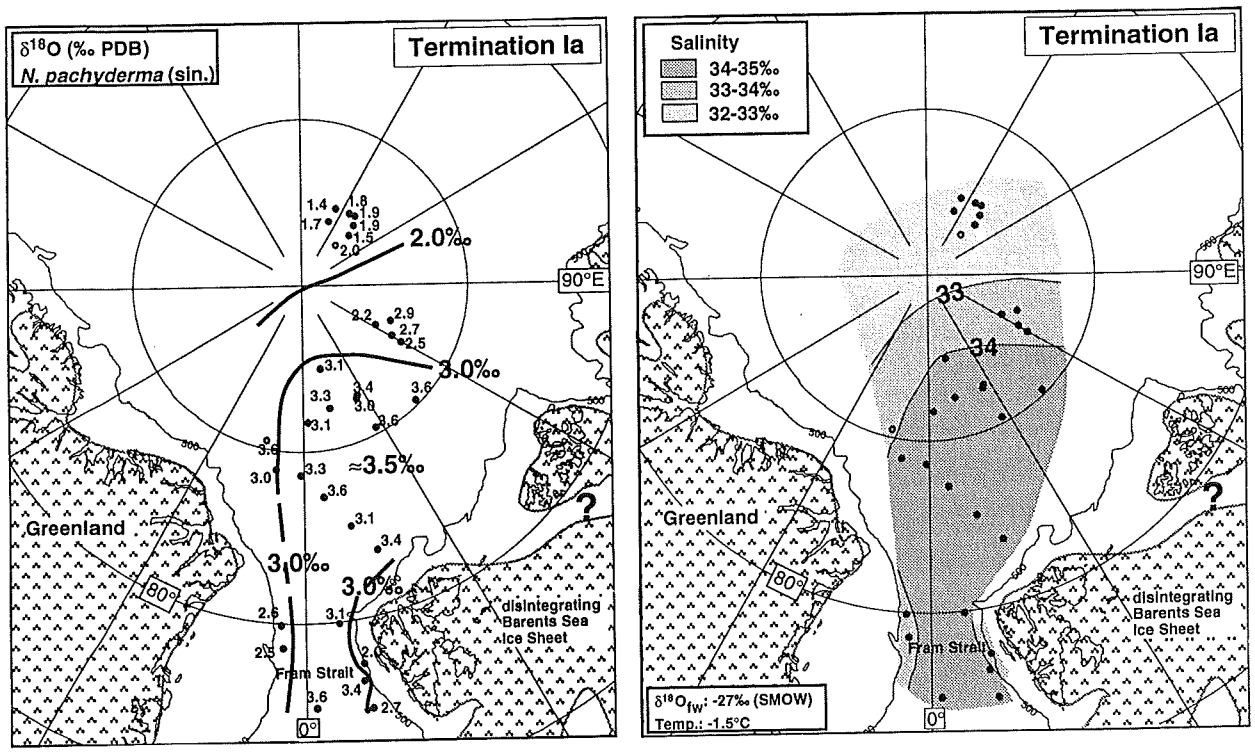

Fig. 28. $\delta^{18}O$ (*N. pachyderma* sin.) distribution and corresponding reconstructed salinity for the Termination Ia (14.5-13 ^{14}C ka).

In general the salinity distribution reconstructed for the Termination Ia time slice is not very different from the modern conditions. Due to the limited time resolution and the effect of bioturbation mixing, however, signals of peak deglacial, low-salinity excursions likely have

been reduced. Evidence of lowered salinities toward the continental margins is poor due to sparse well-dated $\delta^{18}O$ records from these regions. Lowered $\delta^{18}O$ values and derived salinities are inferred for the continental margins adjacent to the Fram Strait. According to Sarnthein et al. (1995) and Seidov et al. (1996) a Termination Ia Meltwater episode (14.2-13.2 ^{14}C ka BP) was characterised by a stop in deep water convection and advection of Atlantic water to the Greenland-Norwegian Sea. The southern Eurasian Basin stable isotope records and paleosalinity distribution may thus, during the early deglaciation, have been less influenced by Atlantic Waters than inferred for the LGM and the Holocene.

c) Modern (late Holocene: 3-0 ^{14}C ka)

The much larger data set of *N. pachyderma* (sin.) $\delta^{18}O$ values from high quality sediment surface samples (Spielhagen & Erlenkeuser, 1994) gave the possibility to compare and calibrate these proxy data directly to modern Arctic Ocean surface water properties (cf. section 5.3). The lateral distribution of $\delta^{18}O$ values (Fig. 29) shows a marked decrease from the southern part of the Nansen Basin (3.4.-3.9‰) toward the central Arctic Lomonosov Ridge and Makarov Basin sites (1.5-1.9‰). The $\delta^{18}O$ values also decrease toward the Svalbard and Barents Sea continental margin and toward the western part of the Fram Strait. The observed $\delta^{18}O$ distribution pattern is in general in accordance with gradients in the modern surface water distribution of $\delta^{18}O_w$ (Bauch, 1995) and salinity (Gorshkov, 1983; Anderson et al., 1994). It shall be emphasized, however, that sea ice formation and melting processes influence the modern salinity distribution (Fig. 22). The reconstructed salinity values shall at first be considered without this effect (see also section 5.2).

The reconstructed modern (late Holocene) salinity distribution shows values varying from about 32‰ in the central Arctic Ocean to about 36‰ in the southern Nansen Basin region characterised by the core of surface-near Atlantic Water advection. As the modern salinity reconstruction is based on the temperature distribution at 100 m (Gorskov, 1983), it should compensate for the expected higher calcification temperature in the southern Nansen Basin, where a deeper habitat (100-200 m) of *N. pachyderma* (sin.) has been documented by Carstens & Wefer (1992). Although a more shallow habitat (0-100 m) can be expected in the central Arctic ocean environment (Carstens & Wefer, 1992), the 100 m temperature data (about -1.5°C) in this area are close to the surface water temperature of about -1.7°C. The calculated salinity values from the central Arctic Ocean and the Eurasian Basin north of 83°N (Fig. 29) reveal reconstructed values about 1‰ lower than the observed values for the 50 m level (Fig. 5), representing the expected calcification depth. This discrepancy can be explained by the effect of sea ice formation, which tends to raise the surface water salinity observed in the central Arctic by at least 1‰ (Fig. 22).

In the southern Nansen Basin, where the highest *N. pachyderma (sin.)* $\delta^{18}O$ values (3.5-3.9‰) are found, the reconstructed salinity (about 36‰) is for most sites about 1‰ higher than the modern Atlantic Water (just below 35‰). Examining the calculated $\delta^{18}O_w$ values obtained for these sites (0.5-0.6‰: Appendix J) with the maximal $\delta^{18}O_w$ values of the Atlantic Water (about 0.25‰: Bauch, 1995), indicates that the calculated $\delta^{18}O_w$ values is too high affecting the reconstructed salinity estimates. Thus using an alternative $\delta^{18}O_w$ /salinity relationship as e.g. the GEOSECS (1987) relation for the salinity calculation in the Southern Nansen Basin area is not the solution to the problem. Calculation examples demonstrate that when the vital effect correction is included (cf. section 5.3), the $\delta^{18}O_w$ discrepancy cannot be explained within a realistic temperature range. E.g. to obtain the modern Atlantic Water salinity value (34.9‰), an unrealistic temperature estimate of about -4°C is needed. Omitting the vital effect correction for the high *N. pachyderma (sin.)* $\delta^{18}O$ values in the southern Nasen Basin area (3.5-3.9‰), however, leads to values of $\delta^{18}O_w$ and salinity close to modern Atlantic Water properties.

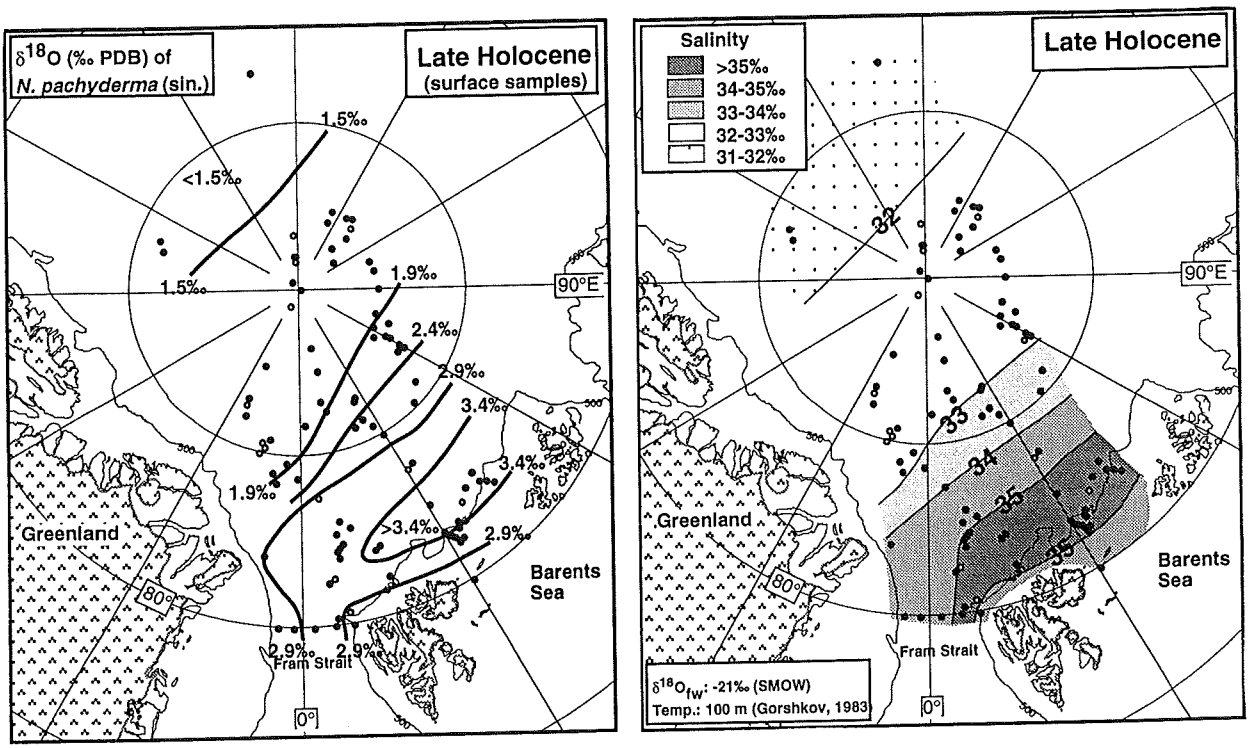

Fig. 29. $\delta^{18}O$ (*N. pachyderma* sin.) distribution and corresponding reconstructed salinity for the late Holocene (3-0 ka).

The above considerations may indicate that the simplified linearity between temperature and potential vital effect derived from data in Bauch (1995) is not well constrained for positive °C

temperatures. Other environmental factors like the degree of sea ice cover, water mass stratification, food supply, etc. may also be decisive for the life cycle and habitat depth of *N. pachyderma* (sin.) and the magnitude of a possible $\delta^{18}O$ vital effect (cf. Kohfeld et al., 1995; Bauch et al., 1997).

6. DISCUSSION

In this section I consider the temporal and spatial variation of the environmental conditions and climatic controls for the Arctic Ocean during the past glacial-interglacial cycle. Selected cores with well established stratigraphies and flux estimations of environmental parameters are basis for the synthesis. The time scale represented by these cores range from between 70,000 -115,000 yr BP to the Holocene. Consequently, emphasis is laid on the mid- to upper Weichselian history. The better constrained age control of the younger part of the record by radiocarbon dating facilitates the more precise estimation of timing and development of paleoceanographic events in relation to the last deglaciation. The same apply to the last deglaciation history of the circum-Arctic ice sheets, and consequently correlation of land-ocean records for this period can be done with more confidence. Due to low sedimentation rates and limited age fix points beyond the range of radiocarbon dating, the results do not permit the identification of climatic variations on timescales shorter than a few thousand years.

The relevant external controls of upper Quaternary paleoclimatic variations in the Arctic include: (1) the size and location of ice sheets which influences both atmospheric circulation, temperature and sea level, (2) insolation and carbon dioxide in the atmosphere, which influence mainly temperature and seasonality, and (3) feedbacks, involving sea ice and snow cover which reinforce the insolation effects (Bartlein et al., 1991).

6.1 Application of sediment proxies to reconstruct paleoenvironmental parameters

The stable isotopic and sedimentological parameters that have been quantified can in a stratigraphic framework be used as proxies for temporal and spatial changes in the Arctic Ocean paleoenvironment. Environmental factors of special interest are: salinity and temperature distribution of surface waters, influx of freshwater (riverine and/or deglacial), surface water stratification and CO_2 transport, degree of sea ice cover (partly open or closed), sediment ice rafting (sea ice or iceberg transport), primary production (planktic and benthic organisms), continental ice sheet build-up and deglaciation, and water mass exchange with the Norwegian-Greenland Sea (e.g. advection of Atlantic Water).

As demonstrated in the previous chapter, the $\delta^{18}O$ values of planktic foraminifers *N. pachyderma* (sin.) can be used as a proxy of changes in surface ocean salinity if major changes in water temperature and/or habitat depth can be ruled out and corrections for the global ice volume effect are done. In addition to the global sea-water ^{13}C variation, which roughly follows glacial-interglacial cycles (Labeyrie & Duplessy, 1985), the $\delta^{13}C$ values of

N. pachyderma (sin.) reflect regional changes in ventilation and stratification of the surface water masses, related to the degree of sea ice cover and influx of freshwater (riverine or deglacial meltwater). AMS-^{14}C dated stable isotope records documenting the last deglacial period in the Arctic Ocean indicate that minimum δ^{13}C values are related to peak deglacial meltwater events (Stein et al., 1994c; this study) .

The lithogenic part of the coarse fraction (>63μm) is, when bottom current activity and/or turbidity currents can be ruled out, a measure of the amount of material released from sea ice or icebergs. A low amount of lithogenic coarse fraction associated with a high planktic foraminifer content (as observed in surface sediment samples) indicates thus dominantly fine-grained (clay and silt) sea-ice rafting and at least seasonally open leads in the pack ice cover. A relative high amount of coarse sand and dropstones (IRD) suggests transport and melt-out from icebergs. The different IRD lithologies give clues to provenance areas of material eroded and incorporated into glacier ice. Identification of specific tracer lithologies with well-defined outcrop regions, as e.g. dolomitic carbonates, is crucial for more accurate reconstructions. The quantified flux of specific tracer IRD components may thus, for specific time slices, give a detailed picture of source regions for iceberg-calving and plausible paleocurrent patterns.

The percentage of lithogenic fragments, planktic foraminifers, and benthic foraminifers in specific grain size fractions is related to the accumulation rate of lithogenic material (dillution), the biogenic production, and the influence of calcium carbonate dissolution. Under assumption that sedimentation rates are constant and no severe dissolution has taken place, the amount of planktic foraminifers/g sediment can be taken as a measure for the planktic productivity, which may be related to the degree of ice cover (light for phytoplankton), nutrient supply, salinity stratification, temperature, etc.

The established stratigraphy and age models for selected key cores allow the determination of accumulation rates of specific components (amount cm^{-2} ky^{-1}). By that means, it is possible to make a direct comparison of the flux (temporally and spatially) of different sediment components. E.g. very low bulk accumulation rates associated with very low fluxes of planktic foraminifers may indicate an almost 100% closed sea ice cover. Flux estimates for the period beyond the ^{14}C dating limit, hovever, are averaged over long time spans. Due to generally low sedimentation rates in the Arctic Ocean, bioturbation mixing is a factor which seriously can have modified the sedimentological records and all quantified environmental proxy.

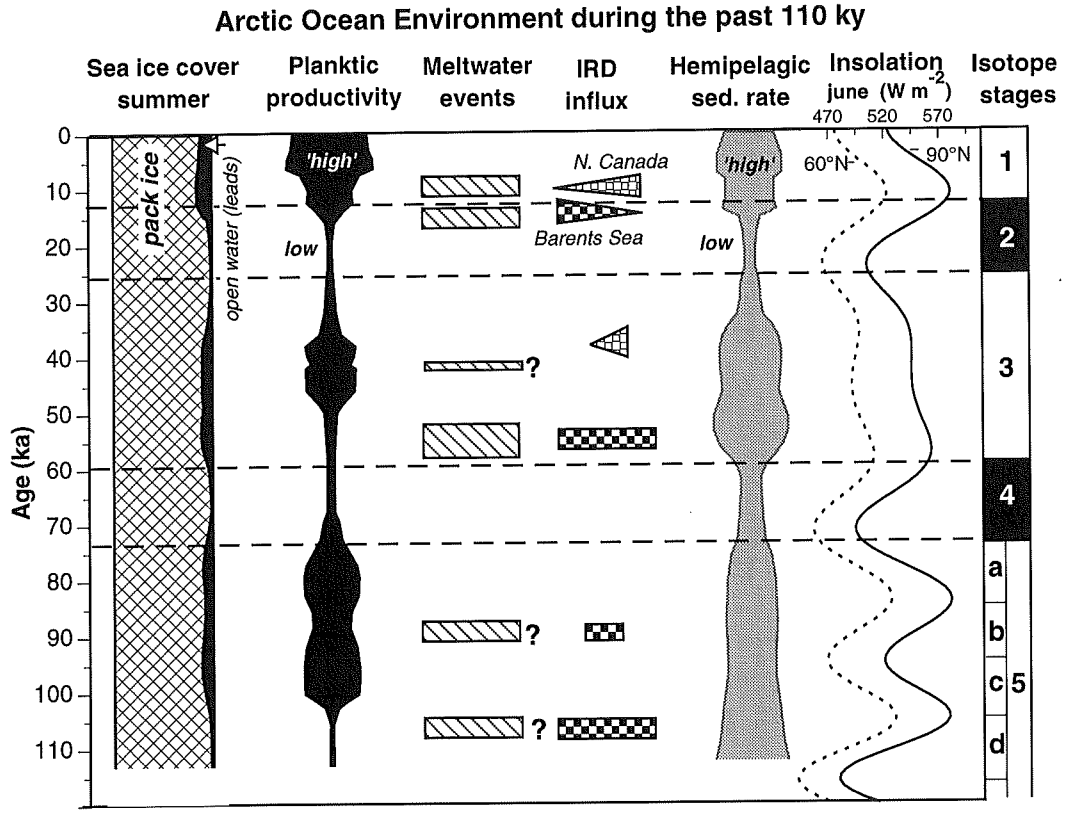

Fig. 30. A simplified compilation of Arctic Ocean environment for the past 110 ka based on the present study. Changes in hemipelagic sedimentation rate, planktic foraminifer productivity, IRD flux, and the timing of major meltwater episodes apparently are connected to changes in summer insolation (Berger & Loutre, 1991). The qualitative estimate of sea ice cover (summer situation) has been interpreted from the rest of the environmental proxy data.

6.2 Paleoceanographic development (oxygen isotope stage 5-1)

In the following the chronological development in separate oxygen isotope stages (sensu Martinson et al. (1987)) will be discussed. The main conclusions are summarised in Fig. 30 and relevant terrestrial/marine climate records are presented in Fig. 31 as basis for a discussion of climate controls and land-ocean linkages.

a) Mid- to late Stage 5 (110-74 ka)

Oxygen isotope stage 5 deposits have only been identified in few of the box cores investigated and paleoceanographic interpretations presented are therefore limited. Positive evidence for stage 5 are the stable isotope records characterised by moderate low $\delta^{18}O$ and relative high $\delta^{13}C$ values, a periodically high estimated flux of planktic foraminifers, and a dominance of *Gephyrocapsa mullerae* coccoliths (Gard, 1993). The $\delta^{18}O$ values (2.5-3.5‰) are in general 0.5-1.0‰ higher than the Holocene level and only single $\delta^{18}O$ values in early

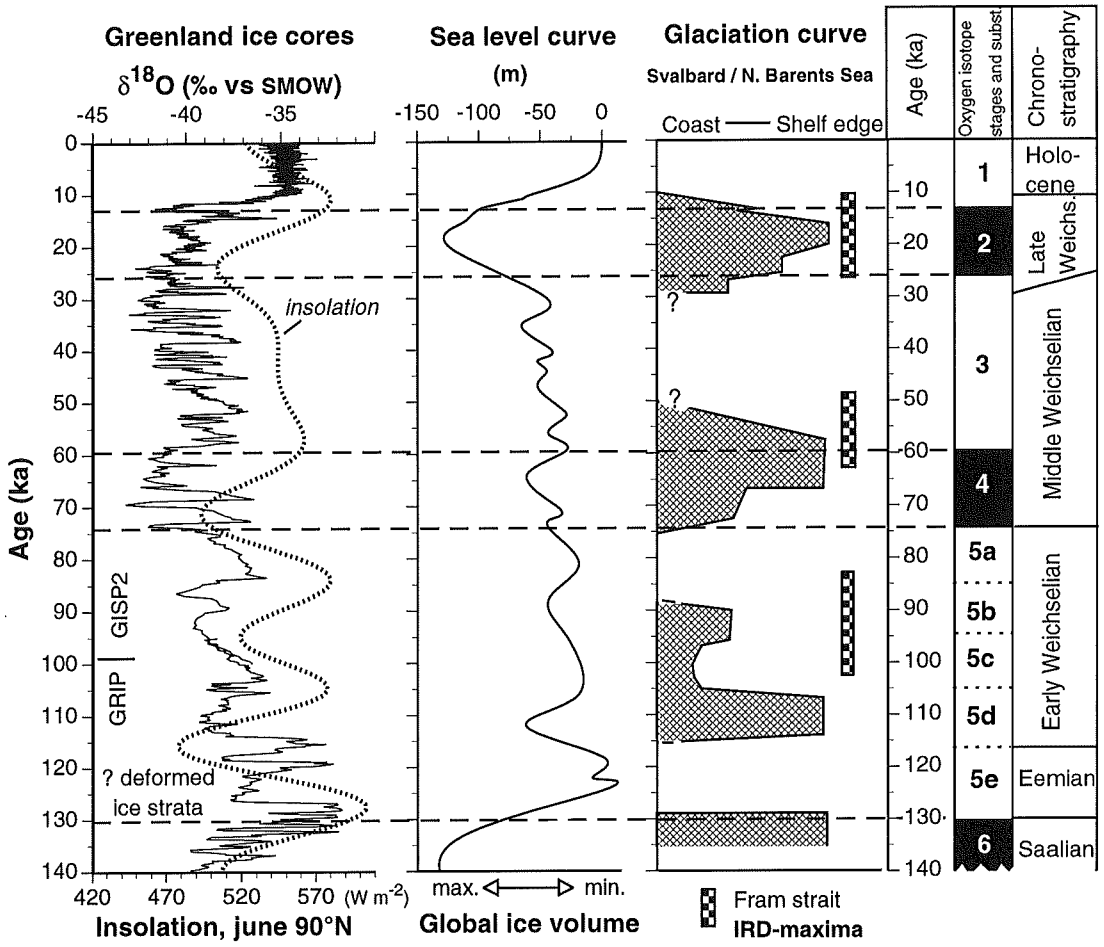

Fig. 31. 140 ka climate records of Greenland ice cores (GRIP, GISP2), june insolation (Berger & Loutre, 1991), sea level (Chappel & Shackleton, 1986) and glaciation curve for the Svalbard and Barents Sea (Mangerud et al., 1996). Data for the GISP2 $\delta^{18}O$ record (0-100 ka) from Grootes et al. (1993), Stuiver et al. (1995), Meese et al. (1994) and Sowers et al. (1993). Data for the GRIP $\delta^{18}O$ record (95-140 ka) are from Dansgaard et al. (1993).

stage 5 (substage 5e?) are as low as the Holocene level. Compared to $\delta^{18}O$ values reported from Fram Strait and Yermak Plateau sites for substages 5d-5a (Köhler, 1992), the central Arctic Ocean values (Morris Jesup Rise, Amundsen Basin, Lomonosov Ridge) is about 1‰ lower. This difference is about half of the one observed in mapped-out $\delta^{18}O$ values of surface sediment samples (late Holocene) from the southern part of the Eurasian Basin to the Lomonosov Ridge (Spielhagen & Erlenkeuser, 1994). Thus, if bioturbation modification and temperature influence can be neglected, a lower than present day regional gradient in salinity is suggested for the mid- to late stage 5. The $\delta^{13}C$ values recorded for that period are

relative high (0.5-1.0‰) suggesting generally well-ventilated Arctic Ocean surface waters comparable to recent conditions.

The planktic productivity during substages 5c? to 5a? (105-74 ka) were, at least locally, close to the Holocene level (based on the calculated flux of planktic foraminifers in core PS2195-4). Indications of severe calcium carbonate dissolution in the Lononosov Ridge and Morris Jesup Rise cores from water depths between 1000 and 2000 m in the sediment units asigned to stage 5, 4 and early stage 3, suggest the influence of corrosive CO_2-rich intermediate water masses during this time period. In cores from deeper sites in the Amundsen Basin (e.g. PS2195-4 and PS2196-2) and the Gakkel Ridge (e.g. PS2164-4) there is no evidence for corrosive bottom waters for the stage 5 period. This is confirmed by the study of Pagels (1992) who for this period found no indications of severe carbonate dissolution in deep (>2900 m) Gakkel Ridge and Nansen Basin cores.

The stage 5 records are characterised by moderate high bulk accumulation rates (0.4-1.0 g cm^{-2} ky^{-1}) of relatively sandy sediments (15-30% >63μm). Larger amounts of IRD >500μm are concentrated in certain levels (substages 5d? and 5b?) and may reflect increased sediment rafting by icebergs associated with ice sheet build-up or deglaciation. There is, however, no positive identification of deglacial events from the (low resolution) stable isotope records (e.g. low-$\delta^{18}O$, low-$\delta^{13}C$ meltwater spikes). The IRD composition is remarkably rich in quartz grains (cores PS2195-4, PS2200-2/5, PS2185-3/6 and PS2164-4), and the amount of siliciclastic sediment rock grains is clearly dominant to the sparse content of detrital carbonate. In comparison, Kubisch (1992) suggested enhanced IRD accumulation rates on Gakkel Ridge sites (close to 30°E) in the early- to middle stage 5 (5e to 5c) followed by a decrease in IRD flux in late stage 5 (5b to 5a). The glaciation curves for the Svalbard-Barents Sea (Mangerud, 1991; Mangerud et al., 1996; Dokken, 1995) and Northern Canada data (e.g. Porter, 1989; Blasco et al., 1990; Dinter et al., 1990; Brigham-Grette & Hopkins, 1995) suggest the build-up of circum-Arctic ice sheets during substages 5d and 5b, coinciding with pronounced summer insolation minima (Berger & Loutre, 1991) and sea level low stands (Chappel & Shackleton, 1986).

b) Stage 4 (74-59 ka)

In oxygen isotope stage 4, glacial conditions associated with a minimum in summer insolation are suggested to have caused a dense sea ice cover of the Arctic Ocean. The accumulation rates on ridges and turbidite protected sites dropped apparently to 0.2-0.5 g cm^{-2} ky^{-1}. These values are comparable to estimates for glacial stage 2 and considerably lower than the accumulation rates estimates for the climatic warmer periods (i.e. stage 5, early stage 3 and the Holocene). In general the sediments are fine-grained, with a low

foraminifer content and a low calcium carbonate content. The calculated flux of planktic foraminifers is <300 shells cm^{-2} ky^{-1}. The Morris Jesup Rise and the Lomonosov Ridge sites may, however, have been subject to calcium carbonate dissolution. The IRD content and calculated IRD flux are very low, but show an increase at the transition to stage 3. In this way, extensive iceberg rafting and sediment release were mainly associated with the subsequent deglaciation of the relative large stage 4 ice sheets documented for the Northern Hemisphere (cf. Mangerud, 1991; Mangerud & Svendsen, 1992; Baumann et al., 1995; Dredge & Thorleifson, 1987; Porter, 1989; Blasco et al., 1990).

The $\delta^{18}O$ values obtained for stage 4 are remarkably uniform (3.5-4.0‰) over the central and eastern Arctic Ocean compared to large regional differences observed in the stage 3 to 1 records. This may indicate that a quite homogeneous surface water mass, without major gradients in salinity, characterised the Arctic Ocean during glacial stage 4. Markedly decreasing $\delta^{13}C$ values throughout stage 4, and minimum $\delta^{13}C$ values at the stage 4/3 transition are observed in the Arctic Ocean records and in Fram Strait and Norwegian-Greenland Sea records as well (cf. Weinelt, 1993; Dokken, 1995). This may partly be due to the global oceanic $\delta^{13}C$ signal which reaches a minimum in stage 4 (cf. Labeyrie & Duplessy, 1985; Jansen, 1989). On the other hand, the $\delta^{13}C$ pattern may also indicate poor ventilation of surface waters due to cooling and increase of ice cover in late stage 4 followed by deglacial meltwater (low $\delta^{13}C$/high $\delta^{18}O$) influx at the stage 4/3 transition, quite similar to the stage 2/1 scenario.

c) Early Stage 3 (59-50 ka)

The middle Weichselian oxygen isotope stage 3 record in the Arctic Ocean can be divided into three intervals representing major changes in environment as a response to climatic changes: An early stage 3 deglacial period (59-50 ka) associated with a Northern Hemisphere summer insolation maximum (Berger & Loutre, 1991), a middle stage 3 period (50-35 ka) with longer lasting warm interstadials (cf. Dansgaard et al., 1993; Bond et al., 1993) in many aspects similar to the present day Arctic Ocean, and a late stage 3 period (35-27 ka) of gradual cooling (decrease in summer insolation).

The early stage 3 was characterised by a major deglacial episode which can be traced from the central Arctic Ocean to the North Atlantic (Fig. 32). Low-$\delta^{18}O$/low-$\delta^{13}C$ meltwater spikes with amplitudes (≥1‰), not inferior to meltwater spikes observed during the last deglaciation, are suggested to correspond to the deglacial event 3.31 (55.45 ka: Martinson et al., 1987) observed in Norwegian-Greenland Sea records (Duplessy et al., 1988; Vogelsang, 1990; Weinelt, 1993; Dokken, 1995) and, less conspicuous, in global oxygen isotope records (Martinson et al., 1987). On the Lomonosov Ridge, only the deeper site

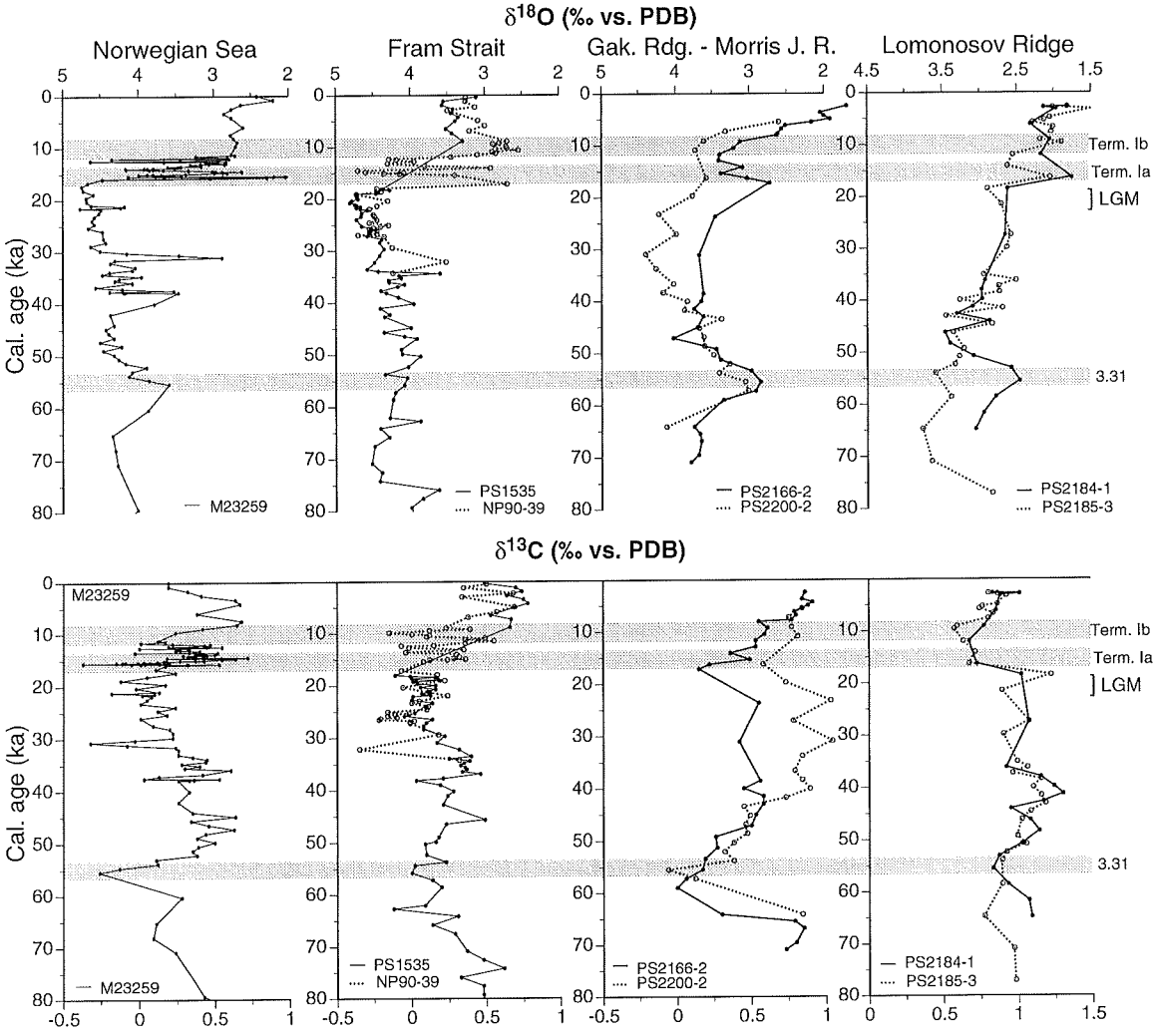

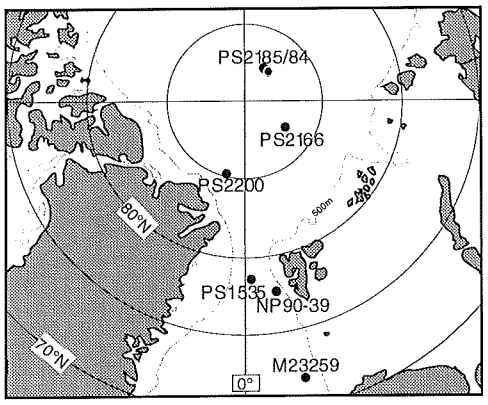

Fig. 32. Comparison of high resolution stable isotope records (*N. pachyderma* sin) from the Norwegian Sea and the Fram Strait with records from the central Arctic Ocean covering the past 80 cal. ky. Major deglacial events (3.31 and Termination I) can be traced in all records. Data for core M23259 (Bear Island Fan are from Weinelt (1993); the NP90-39 record is from Dokken (1995); the PS1535 record is from Köhler (1992) and Spielhagen (unpubl. data); the records of PS2166-2, PS2200-2, PS2185-3, and PS2184-1 are from this study.

PS2184-1 presumably has recorded this deglacial event properly in the stable isotope record. The amplitude and the absolute $\delta^{18}O$ values of the deglacial spike in core PS2184-1 are quite similar to the records obtained on the Gakkel Ridge (e.g. PS2166-2) and the Morris Jesup Rise (PS2200-2). The calculated flux of planktic foraminifers and accumulation rate of calcium carbonate for this deglacial period are extremely low. A combination of low planktic productivity, carbonate dissolution, and terrigenic dilution associated with high deglacial sedimentation rates, may explain the observed pattern. Similar conditions are reflected in the well-dated Yermak Plateau core PS1533-3 (Pagels, 1992; Nowaczyk & Baumann, 1992) and in Norwegian-Greenland sea cores (Baumann et al., 1995) showing practically no planktic foraminifers and nannoplankton in the lowermost part of stage 3. In the Arctic Ocean, the deglaciation in early stage 3 apparently was associated with a prominent increase in bulk accumulation rates reaching peak values of 0.5-1.5 g cm^{-2} ky^{-1}. The limited number of age fix points, however, cause that 'true' accumulation rates, for peak deglacial events cannot be estimated. Over the Gakkel Ridge, the flux of coarse IRD apparently was very modest. At Lomonosov Ridge sites, however, a distinct peak of lithic sandy material indicates considerably higher IRD fluxes. The IRD composition is rich in quartz and shows no detrital carbonate. A correlatable lithic coarse fraction peak was reported from the LOREX core B-8 (Makarov Basin) at about 30 cm below surface (Morris et al., 1985) supporting the true ice-rafted nature of this event. High resolution cores from the Fram Strait and the Yermak Plateau show in the lowermost part of stage 3 also peaks of IRD equal to or exceeding the amplitude reached during the last deglaciation (Pagels, 1992; Hebbeln, 1991; Dokken, 1995). The pattern of stable isotope meltwater spikes, IRD flux and composition suggests that degradation of (stage 4) ice sheets from both the Eurasian margin (Svalbard-Barents Sea) and the Amerasian Margin have influenced the Arctic Ocean during early stage 3.

d) Middle Stage 3 (50-35 cal. ka)

At about 50 ka, an environmental change took place as recorded in a pronounced increase in calcium carbonate accumulation rate and flux of planktic foraminifers. This is paralleled by a return to higher $\delta^{18}O$ and $\delta^{13}C$ values, suggesting a decrease in freshwater/meltwater influx and better ventilation of surface waters. The period 50-35 ka was characterised by moderate high bulk accumulation rates (0.4-1.0 g cm^{-2} ky^{-1}) of relatively fine-grained sediments rich in planktic foraminifers, i.e. quite similar to upper Holocene conditions. The sea ice cover may have been partly open during summer. Despite of poor age control in the period prior to 40 ^{14}C ka, two separate planktic foraminifer maxima, at about 48-45 cal. ka and 41-39 cal. ka, may be recognised from stacked records. The calculated fluxes of planktic foraminifers for these periods are in the range of 1,500-4,000 shells cm^{-2} ky^{-1} almost equaling the upper Holocene level. Several of the stable isotope records show in the intervening period, about

45-41 cal. ka, evidence of a meltwater episode and lowered planktic productivity. The Greenland ice cores (Dansgaard et al., 1993) and correlative high resolution deep sea records from the North Atlantic (Bond et al., 1993; Bond & Lotti, 1995) reveal longer lasting warm interstadials (several thousand years) flickering with shorter cold episodes in the middle part of oxygen isotope stage 3. It is possible that the Arctic Ocean records reflect similar episodes, but due to low sedimentation rates, only the most prominent can be stratigraphically resolved. From the Norwegian-Greenland Sea records it appears that meltwater incursions, during the middle stage 3, were quite modest (Weinelt, 1993).

The present study has documented that the IRD flux, at about 40 cal. ka, dramatically increased close to the north Greenland continental margin. The IRD is rich in dolomitic carbonate suggesting an origin from the extensive outcrops of paleozoic platform carbonates in Arctic Canada and/or northern Greenland (cf. Fig. 34). In Lomonosov Ridge and Gakkel Ridge records, a more modest IRD flux (w. detrital carbonate) are recorded in the mid- to late stage 3. It is suggested that the detrital carbonate-rich IRD record reflect the growth of northern Greenland and northern Canadian ice sheets leading to shelf edge calving of icebergs into the Arctic Ocean. From Ellesmere Island and Hall land of northern Greenland, moraines of mid- to late Weichselian age (the Lake Hazen Moraines and the Peterman and Newman Moraines) have been reported by England & Bradley (1978) and England (1985). Funder (1989) and Kelly & Bennike (1985), however, suggested that major North Greenland glaciation first was initiated at the beginning of oxygen isotope stage 2.

e) Late Stage 3 and Stage 2 (35-17 cal. ka / 30-14.5 ^{14}C ka)

The present study has documented that the Arctic Ocean, during the upper part of oxygen isotope stage 3 and 2 (including the LGM), was characterised by very low accumulation rates (0.2-0.4 g cm^{-2} ky^{-1}) and a very low flux of planktic foraminifers. It is suggested that a dense cover of sea ice developed with reduced summer melting/open leads limiting planktic productivity and deposition of ice-rafted sediment. This was probably a response to Northern Hemisphere cooling and decrease in summer insolation from about 35 ka to 22 ka reported by Berger & Loutre (1991). In contrast, for the eastern Fram Strait and the Yermak Plateau region, a much higher accumulation rate/planktic productivity regime has been documented for stage 2 (Pagels, 1992; Nowaczyk et al., 1994; Hebbeln et al., 1994; Dokken, 1995, Vogt et al., in prep.) and related to periodical advection of Atlantic Water, seasonally ice free waters, and influence of ice sheet margin processes (iceberg calving, sediment plumes, etc.).

In the Arctic Ocean a major peak of calcium carbonate content is ubiquitously found in the foraminifer poor oxygen isotope stage 2 records from turbidite-protected sites. This

phenomenon is less conspicuous in the calcium carbonate accumulation rate records due to the very low bulk accumulaion rates in this interval. Whereas the amount of coarse detrital carbonate IRD is very low in this interval, the content of authigenic calcium carbonate aggregates in some cores is quite high (e.g. cores PS2200-2, PS2166-2). It can be speculated whether diagenetic processes are responsible for the phenomenon, or if enhanced deposition of clay to silt-sized detrital carbonate from the Northern Greenland-Northern Canada continental margin, during the LGM low sea level stand, contributed to the carbonate peak.

The large difference in planktic $\delta^{18}O$ values (1.5-2.5‰) observed between cores from the southern part of the Eurasian Basin and the central Arctic Ocean during late stage 3 and stage 2 suggests that a strong gradient in salinity prevailed. The reconstruction of salinity distribution for the LGM time-slice (Fig. 27) indicates that salinities in the central Arctic Ocean were about 2-3‰ lower than values obtained for the southwestern Nansen Basin and the Fram Strait. The interaction of several factors may explain this salinity gradient which is not far from the present one. Ice core snow accumulation data (e.g. Reeh, 1990; Alley et al., 1993) and general circulation models indicate that the hydrological cycle and precipitation rates over high northern latitudes were dramatically reduced during the LGM. The total influx of freshwater to the Arctic Ocean was likely considerably lower than the present level. The advection of saline Atlantic water may also have been reduced because the Barents Sea Branch was cut off by the lowered sea level and an ice sheet cover. Some advection of Atlantic Water through the Fram Strait probably still took place during intervals (Hebbeln et al., 1994; Dokken, 1995) contributing the moisture supply for the rapid Stage 2 growth of the Barents Sea Ice Sheet (Elverhøi et al., 1995). The import of Pacific Water through the shallow Bering Strait, however, was not possible. With less influx/outflow of freshwater to the Arctic Ocean and reduced advection of Atlantic water, a stable low salinity surface layer may have developed independently of the actual size of the freshwater influx. It is suggested that the residence time of surface water in the Arctic Ocean was considerably higher than the present day value (cf. Lehman et al., 1993; Hunkins, 1991).

Sarnthein et al. (1995) for the LGM suggested that the seasonally open-sea conditions documented for the Grenland-Norwegian Sea (see also Veum et al., 1992) and the Fram Strait (Hebbeln et al., 1994) may even hold true for the Arctic Ocean north of Greenland up to 85°N (high $\delta^{18}O$ values in the FRAM I/4 and I/7 cores: Zahn et al., 1985). The present study supports that the homogeneous pattern of $\delta^{18}O$ values in the southwestern part of the Eurasian Basin (Fig. 27) and the Norwegian-Greenland Sea (Sarnthein et al., 1992) may indicate the advection of (subsurface?) Atlantic Waters to the high north during the LGM. The remarkable reduction in stage 2 accumulation rates and planktic productivity from the

Fram Strait toward the northern part of the Eurasian Basin (this study; Stein et al., 1994c; Vogt, in prep.), however, suggests that open water Arctic Ocean conditions were limited to the region around Svalbard.

f) The last deglaciation (17-8.5 cal. ka / 14.5-7.5 ^{14}C ka)

The beginning of the last deglaciation has been traced by stable isotope signals and radiocarbon dated to about 15-14 ^{14}C ka in the central and eastern Arctic Ocean. This is in agreement with age estimates of early deglaciation given for higher resolution Fram Strait records (Jones & Keigwin, 1988; Elverhøi et al., 1995) and Norwegian-Greenland Sea records (Blaume, 1992; Weinelt, 1993; Sarnthein et al., 1992). Based on a single AMS-^{14}C dating from a core on the Gakkel Ridge, Stein et al. (1994b) suggested that major influx of meltwater to the Arctic Ocean commenced as early as 15.7 ^{14}C ka.

The present work documents two major deglacial episodes, Termination Ia and Termination Ib, in the radiocarbon dated stable isotope records. Low-δ^{18}O meltwater excursions with an amplitude of about 1‰ culminate about 14-12 ^{14}C ka (Termination Ia). This is followed by a return to heavier values about 11-10 ^{14}C ka (12.5-11.4 cal. ka) associated with the Younger Dryas cooling episode (12.8-11.7 cal. ka: Stuiver et al., 1995). In the subsequent period 10-7.5 ^{14}C ka a rapid decrease of δ^{18}O values is associated with Termination Ib. Meltwater spikes during Termination Ib are more pronounced in the Lomonosov Ridge records whereas the Gakkel Ridge records more or less parallel the global oxygen isotope curve. Extremely low δ^{13}C values associated with the meltwater spikes, suggest that a low saline and poor-ventilated surface layer covered the Arctic Ocean during the Termination Ia and Ib. The salinity reconstruction performed for the Termination Ia time slice indicates that surface salinities in the southwestern Nansen Basin were in the range 34.3-34.9‰ and that the central Arctic showed salinities in the range 32.1-32.8‰ (Fig. 28). Compared to modern conditions, salinities in the southwestern Nansen Basin were slightly lowered, whereas salinities in the central Arctic apparently were close to the modern level. Due to the limited time resolution, however, signals of peak deglacial salinity excursions likely have been reduced.

A pronounced increase in sedimentation rates (0.5-1.0 g cm^{-2} ky^{-1}) and planktic foraminifer productivity characterised the deglacial period. The higher-resolution records, PS2166-2 and PS2177-1, show an increase in the flux of planktic foraminifers taking place in two steps, following the peak deglacial meltwater episodes with a lag of about 1000-2000 years. It is suggested that meltwater stratification prevented vertical mixing and subdued planktic productivity during the peak deglacial episodes. Moreover the effect of increasing summer insolation, peaking at about 10 ka (Berger & Loutre, 1991), and reestablishment of the

Atlantic Water advection (Hebbeln et al., 1994; Dokken, 1995; Sarnthein et al., 1995) may have created favourable conditions (more open water, more nutrients) for a relative high planktic productivity during the upper part of Termination Ib (i.e. early Holocene).

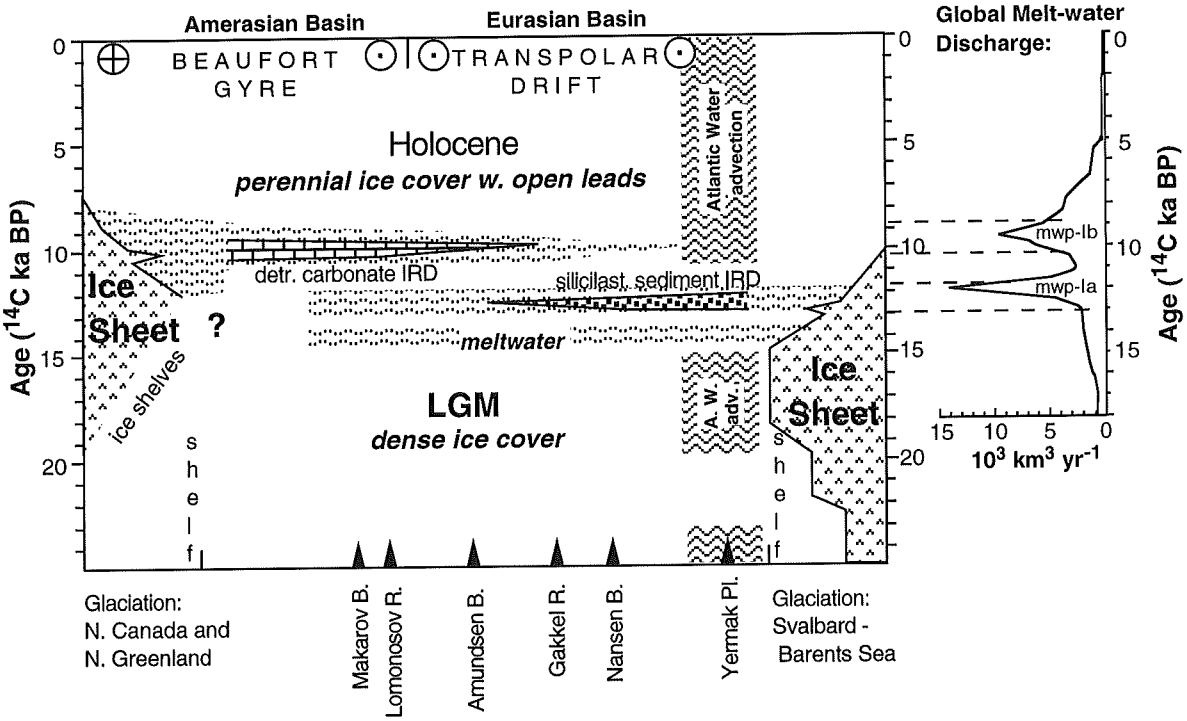

Fig. 33. a) Timing and inferred provenance of major deglacial meltwater and IRD events in the Arctic Ocean during the last deglaciation. The ice sheet extent (relative to shelf margin) for the Svalbard-Barents Sea is based on Elverhøi et al. (1995). The Northern Canada/ Northern Greenland ice sheet-retreat history is based on Hodgson (1994) and Funder & Hansen (1996). The global meltwater signal according to Fairbanks (1989) is shown for comparison. The inferred Atlantic Water advection (seasonally open water conditions) is based on Hebbeln et al. (1994).

The regional pattern of meltwater spikes and IRD influx is suggested to reflect the diachronic course of deglaciation of the Barents Sea Ice Sheet compared with the Innutian-Greenland and Northern Laurentide Ice Sheets (Fig. 33). During Termination Ia, the main part of the Barents Sea Ice Sheet and the northwestern sector of the Laurentide Ice Sheet disappeared within a few thousand years (Elverhøi et al., 1995; Peltier, 1994; Hodgson, 1991, 1994) and discharged huge amounts of isotopically light meltwater into the Arctic Ocean and the Norwegian-Greenland Sea (Jones & Keigwin, 1988; Weinelt, 1993; Sarnthein, 1995) accompanied by a rapid rise in sea level and reflooding of the continental shelves. Termination Ia deglacial events are well reflected in the Gakkel Ridge, Nansen Basin and Yermak Plateau records where IRD peaks dominated by clastic sedimentary rock fragments,

dated to about 13-12 ^{14}C ka, apparently lag about 1000-2000 years after the first main incursion of meltwater. In the Fram Strait, a comparable lag of IRD spikes to Termination Ia meltwater spikes has also been reported (Elverhøi et al., 1995; Dokken, 1995). The observation that the stable isotopic meltwater spikes during Termination Ib are more pronounced in the central Arctic Ocean compared to the Eurasian Basin records, and that the peak flux of detrital carbonate IRD took place about 10-8 ^{14}C ka, suggest that during Termination Ib meltwater and melting icebergs were mainly discharged from the remaining northeastern sector of the Laurentide Ice Sheet and the retreating Innutian and north Greenland ice sheets. The present study has made it possible to map out the distribution of Termination I detrital carbonate IRD in detail (Figs. 16, 34). A peak of detrital carbonate IRD is found in cores from the Makarov Basin, the Lomonosov Ridge, the western Amundsen Basin and the Morris Jesup Rise. In contrast, the cores from the Gakkel Ridge (60°E), the Nansen Basin and the Yermak Plateau show almost no detrital carbonate fragments during the Termination I. An ice drift pattern comparable to the present, with a Beaufort Gyre export branch over the Lomonosov Ridge and the western Amundsen Basin (Fig. 4), could explain the observed depositional pattern of IRD (Fig. 34). It is remarkable that in the two Makarov Basin cores the flux of detrital carbonate IRD for the Termination Ib peak is considerably larger than the flux documented in the Lomonosov Ridge cores nearby. This pattern may indicate the existence of a sharp boundary zone of surface and subsurface water masses over the Lomonosov Ridge comparable to the present day conditions (Anderson et al., 1994; Rudels, 1994; Aagaard, 1996). Icebergs undergoing slow degradation might thus have been trapped in the Beaufort Gyre for several decades.

g) Mid- to late Holocene (7.5 - O ^{14}C ka)

Quite uniform conditions characterised the Arctic Ocean during the mid- to late Holocene. Bulk sedimentation rates have been relative high, 0.5-1.0 g cm^{-2} ky^{-1}, with a relative high planktic foraminifer flux (about 5000 shells cm^{-2} ky^{-1}) and a moderate to low IRD accumulation rate. With reference to the present day processes, sea ice-rafted, fine-grained sediments entrained on the shallow shelf seas and river mouths possibly are the main contributer to the hemipelagic sea floor cover. The highest accumulation rates were apparently reached about 7-5 ^{14}C ka concurrently to the Holocene climatic optimum. It cannot, however, be ruled out that this is a bioturbation artefact influencing the planktic foraminifer distribution and radiocarbon datings.

The steadily increasing $\delta^{18}O$ values documented in the Eurasian Basin cores for the Holocene, suggest that surface water there was relatively more saline in the early Holocene.

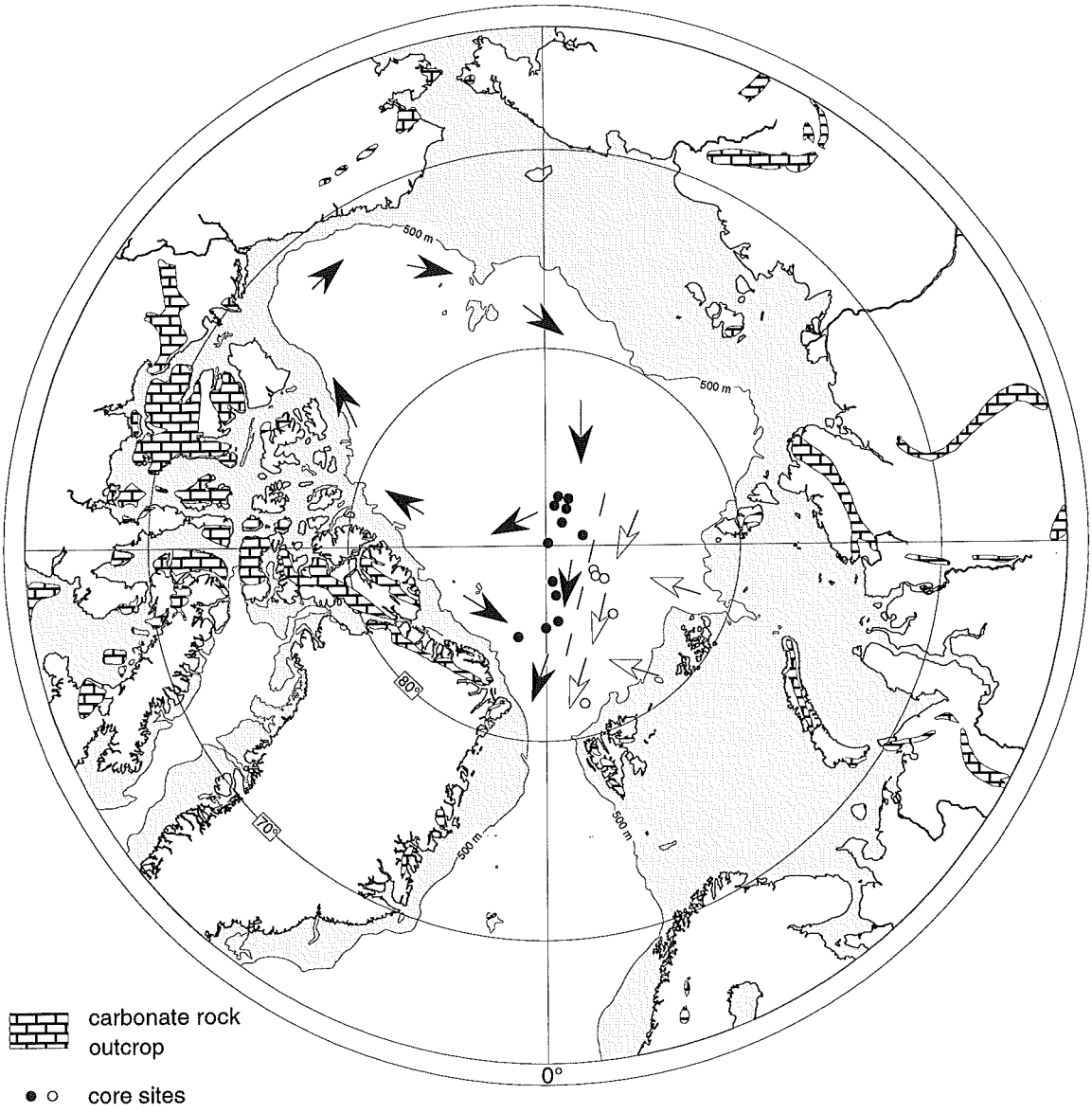

Fig. 34. Major outcrops of carbonate rocks in the circum-Arctic region (compiled from Okulitch et al. (1989) and Okulitch (1991)). Two zones of different IRD signature have been mapped out for the last deglacial period: 14.5-8.0 ^{14}C ka. Black dots represent core sites with abundant detrital carbonate IRD. White dots represent core sites where detrital carbonate is rare (dominated by siliciclastic sediment IRD). The inferred ice drift pattern is largely identical to the present one (cf. Fig. 3), but might have varied temporally as a response to rising sea-level, deglaciation and drowning of shelf areas and gate-ways, and atmospheric pressure changes subsequent to ice sheet retreat.

It is likely, however, that bioturbation has influenced the trend by mixing of high-$\delta^{18}O$ glacial signals with low-$\delta^{18}O$ deglacial and Holocene signals. In the central Arctic Ocean more uniform low salinities apparently have prevailed. The marked decrease in modern surface ocean salinity that can be observed from the southern Nansen Basin to the Lomonosov Ridge (about 3‰) thus seem to have prevailed throughout the Holocene. Comparison of $\delta^{18}O$ of water samples, of net-sampled *N. pachyderma* (sin.), and of surface sediment samples reveal that reconstructed $\delta^{18}O_W$ values and salinities for the modern central Arctic ocean are influenced by halocline properties (50 m average habitat), but that gradients in surface salinities are reasonably well recorded. The deeper 'Atlantic Water'-habitat (100-200m) in the southern Nansen Basin implies that, using $\delta^{18}O$ values of *N. pachyderma* (sin.) as a salinity proxy, surface water salinities cannot be reconstructed properly there. For time-slices where a significant Atlantic Water advection can be documented, similar habitat conditions can be expected.

The high and uniform $\delta^{13}C$ values imply that ventilation has been good throughout the mid- to late Holocene. This may be due to partly ice-free shelf seas during late summer where atmosphere-ocean CO_2 excange can take place. Due to low total biogenic productivity under the perennial sea ice cover, modification of the $\delta^{13}C$ ratio is probably limited during the trans-Arctic drift (Spielhagen & Erlenkeuser, 1994).

6.3 The Arctic Ocean - an active or passive link in the climate system?

The present study, and other studies as well, have shown that major climatic changes observed in lower latitude marine and terrestrial records indeed are reflected in deep Arctic Ocean sediments. This can be observed as changes in basic parameters as the accumulation rate of sediment, the flux and composition of ice-rafted debris, the flux of foraminifers and coccoliths, and the down-core pattern of stable isotope records. Apparently the gross changes occur more or less parallel to the oscillation in Northern Hemisphere insolation (Fig. 30) which, partly indirectly, have controlled the growth and decay of major ice sheets, the fall and rise in sea level, and the influx of fresh water to the Arctic Ocean (Fig. 31). It has been documented that the Arctic Ocean environment reacts more or less synchronous to rapid climatic changes. Unlike terrestrial ice sheets with their build-in inertia, the thin character of the Arctic Ocean sea ice cover makes it very sensible to external influence. The Arctic Ocean is bounded by continents and shallow seas which repeatedly have been glaciated and therefore have exerted a profound control on the fresh water balance and the sediment transport and deposition in the Arctic Ocean and the North Atlantic. The glacial-interglacial deep sea record therefore reflects both rapid climatic changes in the environment and retarded effects linked to the inertia of continents and ice sheets. The low hemipelagic sedimentation

rate in the Arctic Ocean, however, causes that short millenia scale events may not be resolved due to bioturbation mixing and a limited sample resolution.

A key feature of the Greenland ice core record and high resolution marine records from the North Atlantic during the last glaciation is the occurrence of more than 20 abrupt millenial-scale warming events, referred to as 'Dansgaard-Oeschger interstadials' (Dansgaard et al., 1993). Warming was extremely rapid for most events, occurring within decades. The warming was followed by a slower return to glacial conditions over hundreds of years. The frequency of this flickering climate change is an order higher than the major climate oscillations tied to orbital insolation forcing. The actual driving force is currently under debate, but it seems that changing intensity and/or direction of the North Atlantic Current, associated with changing sea ice cover, iceberg surging (Bond & Lotti, 1995) and deep water formation took an active part in the scenario. The formation of North Atlantic Deep Water (NADW) - on/off switching driven by changes in the salinity budget - may induce instability of the circulation pattern which could destabilise the climate (Broecker et al., 1990). The advection of Atlantic Water to the Fram Strait and the Arctic Ocean may be an important factor influencing latitudinal heat flux, precipitation, salinity, temperature, currents, sea ice distribution and exchange of energy between the ocean and the atmosphere. Dokken (1995) has recently presented evidence from Fram Strait sediment cores of six periods of sea ice break-up and surface ocean warming during isotope stages 4, 3 and 2. These warming episodes, lasting from about 2000 years to >10,000 years, are associated with an increase in meltwater and iceberg rafting and constitute c. 50% of the total time interval. They correlate temporarily to the early temperature maxima in 'Bond cycles' of the North Alantic (Bond et al., 1993) and Greenland ice record (Dansgaard et al., 1993), that immediately follow a Heinrich Event (Broecker et al., 1992). These data document a link between Arctic oceanic climate fluctuations, Northern Hempisphere ice sheet dynamics and ocean-atmosphere temperature changes.

Based on the last 100 ka record for the Arctic Ocean, three simple end-member scenarios can be presented (Fig. 35): a) a full glacial situation (e.g. oxygen isotope stage 4 and 2) with minimum summer insolation, maximum terrestrial ice sheet extension, a dense thick cover of sea ice, very restricted planktic productivity, and extremely low sediment accumulation rates; b) a deglacial situation (e.g. early stage 3 and Termination I) with maximum or increasing summer insolation, decaying terrestrial ice sheets, high discharge of meltwater and icebergs to the Arctic Ocean, a poor ventilated, low saline surface water layer, increased planktic productivity following meltwater episodes and increased bulk and IRD accumulation rates; and c) an interglacial or warm interstadial situation (e.g. late stage 5, middle stage 3 and the Holocene) with moderate high summer insolation, minimum terrestrial ice sheet extent, high

freshwater river influx, well-ventilated surface waters, a perennial sea ice cover with open leads during summer, relative high planktic productivity, and relative high accumulation rates. For periods characterised by rapid changes as deglaciations, this simple model may not reflect the actual climatic/paleoceanographic development very well. For the last deglaciation can major regional diachronic developments and a lag in reaction to climatic controls be documented.

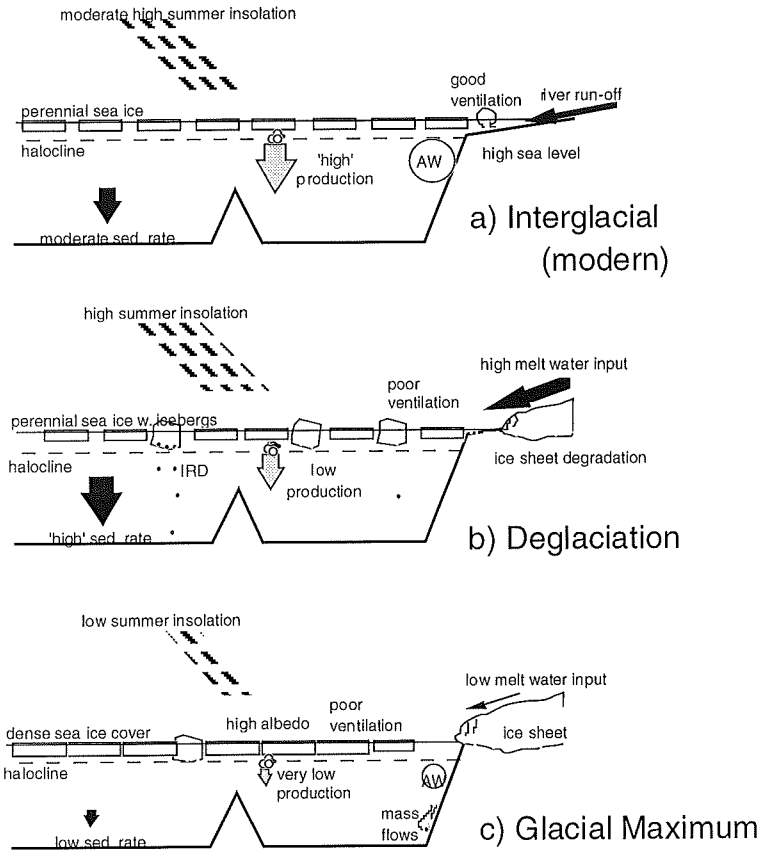

Fig. 35. Models of late Quaternary Arctic surface ocean conditions and sedimentation patterns for three end-member climate situations. a) interglacial conditions, b) deglacial conditions, and c) peak glacial conditions.

Based primarily on studies in the Amerasian Basin, Morris & Clark (1986) suggested that fine-grained sediments with a high foraminifer content are found both in glacial and interglacial intervals, whereas coarse-grained sediment with a low foraminifer content should be associated with deglacial periods. This model was modified by Phillips et al. (1992) and Poore et al. (1993) which, for all climate cycles within the Brunhes magnetochron on the Northwind Ridge, suggested that fine-grained, abiotic, greyish deposits are of 'glacial origin' whereas fine-grained, foraminifer-rich, brownish layers represent interglacial periods. The present study generally supports the latter interpretation but also indicates that climatic favourable periods within 'glacials' (e.g. late stage 5 and middle stage 3) may be characterised by a relative high planktic productivity.

7. CONCLUSIONS

- Major environmental changes in the Arctic Ocean seem to be in phase with the variation of Northern Hemisphere glaciations and summer insolation. This affects the extension and thickness of sea ice, the salinity and density stratification of surface waters, the productivity of planktic and benthic life, the sediment rafting and sedimentation pattern, and the export of freshwater to the North Atlantic.

- During glacial maxima in oxygen stage 2 and 4 the Arctic Ocean was characterised by a dense cover of sea ice with decreased seasonal variation limiting planktic productivity, deposition of terrigenic sediment, and bulk accumulation rates. For the Last Glacial Maximum, the reconstructed low-salinity conditions in the central Arctic Ocean are suggested to reflect a longer residence time of freshwater in the surface layer. The total influx of freshwater to the Arctic, however, might have been considerably lower than the present level.

- Meltwater incursions from major deglaciations of various continental ice sheets can be traced almost synchronous in the central Arctic Ocean surface layer by the stable isotope signature of planktic foraminifers *N. pachyderma* (sin.). The initial meltwater influx led the peak IRD events by at least 1000 years and also planktic productivity was subdued during the peak deglacial meltwater episodes.

- A deglacial event suggested for the early stage 3 had a strong influence on the Arctic Ocean surface water and caused a locally high IRD accumulation. This event, reflecting major circum-Arctic deglaciation of lower- to middle Weichselian ice sheets, is suggested to correspond to isotopic event 3.31 (about 55 ka) which is also the most conspicuous stage 3 deglacial event in Norwegian-Greenland Sea and North Atlantic records. In mid- to late stage 3, the IRD records document enhanced iceberg rafting of dolomitic carbonate rocks, suggested to originate from extensive outcrops of paleozoic platform carbonates in northern Greenland and arctic Canada. These inputs may be the result of expansion or surging events of the margins of the northern Greenland-, Innutian-, and/or Laurentide Ice Sheets. No shorter-lived meltwater/ice-rafting events corresponding to the North Alantic 'Heinrich Events' or 'Bond Cycles' have been positively identified in the sediment cores investigated. This may be due to very low sedimentation rates and bioturbation mixing of signals. On the other hand, high Arctic cold-based ice sheets (apart from the Barents Sea?) in low precipitation regions may be far less vulnerable to surging and rapid atmospheric/ocean temperature shifts, as e.g. the mid-latitude Laurentide Ice Sheet was.

- The diachronic Termination I deglaciation of the Barents Sea Ice Sheet and the western and eastern sector of the Laurentide Ice Sheet is reflected in the sediments of the Arctic Ocean. The rapid deglaciation of the marine-based Barents Sea Ice Sheet, associated with Termination Ia (14.5-11 ^{14}C ka), can be traced by meltwater spikes in sediment records from the Gakkel Ridge, the Fram Strait, and the Norwegian-Greenland Sea. A Termination Ia IRD peak, mainly consisting of sedimentary rock fragments of ?Barents Sea-Kara Sea origin, is limited to the southern Eurasian Basin. A second major meltwater event associated with Termination Ib (10-8 ^{14}C ka) is most conspicuous in isotope records from the central Arctic Ocean. The association with detrital carbonate IRD increasing in abundance toward the Makarov Basin and the northern Greenland margin indicates an origin of deglaciation/surging events from the northeastern Laurentide-, Innutian-, and Greenland Ice Sheets (cf. Hodgson, 1994; Funder and Hansen, 1996).

- The Holocene after 8 ^{14}C ka, longer lasting interstadials in middle stage 3 (50-35 cal. ka), and substages ?5c and 5a have left alike hemipelagic sediment records with relative high accumulation rates of fine-grained sediment rich in planktic foraminifers. With reference to the present day 'interglacial' environment these periods were likely characterised by a higher open water (lead) fraction during summers, extensive sea ice rafting and melting release of sediments incorporated on the wide shallow shelf seas, and a moderate to high freshwater influx from rivers.

8. Acknowledgments

I gratefully thank Prof. Dr. Jörn Thiede for supervising this work and for fruitful comments on an earlier version of this manuscript. My special thanks go to Robert F. Spielhagen for introducing me to the mysteries and dirty work of high latitude sedimentology and paleoceanography. His experienced guidance, friendly collaboration, and critical reviews over the last years contributed in particular to the completion of this study. I sincerely thank the Alfred Wegener Institute for Polar and Marine Research and the crew of RV *Polarstern* for providing samples and for giving me the possibility to participate in exciting cruises to the icy top of the Earth (ARK IX/4, ARK XI/1) during 1993 and 1995. For many fruitful discussions on stratigraphical aspects, I am grateful to my brothers in arms from the Alfred Wegener Institute, Christoph Vogt and Carsten Schubert. Christoph Vogt also performed XRD measurements. For measurements of stable isotopes I am indebted to Dr. Helmuth Erlenkeuser and his staff at the Radiocarbon Laboratory, Christian-Albrechts-University, Kiel. For providing oxygen isotope data on water samples, and for valuable discussions of salinity proxy data, I am grateful to Dorothea Bauch. For sample preparation and for performing radiocarbon datings, I thank Dr. Jan Heinemeier and his staff at the AMS-^{14}C Dating Laboratory, Institute of Physics and Astronomy, University of Aarhus, as well as Dr. Bernd Kromer, Heidelberg Academy of Sciences, and the ETH AMS-facility, Zürich. I also want to express my gratitude to Sven Ole Bude, Ralf Freitag, Silke Marczinek, Nina Schmidt, Stefan Steincke, and Dagmar Rau who helped to process the sediment samples used in this study. I acknowledge Heidi Kassens for her friendly assistance, for providing physical property data, and for letting me take over her green wreck. Finally, I would like to express my gratitude to other colleagues who have been supportive in professionel as well as social aspects during my stay at GEOMAR. In this capacity I would like to acknowledge Andreas Aichinger, Henning Bauch, Warner Brückmann, Nicole Biebow, Dirk Dethleff, Betina Gehrke, Harry Hommers, Susan Kinsey, Klas Lackschewitz, Frank Lindemann, Dirk Nürnberg, Xin Su, Martin Weinelt, and many others. My special thanks go to Ortrud Runze for her self-sacrificing coffee-support and for weeding the reference list. For financiel support of the project: "Paläoklima im Arktischen Ozean" (FKZ 03F0131A) I am grateful to the German Ministery of Education and Research (BMBF).

9. References

Aagaard, K., Barry, L.A., Carmack, E.C., Garrity C., Jones, E.P., Lubin, D., MacDonald, R.W., Swift, J.H., Tucker, W.B., Wheeler, P.A., and Whritner, R.H. 1996. U.S., Canadian researchers explore Arctic Ocean. EOS Transactions, American Geophysical Union, 77(22).

Aagaard, K. and Carmack, E.C. 1989. The role of sea ice and other fresh water in the arctic cirkulation. J. Geophys. Res. 94, 14485-14498.

Aagaard, K. and Carmack, E.C. 1994. The Arctic Ocean and climate: a perpective. In: Johannesen, O.M., Muench, R.D., and Overland, J.E. (eds.): The Polar Oceans and their role in shaping the global environment. Geophysical Monograph 85, American Geophysical Union, 33-46.

Aagaard, K., Swift, J.H., and Carmack, E.C. 1985. Thermohaline circulation in the arctic mediterranean seas. J. Geophys. Res. 90 (C5), 4833-4846.

Aksu, A. E. and Mudie, P. J. 1985. Magnetostratigraphy and palynology demonstrates at least 4 million years of Arctic Ocean sedimentation. Nature 318, 280-283.

Aksu, A. E. and Vilks, G. 1988. Stable isotopes in planktonic and benthic foraminifera from Arctic Ocean surface sediments. Can. J. Earth Sci. 25, 701-709.

Alley, R. B., Meese, D. A., Schuman, C. A., Gow, A. J., Taylor K. C., Grootes, P. M., White, J. W. C., Ram, M., Waddington, E. D. Mayeewski, P. A., and Zielinski, G. A. 1993. Abrupt increase in Greenland snow accumulation at the end of the Younger Dryas event. Nature 362, 527-529.

Anderson, L. G., Björk, G., Holby, O., Jones, E. P., Kattner, G., Koltermann, K. P., Liljeblad, B., Lindegren, R., Rudels, B., and Swift, J. H. 1994. Watermasses and cirkulation in the Eurasian Basin: Results from the *Oden* 91 expedition. J. Geophys. Res. 99(C2), 3273-3283.

Andrews, J.T. 1987. The late Wisconsian glaciation and deglaciation of the Laurentide Ice Sheet. In: Ruddimann, W.F. and Wright, H.E. Jr. (eds.). The Geology of North America, vol. K-3. North America and adjacent oceans during the last deglaciation, Geological Society of America, 13-38.

Astakhov, V. 1992. Last glaciation of West Siberia. Sveriges Geologiska Undersökning, Serie Ca 78, 21-30.

Bard, E., Arnold, M., Fairbanks R.G., and Hamelin, B. 1993. ^{230}Th-^{234}U and ^{14}C ages obtained by mass spectromertry on corals. Radiocarbon 35, 191-199.

Bard, E., Arnold, M., Mangerud, J., Paterne, M., Labeyrie, L., Duprat, J., Mélières, M.-A., Sønstegaard, E., and Duplessy, J.-C. 1994. The North Atlantic atmosphere-sea surface gradient during the Younger Dryas climatic event. Earth Planet. Sci. Lett. 126, 275-287.

Bard, E., Hamelin, B., Fairbanks R.G., and Zindler, A. 1990. Calibration of ^{14}C timescale over the past 30,000 years using mass spectrometric U-Th ages from the Barbados corals. Nature 345, 405-410.

Bartlein, P.J., Anderson, P. M., Edwards, M.E., and McDowell, P.F. 1991. A framework for interpreting paleoclimatic variations in eastern Beringia. Quaternary International, vol. 10-12, 73-83.

Bauch, D. 1995. The distribution of $\delta^{18}O$ in the Arctic Ocean: implications for the freshwater balance of the halocline and the sources of deep and bottom waters. Ber. Polarforsch. 159, 144pp.

Bauch, D., Carstens, J., and Wefer, G. 1997. Oxygen isotope composition of living *Neogloboquadrina pachyderma* (sin.) in the Arctic Ocean. Earth Planet. Sci. Lett. 146 (1-2), 47-58.

Baumann, K-H., Lackschewitz, K.S., Mangerud, J., Spielhagen, R., Wolf-Welling, T.C.W., Henrich, R., and Kassens, H. 1995. Reflection of Scandinavian Ice Sheet fluctuations in Norwegian Sea sediments during the past 150,000 years. Quaternary Research 43, 185-197.

Baumann, M. 1990. Coccoliths in sediment cores of the Eastern Arctic Basin. In: Bleil, U. & Thiede, J. (eds.). Geological history of the Polar Oceans: Arctic versus Antarctic. NATO ASI Series C, 308, Kluwer Academic Publ., Dordrecht, Netherlands, 437-446.

Bé, A.W.H. 1980. Gametogenetic calcification in a spinose planktonic foraminifera, *Globigerinoides sacculifer* (Brady). Marine Micropaleontology 5, 283-310.

Berger, A. and Loutre, M.F. 1991. Insolation values for the climate of the past 10 million years. Quaternary Science Reviews 10, 297-317.

Bischof, J., Koch, J., Kubisch, M., Spielhagen, R.F., and Thiede, J. 1990. Nordic Seas surface ice drift reconstructions: evidence from ice rafted coal fragments during oxygen isotope stage 6. In: Dowdeswell, J. A. & Scourse, J. D. (eds.). Glacimarine environments: Processes & sediments. Geol. Soc. Spec. Publ. 53, 275-291.

Blasco, S.M., Fortin, G., Hill, P.R., O'Connor, M.J., and Brigham-Grette, J. 1990. The Late Neogene and Quaternary stratigraphy of the Canadian Beaufort continental shelf. In: Grantz, A., Johnson, L., and Sweeney, J.F. (eds.). The Arctic Ocean region, The geology of North America, vol. L., Geological Society of America, Boulder, Colorado, 491-502.

Blaume, F. 1992. Hochakkumulationsgebiete am norwegischen Kontinentalhang: Sedimentologische Abbilder topographie-geführter Strömungsmuster. Ber. Sonderforschungsbereich 313, 36, Universität Kiel, 149pp.

Bleil, U. and Thiede, J. 1990. Geological history of the Polar Oceans: Arctic versus Antarctic, NATO ASI Series C, 308, Kluwer Academic Publ., Dordrecht, Netherlands, 823pp.

Bohrmann, H. (1991): Radioisotopenstratigraphie, Sedimentologie und Geochemie jungquartärer Sedimente des östlichen Arktischen Ozean. Ber. Polarforsch. 95, 133pp.

Bond, G., Broecker, W., Johnsen, S., McManus, J., Labeyrie, L. Jouzel, J., and Bonani, G. 1993. Correlation between climate records from North Atlantic sediments and Greenland ice. Nature 365, 143-147.

Bond, G., Heinrich, H., Broecker, W., Labeyrie, L., McManus, J., Andrews, J., Huon, S., Jantschik, R., Clasen, S., Simmet, C., Tedesco, K., Klas, M., Bonani, G., and Ivy, S. 1992. Evidence of massive discharges of icebergs into the North Atlantic ocean during the last glacial period. Nature 360, 245-249.

Bond, G. and Lotti, R. 1995. Iceberg discharges into the North Atlantic on millenial time scales during the last glaciation. Science 267, 1005pp.

Brigham-Grette, J. and Hopkins, D.M. 1995. Emergent marine record and paleoclimate of the last interglaciation along the northwest Alaskan coast. Quaternary Research 43, 159-173.

Broecker, W.S., Bond, G., Klas, M., Bonani, G., and Wolfi, W. 1990. A salt oscillator in the glacial North Atlantic? - the concept. Paleoceanography 5, 469-477.

Broecker, W.S., Bond, G., Mieczyslawa, K., Clark, E., and McManus, J. 1992. Origin of the northern Atlantic's Heinrich events. Climate Dynamics 6, 265-273.

Carmack, E.C. 1990. Large-scale physical oceanography of polar oceans. In: Smith Jr., W.O. (ed.). Polar oceanography, Part A, Academic, San Diego, Calif., 171-212.

Carstens, J. and Wefer, G. 1992. Recent distribution of planktonic foraminifera in the Nansen Basin, Arctic Ocean. Deep-Sea Research 39, 507-524.

Chappel, J. and Shackleton, N.J. 1986. Oxygen isotopes and sea level. Nature 324, 137-140.

Charles, C.D., Rind, D., Jouzel, J., Koster, R.D., and Fairbanks, R.G. 1994. Glacial-Interglacial changes in moisture sources for Greenland: influences on the ice core record of climate. Science 263, 508-511.

Clark, D. L. and Hanson, A. 1983. Central Arctic Ocean sediment texture: a key to ice transport mechanisms. In: Molnia, B. F. (ed.). Glacial-marine sedimentation. Plenum Press, New York, 301-330.

Clark, D. L., Whitman, R. R., Morgan, K. A., and Mackey, S. 1980. Stratigraphy and glacial-marine sediment of the Amerasiam Basin, Central Arctic Ocean. Geol. Soc. Am. Spec. Pap. 181, 57pp.

Clark, D. L., Wincent, J.-S., Jones, G.A., and Morris, W.A. 1984. Correlation of marine and continental glacial and interglacial events, Arctic Ocean and Banks Island. Nature 311, 147-149.

Craig, H. 1961. Standards for reporting concentrations of deuterium and ^{18}O in natural waters. Science 133, 1833-1834.

Craig, H. and Gordon, L.I. 1965. Isotopic oceanography. In: Symp. Marine Geochemistry, 3. Narragansett Marine Lab., Univ. Rhode Island, 277-374.

Dansgaard, W., Johnsen S. J., Clausen, H.B., Dahl-Jensen, D., Gundestrup, N.S., Hammer, C.U., Hvidberg, C.S., Steffensen, J.P. Sveinsbjornsdottir, A.E., Jouzel, J., and Bond, G. 1993. Evidence for general instability of past climate from a 250-kyr ice-core record. Nature 364, 218-220.

Dansgaard, W., Johnsen S. J., Clausen, H.B., and Gundestrup, N.S. 1973. Stable isotope glaciology. Meddelelser om Grønland 197(2), 1-53.

Dansgaard W., White, J.W.C. and Johnsen, S.J. 1989. The abrupt termination of the Younger Dryas climate event. Nature 339, 532-534.

Dethleff, D. 1995. Die Laptevsee - eine Schlüsselregion für den Fremdstoffeintrag in das arktische Meereis. Dissertation, Mat.-Nat. Fak. Univ. Kiel., 111pp.

Dethleff, D., Nürnberg, D., Reimnitz, E., Saarso, M., and Savchenko, Y. P. 1993. East Siberian Arctic Region Expedition 1992: The Laptev Sea - its significance for arctic sea-ice formation and transpolar sediment flux. Ber. Polarforschung 120, 44pp.

Dinter, D.A., Carter, L., and Brigham-Grette, J. 1990. Late Cenozoic geologic evolution of the Alaskan North Slope and adjacent continental shelves. In: Grantz, A., Johnson, L. and Sweeney, J. F. (eds.). The Arctic Ocean Region, The Geology of North America , vol. L., Geological Society of America, Boulder, Colorado, 459-490.

Dokken, T. 1995. Last interglacial/glacial cycle on the Svalbard/Barents Sea margin. Ph.D. dissertation, University of Tromsø.

Donk, J. V. and Mathieu, G. 1969. Oxygen isotope compositions of foraminifera and water samples from the Arctic Ocean. J. Geophys. Res. 74 (13), 3396-3407.

Dredge, L.A. and Thorleifson, L.H. 1987. The middle Wisconsian history of the Laurentide Ice Sheet. Géographie Physique et Quaternaire 41, 215-235.

Duplessy, J.-C., Labeyrie, L., Arnold, M., Paterne, M., Duprat, J., and van Weering, T. C. E. 1992. Changes in surface salinity of the North Atlantic Ocean during the last deglaciation. Nature 358, 485-487.

Duplessy, J.-C., Labeyrie, L., Juillet-Leclerc, A., Maitre, F., Duprat, J., and Sarnthein, M. 1991. Surface salinity reconstruction of the North Atlantic Ocean during the last glacial maximum. Oceanologica Acta, 14(4), 311-324.

Duplessy, J.-C. and Bé, A.W.H. 1981. Oxygen-18 enrichment of planktonic foraminifera due to gametogenic calcification below the euphotic zone. Science Reprint Series 213, 1247-1250.

Duplessy, J.-C., Shackleton, N.J., Fairbanks, R.G., Labeyrie, L.D., Oppo, D., and Kallel, N. 1988. Deepwater source variations during the last climatic cycle and their impact on the global deepwater cirkulation. Paleoceanography 3(3), 343-360.

Dyke, A.S. and Prest, V.K. 1987. Late Wisconsian and Holocene record of the Laurentide Ice Sheet. Géographie Physique et Quaternaire 41, 237-263.

Eisenhauer, A., Mangini, A., Botz, R., Walter, P., Bonani, G., Suter, M., Hofmann, H. J., and Wölfli, W. 1990. High resolution ^{230}Th and ^{10}Be stratigraphy of late Quaternary sediments from the Fram Strait (core 23235). In: Bleil, U. and Thiede, J. (eds.), Geological history of the Polar Oceans: Arctic versus Antarctic, NATO ASI Series C 308, Kluwer Academic Publishers, Dordrecht, Netherlands, 475-487.

Eisenhauer, A., Spielhagen, R. F., Frank, M., Hentzschel, G., Mangini, A., Kubik, P.W., Dietrich-Hannen, B., and Billen, T. 1994. ^{10}Be records of sediment cores from high northern latitudes: Implications for environmental and climatic changes. Earth Planet. Sci. Lett. 124, 171-184.

Elverhøi, A., Andersen, E.S., Dokken, T., Hebbeln, D., Spielhagen, R., Svendsen, J. I., Sørflaten, M., Rørnes, A., Hald., M., and Forsberg, C.F. 1995. The growth and decay of the late Weichselian ice sheets in western Svalbard and adjacent areas based on provenance studies of marine sediments. Quaternary Research 44(3), 303-316.

Elverhøi, A., Fjeldskaar, W., Solheim, A., Nyland-Berg, M., and Russwurm, L. 1993. The Barents Sea ice sheet - a model of its growth and decay during the last ice maximum. Quaternary Science Review 12, 863-873.

England, J. 1985. The late Quaternary history of Hall Land, Northwest Greenland. Canad. J. Earth Sci. 23, 1-17.

England, J. and Bradley, R.S. 1978. Past glacial activity in the Canadian high Arctic. Science 200, 265-270.

Epstein, S., Buchsbaum, H., Lowenstam, H., and Urey, H.C. 1953. Revised carbonate-water isotopic temperature scale. Geol. Soc. Am. Bull. 64, 1315-1325.

Fairbanks, R. G. 1989. A 17,000-year glacio-eustatic sea level record: influence of glacial melting rates on the Younger Dryas event and deep-ocean cirkulation. Nature 342, 637-642.

Fillon, R. H. 1984. Ice-age Arctic Ocean ice-sheets: a possible direct link with insolation. In: Berger, A.L. Hays, J.D. Kukla, G.J., and Salzman, B. (eds.). Milankovitch and climate. Reidel, Dordrecht, 223-240.

Frederichs, T. 1995. Regionale und altersabhängige Variation gesteinsmagnetischer Parameter in marinen Sedimenten der Arktis. Ber. Polarforsch. 164, 174pp.

Funder, S. 1989. Quaternary geology of the ice-free areas and adjacent shelves of Greenland. Quaternary geology of Canada and Greenland. In: Fulton, R.J. (ed.). The Geology of North America, vol. K-1, Geological Society of America, Boulder, Colorado, 743-792.

Funder, S. and Hansen., L. 1996. The Greenland ice sheet - a model for its culmination and decay during and after the last glacial maximum. Bull. Geol. Soc. Denmark 42(2), 137-152.

Fütterer, D. (1992). ARCTIC'91: The expedition ARK-VIII/3 with RV 'Polarstern' 1991. Ber. Polarforschung 107, 267pp.

Gard, G. 1986. Calcareous nannofossil biostratigraphy of Late Quaternary Arctic sediments. Boreas 15, 217-229.

Gard, G. 1993. Late Quaternary coccoliths at the North Pole: Evidence of ice-free conditions and rapid sedimentation in the central Arctic Ocean. Geology 21, 227-230.

GEOSECS 1987. Atlantic, Pacific, and Indian Ocean expeditions: shorebased data and graphics. In: Östlund, H.G., Craig, H., Broecker, W.S. and Spencer, I.D.O.E., GEOSECS Executive Committee, National Science Foundation, 7.

Gloersen, P., Campbell, W.J., Cavalieri, D.J., Comiso, J.C., Parkinson, C.L., and Zwally, H.J. 1992. Arctic and Antarctic sea ice, 1978-1987: satellite passive-microwave observations and analysis. NASA SP-511, National Aeronautics and Space Administration, Washington D.C., 290pp.

Gordienko, P. A. and Laktionov, A. F. 1969. Circulation and physics of the Arctic Basin waters. In: Annals Int. Geophys. Year, XLVI Oceanography, Pergamon Press, New York, 94-112.

Gorshkov, S. E. 1983. World Ocean Atlas, vol. 3, Arctic Ocean (in russian), Pergamon, New York, 189pp.

Grantz, A., Johnson, L. and Sweeney, J. F. (eds.) 1990. The Arctic Ocean Region, The Geology of North America, vol. L. Geological Society of America, Boulder, Colorado, 644pp.

Grootes, P.M., Stuiver, M., White, J.W.C., Johnsen, S., and Jouzel, J. 1993. Comparison of oxygen isotope records from the GISP2 and GRIP Greenland ice cores. Nature 366, 552-554.

Grosswald, M.G. 1980. Late Weichselian Ice Sheet of northern Eurasia. Quaternary Research 13, 1-32.

Grosswald, M.G 1993. Extent and melting history of the Late Weichselian Ice Sheet, the Barents-Kara Continental Margin. In: Peltier, W.R. (ed.), Ice in the climate system, NATO ASI Series, vol. I 12, Springer-Verlag, Berlin Heildelberg, 1-20.

Grousset, F. E., Labeyrie, L., Sinko, J. A., Cremer, M., Bond, G., Duprat, J., Cortijo, E., and Huon, S. 1993. Patterns of ice-rafted debris in the glacial North Atlantic (40-55°N). Paleoceanography 8, 175-192.

Hebbeln, D. 1991. Spätquartäre Stratigraphie und Paläozeanographie in der Fram-Straße. Dissertation Fachbereich Geowissenschaften der Universität Bremen, 139pp.

Hebbeln, D., Dokken, T., Andersen, E. S., Hald, M., and Elverhøj, A. 1994. Moisture supply for northern ice-sheet growth during the Last Glacial Maximum. Nature 370, 357-360.

Hebbeln, D. and Wefer, G. 1991. Effect of ice coverage and ice-rafted material on sedimentation in the Fram Strait. Nature 350, 409-411.

Heinrich, H. 1988. Origin and consequences of cyclic ice rafting in the northeast Atlantic Ocean during the past 130,000 years. Quaternary Research 29, 143-152.

Henrich, R., Wolf, T., Bohrmann, G., and Thiede, J. 1989. Cenozoic paleoclimatic and paleoceanographic changes in the northern hemisphere revealed by variability of coarse fraction composition in sediments from the Vøring Plateau - ODP Leg 104 Drill sites. In: Eldholm, O., Thiede, J., and Taylor, E. (eds.), Proc. ODP Scientific Results 104, College Station, Texas, Ocean Drilling Program, 77-188.

Herman, Y. 1989. The Arctic Seas: climatology, oceanograhy, geology, and biology. Van Nostrand Reinhold Company, New York, 888pp.

Herman, Y., Osmond, J.K., and Somayajulu, B.L.K. 1989. Late Neogene Arctic paleoceanography: micropaleontology, stable isotopes, and chronology. In: Herman, Y. (ed.). The Arctic Seas: climatology, oceanograhy, geology, and biology. Van Nostrand Reinhold Company, New York, 581-655.

Hemleben, C., Spindler, M., and Anderson, O.R. 1989. Modern planktonic foraminifera. Springer Verlag, New York, 1989, 363pp.

Hodgson, D.A. 1989. Quaternary geology of the Queen Elizabeth Islands. In: Fulton (ed.). Quaternary geology of Canada and Greenland. The Geology of North America, vol. K-1, Geological Society of America., 443-477.

Hodgson, D.A. 1991. The Quaternary record. In: Trettin, H.P. (ed.). Geology of the Innutian Orogen and Arctic Platform of Canada and Greenland. The Geology of North America, vol. E., Geological Society of America, 499-513.

Hodgson, D.A. 1994. Episodic ice streams and ice shelves during retreat of the northwesternmost sector of the late Wisconsian Laurentide Ice Sheet over the central Canadian arctic archipelago. Boreas 23, 14-28.

Holmes, M.L. and Creager, J.S. 1974. Holocene history of the Laptev Sea continental shelf. In: Herman, Y. (ed.). Marine geology and oceanography of the Arctic Seas. Springer Verlag, Berlin, 211-230.

Hughes, T.J., Denton, G.H., and Grosswald, M.G. 1977. Was there a late Würm Arctic ice-sheet? Nature 266, 596-602.

Hunkins, K. 1991. Laboratory studies of exchange between a polar and a subpolar basin. In: Weller, I.G., Wilson, C.L. and Severin, B.A.B. (eds.). Proceedings of the international conference on the role of the polar regions in global change, june 11-15, 1990, University of Fairbanks, 304-309.

Imbrie, J., Hays, J.D. , Martinson, D.G., McIntyre, A., Mix, A.C., Morley, J. J., Pisias, N.G., Prell, W.L., and Shackleton, N.J. 1984. The orbital theory of Pleistocene climate: support from a revised chronology of the marine $\delta^{18}O$ record. In: Berger, A.L. et al. (eds.) Milankovitch and climate, Part 1, Reidel Publ. Company, Dordrecht, Netherlands, 269-305.

Imbrie, J. and Kipp, N.G. 1971. A new micropaleontological method for quantitative paleoclimatology: application to a late Pleistocene Caribbean core. In: Turekian, K.K. (ed.). The Late Cenozoic glacial ages. Yale University Press, New Haven, Connecticut.

International Arctic Buoy Program (IABP) brochure 1994.

Jansen, E. 1989. The use of stable oxygen and carbon isotope stratigraphy as a dating tool. Quaternary International 1, 151-166.

Jeffries, M.O., Krouse, H.R., Sackinger, W.M., and Serson, H.V. 1989. Stable-isotope ($^{18}O/^{16}O$) tracing of fresh, brackish, and sea ice in multi-year land-fast ice, Ellesmere Island, Canada. J. Glaciol. 35, 9-16.

Johnsen S. J., Clausen, H.B., Dansgaard W., Fuhrer, K., Gundestrup, N.S., Hammer, C.U., Iversen, P., Steffensen, J.P., Jouzel, J., and Stauffer, B. 1992. Irregular glacial interstadials recorded in a new Greenland ice core. Nature 359, 311-313.

Jones, G.A., Gagnon, A., von Reden, K.F., McNichol, A.P., and Schneider, R.J. 1994. High precision AMS radiocarbon measurements of central Arctic Ocean sea waters. Nucl. Instr. Meth. B(92), 426-430.

Jones, G.A. and Keigwin, L.D. 1988. Evidence from Fram Strait (78°N) for early deglaciation. Nature 336, 56-59.

Kassens , H. and Thiede, J. 1994. Climatological significance of arctic sea ice at present and in the past. In: Kassens, H., Hubberten, H.-W., Pryamikov, S. M., and Stein, R. (eds.). Russian-German cooperation in the Siberian Shelf Seas: Geo-system Laptev-Sea. Ber. Polarforsch. 144, 81-85.

Keigwin, L. D. 1982. An Arctic Ocean ice-sheet in the Pleistocene? Nature 296, 808-809.

Kelly, M. and Bennike, O. 1985. Quaternary geology of parts of central and western North Greenland. Geol. Survey of Greenland, Report 126, 111-116.

Kempena, E. W., Reimnitz, E., and Barnes, P. 1989. Sea ice sediment entrainment and rafting in the Arctic. J. Sediment. Petrol. 59, 308-317.

Koc, N. and Jansen, E. 1994. Response of the high-latitude Northern Hemisphere to orbital climate forcing: evidence from the Nordic Seas. Geology 22, 523-526.

Kohfeld, K.E., Fairbanks, R.G., Smith, S.L., and Walsh, I.D. 1995. Decoupling of abundance and geochemical signals of *Neogloboquadrina pachyderma* (left) in polar marine sediments, as seen in plankton tows and sediment traps. ICP V program and abstracts, 163. 5th International Conference on Paleoceanography, October 10-14, 1995, Halifax , Canada, 163pp.

Köhler, S. E. I. 1992. Spätquartäre paläo-ozeanographische Entwicklung des Nordpolarmeeres und Europäischen Nordmeeres anhand von Sauerstoff- und Kohlenstoffisotopenverhältnissen der planktischen Foraminifere *Neogloboquadrina pachyderma* (sin.). GEOMAR Report 13, 103pp.

Kubisch, M. 1992. Die Eisdrift im Arktischen Ozean während der letzen 250.000 Jahre. GEOMAR Report 16, 100pp.

Labeyrie, L., Duplessy, J-C. 1985. Changes in the oceanic $^{13}C/^{12}C$ ratio during the last 140,000 years: high-latitude surface water records. Palaeogeogr., Palaeoclimatol., Palaeoecol. 50, 217-240.

Lambeck, K. 1996. Limits on the areal extent of the Barents Sea Ice Sheet in Late Weichselian time. Global and Planetary Change 12, 41-51.

Larssen, B. B., Elverhøi, A., and Aagaard, P. 1987. Study of particulate material in sea ice in the Fram Strait. Polar Res. 5, 313-315.

Lehman, S. J., Wright, D.G., and Stocker, T.S. 1993. Transport of freshwater into the deep ocean by the conveyor. In: Peltier, W.R. (ed.). Ice in the climate system. NATO ASI Series, Vol. I12. Springer-Verlag, Berlin, Heidelberg, 187-208.

Letzig, T. 1995. Meereistransportiertes lithogenes Feinmaterial in spätquartären Tiefseesedimenten des östlichen Arktischen Ozeans und der Fram Straße. Ber. Polarforschung 162, 98pp.

MacDonald, R. 1996. Awakenings in the Arctic. Nature 380, 286-287.

MacDonald, R.W. and Carmack, E.C. 1991. Age of Canada Basin deep waters: A way to estimate primary production for the Arctic Ocean. Science 254, 1348pp.

MacDonald, R.W., Carmack, E.C., and Wallace, D.W.R. 1993. Tritium and radiocarbon dating of Canada Basin deep waters. Science 259, 103pp.

Mangerud, J. 1991. The Scandinavian Ice Sheet through the last interglacial/glacial cycle. In: Frenzel, B. (ed). Klimageschichtliche Probleme der letzten 130,000 Jahre. Paläoklimaforschung 1, G. Fischer, Stuttgart, New York, 307-330.

Mangerud, J., Bolstad, M., Elgersma, A., Helliksen, D., Landvik, J.Y., Lønne, I., Lycke, A.K., Sandahl, T., and Svendsen, J.I. 1992. The last glacial maximum on western Svalbard. Quaternary Research 38, 1-31.

Mangerud, J., Jansen, E., and Landvik, J. Y. 1996. Late Cenozoic history of the Scandinavian and Barents Sea ice sheets. Global and Planetary Change 12, 11-26.

Mangerud, J. and Svendsen, J.I. 1992. The last interglacial-glacial period on Spitsbergen, Svalbard. Quaternary Science Reviews 11, 633-644.

Markussen, B. 1986. Late Quarternary sedimentation and paleoceanography in the eastern Arctic Ocean. Dr. Scient Thesis, Dept. of Geology, University of Oslo, 174pp.

Markussen, B., Zahn, R., and Thiede, J. 1985. Late Quaternary sedimentation in the eastern Arctic basin: stratigraphy and depositional environment. Palaeogeogr., Palaeoclimatol., Palaeoecol. 50, 271-284.

Martinson, D.G., Pisias, N.G., Hays, N.D., Imbrie, J., Moore, T.C., and Shackleton, N.J. (1987): Age dating and the orbital theory of the ice ages: development of a high-resolution 0 to 300,000 year chronostratigraphy. Quaternary Research 27, 1-29.

Meese, D., Alley, R., Gow, T., Grootes, P.M., Mayewski, P., Ram, M., Taylor, K., Waddington, E., and Zielinski, G., 1994. Preliminary depth-age scale of the GISP2 ice core. CRREL Special Report 94-1.

Melling, H. and Moore, R.M. 1995. Modification of halocline source waters during freezing on the Beaufort Sea Shelf: evidence from oxygen isotopes and dissolved nutrients. Continental Shelf Research 15 (1), 89-113.

Mienert, J., Mayer, L., Jones, G.A., and King, J.W. 1990. Physical and acoustic properties of Arctic Ocean deep-sea sediments: Paleoenvironmental implications. In: Bleil, U. & Thiede, J. (eds). Geological history of the Polar Oceans: Arctic versus Antarctic. NATO ASI Series C 308, Kluwer Academic Publishers, Dordrecht, 455-473.

Minicucci, D. A. and Clark, D. L. 1983. A late Cenozoic stratigraphy for glacial-marine sediments of the eastern Alpha Cordillera, Central Arctic Ocean. In: Molnia, B.F. (ed.). Glacial-marine sedimentation, Plenum, New York, 331-366.

Molfino, B. 1992. Technique and calibration bias in paleoestimation. Ber. Rep. Geol. Paläont. Inst. Univ. Kiel, 57, 204-205.

Molnar, M. 1995. Die Datierung von Sedimentkernen aus dem Arktischen Ozean. Diplomarbeit, Fakultät für Physik und Astronomie, Universität Heidelberg.

Molnia, B. F. 1972. Pleistocene ice rafting in the North Atlantic Ocean. Ph. D. dissertation. Columbia, Univ., South Carolina, 103pp.

Morris, T.H. and Clark, D.L. 1986. Pleistocene calcite lysocline and paleocurrents of the central Arctic Ocean and their paleoclimatic significance. Paleoceanography 1(2), 181-195.

Morris, T.H., Clark, D.L., and Blasco, S.M. 1985. Sediments of the Lomonosov Ridge and Makarov Basin: a Pleistocene stratigraphy for the North Pole. Geol. Soc. America Bull. 96, 901-910.

Naidu, S.A. and Mowatt, T.C. 1992. Origin of gravels from the southern coast and continental shelf of the Beaufort Sea. ICAM Proceedings, Anchorage, Alaska, 351-356.

Nansen, F. 1897. Farthest North. Archibald Constable & Co., Whitehall Gardens, 510pp.

Nansen, F. 1902. The oceanography of the North Polar Basin, Norwegian North Polar Expedition, 1893-1896. Sci. Res. V(IX), 427pp.

Nansen Arctic Drilling Program NAD Science Committee 1991. The Arctic Ocean record: key to global change (Initial Science Plan). Polarforschung 61(1), 102pp.

Nowaczyk, N.R. and Baumann, M. 1992. Combined high-resolution magnetostratigraphy and nannofossil biostratigraphy for late Quaternary Arctic Ocean sediments. Deep-Sea Reseach 39, Suppl. 2, 567-601.

Nowaczyk, N.R., Frederichs, T.W., Eisenhauer, A., and Gard, G. 1994. Magnetostratigraphic data from the late Quaternary sediments from the Yermak Plateau, Arctic Ocean: evidence for four geomagnetic polarity events within the last 170 Ka of the Brunhes Chron. Geophys. J. Int. 117, 453-471.

Nürnberg, D., Fütterer, D.K., Niessen, F., Nørgaard-Pedersen, N., Schubert, C.J., Spielhagen, R.F., and Washner, M. 1995. The depositional environment of the Laptev Sea continental margin: preliminary results from the R/V POLARSTERN ARK IX-4 cruise. Polar Research 14(1), 43-54.

Nürnberg, D., Wollenburg, I., Dethleff, D., Eicken, H., Kassens, H., Letzig, T., Reimnitz, E., and Thiede, J. 1994. Sediments in arctic sea ice - implications for entrainment, transport and release. Marine Geology 119, 185-214.

Okulitch, A.V. 1991. Geology of the Innutian Orogen and Arctic Platform of Canada and Greenland, map sheet, 1:200,000. In: Trettin, H.P. (ed.). Geology of the Innutian Orogen and Arctic Platform of Canada and Greenland. Geology of Canada, no 3., Geological Survey of Canada.

Okulitch, A.V., Lopatin, B.G., and Jackson, H.R. 1989. Circumpolar geological map of the Arctic, Geol. Surv. Canada, Map 1765A, 1:600,000.

Olausson, E. 1985. The glacial oceans. palaeogeogr., palaeoclimatol., palaeoecol. 50, 291-301.

Östlund, G., Possnert, G., and Swift, J.H. 1987. Ventilation rate of the deep Arctic Ocean from carbon 14 data. J. Geophys. Res. 92(C4), 3769-3777.

Pagels, U. 1992. Sedimentologische Untersuchtungen und Bestimmung der Karbonatlösung in spätquartären Sedimenten des östlichen Arktischen Ozeans. GEOMAR Report 10, 106p.

Paterson, W.S.B. and Hammer, C.U. 1987. Ice core and other glaciological data. In: Ruddimann, W.F. and Wright, H.E. Jr. (eds.). North America and adjacent oceans during the last deglaciation. The geology of North America, vol. K-3, Geological Society of America, Boulder, Colorado, 91-109.

Peltier, W.R. 1994. Ice age paleotopography. Science 265, 195-201.

Pfirman, S., Lange, M.A., Wollenburg, I., and Schlosser, P. 1990. Sea ice characteristics and the role of sediment inclusions in deep-sea deposition: Arctic-Antarctic comparison. In: Bleil, U. and Thiede, J., (eds.). Geological history of the Polar Oceans: Arctic versus Antarctic, NATO ASI Series C 308, Kluwer Academic Publishers, Dordrecht, 187-211.

Pflaumann, U., Duprat, J., Pujol, C., and Labeyrie, L.D. 1996. SIMMAX: a modern analog technique to deduce Atlantic sea surface temperatures from planktonic foraminifera in deep sea sediments. Paleoceanography 11(1), 15-35.

Phillips, R.L. and Grantz, A. 1995. Variations in provenance and abundance of ice-rafted clasts in Arctic Ocean sediments: implications for configuration and stability of latest Wisconsin and Holocene paleocurrents. ICP V program and abstracts, 5th International Conference on Paleoceanography, October 10-14, 1995, Halifax, Canada, 168pp.

Phillips, R.L., Grantz, A., Mullen, M.W., Rieck, H.J., McLaughlin, M.W., and Selkirk, T.L. 1992. Summary of lithostratigraphy and stratigraphic correlations in piston cores from Northwind Ridge, Arctic Ocean, from USGGC Polar Star, 1988. U.S. Geol. Surv. open-file report, 110pp.

Pisias, N.G., Martinson, D.G., Moore, T.C., Jr., Shackleton, N.J., Hays, N.D., and Boden, G. 1984. High resolution stratigraphic correlation of benthic oxygen isotopic records spanning the last 300,000 years. Marine Geology 56, 119-136.

Poore, R.Z., Ishman, S.E., Phillips, R.L., and McNeil, D.H. 1994. Quaternary stratigraphy and paleoceanography of the Canada Basin, western Arctic Ocean. U.S. Geol. Surv. Bull. 2080, 32pp.

Poore, R.Z., Phillips, R.L., and Rieck, H.J. 1993. Paleoclimate record for Northwind Ridge, western Arctic Ocean. Paleoceanography 8, 149-159.

Porter, S.C. 1989. Some geological implications of average Quaternary glacial conditions. Quaternary Research 32, 245-261.

Rachor, E. 1997. Arctic Expedition ARK XI/1 of RV 'Polarstern' in 1995. Ber. Polarforschung 226, 157pp.

Reeh, N. 1990. Past changes in precipitation rate and ice thickness as derived from age - depth profiles in ice-sheets; application to Greenland and Canadian Arctic ice core records. In: Bleil, U. and Thiede, J. (eds.). Geological history of the Polar Oceans: Arctic versus Antarctic, NATO ASI Series C308, Kluwer Academic Publishers, Dordrecht, 255-271.

Reimnitz, E. 1994. The Laptev Sea shelf regime from a western perspective. In: Kassens, H., Hubberten, H.-W., Pryamikov, S.M., and Stein, R. (eds.). Russian-German cooperation in the Siberian Shelf Seas: Geo-system Laptev-Sea. Ber. Polarforsch. 144, 45-47.

Reimnitz, E. and Kempena, E.W. 1987. Field observations of slush ice generated during freeze-up in arctic coastal waters. Marine Geology 77, 219-231.

Reimnitz, E., Kempena, E.W., and Barnes, P. 1987. Anchor ice, seabed freezing, and sediment dynamics in shallow arctic seas. J. Geophys. Res. 92 (C13), 14671-14678.

Rudels, B. 1987. On the mass balance of the Polar Ocean with special emphasis on the Fram Strait. Norsk Polar Skr. 188, 1-53.

Rudels, B., Jones, E.P., Anderson, L.G. and Kattner, G. 1994. On the intermediate waters of the Arctic Ocean. In: Johannesen, O.M., Muench, R.D., and Overland, J.E. (eds.). The Polar Oceans and their role in shaping the global environment. Geophysical Monograph 85, American Geophysical Union, 33-46.

Rudels, B. and Quadfasel, D. 1991. Convection and deep water formation in the Arctic Ocean - Greenland Sea system. J. Marine Systems 2, 435-450.

Rutter, N. 1995. Problematic ice sheets. Quaternary International 28, 19-37.

Sarnthein, M. 1971. Oberflächensedimente im Persischen Golf und dem Golf von Oman II. Quantitative Komponentenanalyse der Grobfraktion. "Meteor" Forschungsergebnisse, Reihe C5, 1-113.

Sarnthein, M. Jansen, E. Arnold, M., Duplessy, J.-C., Erlenkeuser, H., Flatoy, A., Veum, T., Vogelsang, E., and Weinelt, M. S. 1992. $\delta^{18}O$ time-slice reconstruction of melt-water anomalies at Termination I in the North Atlantic between 50 and 80 °N. In: Bard, E. and Broecker, W. S. (eds.). The last deglaciation: absolute and radiocarbon chronologies. Series I: Global Environmental Change, Vol. 2. NATO ASI Series, Springer Verlag, 183-200.

Sarnthein, M. Jansen, E., Weinelt, M., Arnold, M., Duplessy, J.-C. Erlenkeuser, H., Flatoy, A., Johannessen, G., Johannessen, T., Jung, S., Koc, N., Labeyrie, L., Maslin, M., Pflaumann, U., and Schultz, H. 1995. Variations in Atlantic surface ocean paleoceanography, 50°-80°N: A time-slice record of the last 30,000 years. Paleoceanography 10(6), 1063-1094.

Schauer, U., Rudels, B., Muench, R.D., and Timokhov, L. 1995. Cirkulation and water mass modifications along the Nansen Basin slope. Ber. Polarforsch. 176, 94-106.

Schäfer-Neth, C. 1994. Modellierung der Paleoozeanographie des nördlichen Nordatlantiks zur letzen Maximalvereisung. Ber. Sonderforschungsbereich 313, 51, Universität Kiel, 105pp.

Schäper, S. 1994. Quartäre Sedimentation im polnahen Arktischen Ozean. Diplomarbeit, Fak. für Physik und Astronomie, Ruprecht-Karls-Universität, Heidelberg, 113pp.

Schlosser, P., Bönisch, G., Kromer, B., Münnich, K.O., and Koltermann, P. 1990. Ventilation rates of the waters in the Nansen Basin of the Arctic Ocean derived from a multitracer approach. J. Geophys. Res. 95(C3), 3265-3272.

Schneider, D.A., Backman, J., Curry, W.B., and Possnert, G. 1996. Paleomagnetic constraints on sedimentation rates in the eastern Arctic Ocean. Quaternary Research 46, 62-71.

Schubert, C.J. 1995. Organischer Kohlenstoff in spätquartären Sedimenten des Arktischen Ozeans: terrigener Eintrag und marine Produktivität. Ber. Polarforsch. 177, 178pp.

Seidov, D, Sarnthein, M., Stattegger, K., Prien, R., and Weinelt, M. 1996. North Atlantic ocean circulation during the last glacial maximum and subsequent meltwater event: A numerical model. J. Geophys. Research 101(C7), 16305-16333.

Shackleton, N.J. 1974. Attainment of isotopic equilibrium between ocean water and the benthonic foraminifera *Uvigerina*: isotopic changes in the ocean during the last glacial. Coll. Int. CNRS, 219, 203-209.

Sowers, T., Bender, M., Labeyrie, L., Martinson, D., Jouzel, J., Raynaud, D., Pichon, J.J., and Korotkevich, Y. 1993. 135,000 year Vostok-SPECMAP common temporal framework. Paleoceanography 8, 737-766.

Spielhagen, R.F. 1991. Die Eisdrift in der Framstrasse während der letzten 200,000 Jahre. GEOMAR Report 4, 133pp.

Spielhagen. R. F., Eisenhauer, A., Frank, M., Frederichs, T., Kassens, H., Mangini, A., Nowaczyk, N.R., Nørgaard-Pedersen, N., Schäper, S., Stein, R., Thiede, J., Tiedemann, R., Wahsner, M., Bonani, G., and Kubik, P.W. (subm.). Arctic Ocean evidence for Late Quaternary initiation of northern Eurasian ice sheets. Geology.

Spielhagen. R. F. and Erlenkeuser, H. 1994. Stable oxygen and carbon iostopes in planktic foraminifers from Arctic Ocean surface sediments: Reflection of the low salinity surface water layer. Marine Geology 119, 227-250.

Spielhagen. R. F. and Thiede, J. 1994. Late Quaternary changes in the Arctic Ocean ice cover. In: H. Kassens, H.-W. Hubberten, S. M. Pryamikov and R. Stein (eds.). Russian-German Cooperation in the Siberian Shelf Seas: Geo-system Laptev-Sea. Ber. Polarforschung 144, 101-105.

Stein, R., Grobe, H., and Washner, M. 1994a. Organic carbon, carbonate, and clay mineral distribution in eastern central Arctic Ocean surface sediments. Marine Geology 119, 269-285.

Stein, R., Nam, S.I., Schubert, C., Vogt, C., Fütterer, D., and Heinemeier 1994b. The last deglaciation event in the eastern Central Arctic Ocean. Science 264, 692-696.

Stein, R., Schubert, C., Vogt, C., and Fütterer, D. 1994c. Stable isotope stratigraphy, sedimentation rates and paleosalinity in the latest Pleistocene to Holocene Central Arctic Ozean. Marine Geology 119, 333-355.

Stuiver, M., Pearson, G.W., and Braziunas, T. 1986. Radiocarbon age calibration of marine samples back to 9000 cal yr BP. Radiocarbon 28(2B), 980-1021.

Streeter, S.S., Belanger, P.E., Kellogg, T.B., and Duplessy, J.-C. 1982. Late Pleistocene paleoceanography of the Norwegian-Greenland Sea : benthic foraminiferal evidence. Quaternary Research 18, 72-90.

Stuiver, M., Grootes, P.M., and Braziunas, T. 1995. The GISP2 $\delta^{18}O$ climate record of the past 16,500 years and the role of the sun, ocean, and volcanoes. Quaternary Research 44, 341-354.

Tauber, H. and Funder, S. 1975. ^{14}C content of recent molluscs from Scoresby Sund, central East Greenland, Geol. Survey of Greenland, Report 75, 95-99.

Taylor, K.C., Lamorey, G.W., Doyle, G.A., Alley, R.B., Grootes, P.M., Mayewski, P.A., White, J.W.C., and Barlow, L.K. 1993. The 'flickering' switch of Late Pleistocene climate change. Nature 361, 432-436.

Thiede, J. 1988. Scientific cruise report of Arctic Expedition ARK IV/3. Ber. Polarforsch. 43. 237pp.

Thiede, J., Clark, D.L., and Herman, Y. 1990. Late Mesozoic and Cenozoic paleoceanography of the northern polar oceans. In: Grantz, A., Johnson, L. and Sweeney, J.F. (eds.). The Arctic Ocean Region, The Geology of North America, vol. L., The Geological Society of America, Boulder, Colorado, 427-458.

Thiede, J. and Myhre, A.M. 1995. Non-steady behaviour in the Cenozoic polar North Atlantic system: the onset and variability of Northern Hemisphere glaciations. Phil. Trans. R. Soc. Lond. A, 352, 373-385.

Untersteiner, N. 1990. Structure and dynamics of the Arctic Ocean ice cover. In: Grantz, A., Johnson, L. and Sweeney, J. F. (eds.). The geology of North America, The Arctic Ocean region, vol. L., The Geological Society of America, Boulder Colorado, 37-51.

Veum, T., Jansen, E., Arnold, M., Beyer, I., and Duplessy, J.-C. 1992. Water mass exchange between the North Atlantic and the Norwegian Sea during the past 28,000 years. Nature 356, 783-785.

Vogelsang, E. 1990. Paläo-Ozeanographie des Europäischen Nordmeeres an Hand stabiler Kohlenstoff- und Sauerstoffisotope. Ber. Sonderforschungsbereich 313, 23, Universität Kiel, 136pp.

Vogt, C., Knies, J., Grobe, H., Spielhagen, R.F., and Stein, R. (in prep.). Late Quaternary paleoceanography near the NW-Spitsbergen coast and on the Yermak Plateau.

Vogt, C. (in prep.). Zeitliche und räumliche Verteilung von Mineralvergesellschaftungen in spätquartären Sedimenten des Arktischen Ozeans während Glazialen und Interglazialen und ihre Nützlichkeit als Klimaindikatoren. Dissertation, Fachbereich Geowissenschaften der Universität Bremen.

Vorren, T.O. and Laberg, J.S. 1996. Late glacial temperature, oceanographic and ice sheet interactions in the southern Barents Sea region. In: Andrews, J.T., Austin, W.E.N., Bergsten, H. and Jennings, A.E. (eds.). Late Qaternary paleoceanography of the North Atlantic margins, Geol. Soc. Spec. Publ. 111, 303-321.

Weinelt. M. 1993. Veränderungen der Oberflächenzirkulation im Europäischen Nordmeer während der letzten 60,000 Jahre - Hinweise aus stabilen Isotopen. Dissertation Mat.-Nat.-Fak., Universität Kiel, 106pp.

Winn, K., Sarnthein, M., and Erlenkeuser, H. 1991. $\delta^{18}O$ stratigraphy and chronology of Kiel sediment cores from the East Atlantic. Ber. Geol.-Paläont. Inst. u. Museum, Universität Kiel 45, 99pp.

Wollenburg, I. 1993. Sediment-transport durch das arktische Meereis: die rezente lithogene und biogene Materialfracht. Ber. Polarforsch. 127, 159pp.

Zahn, R., Markussen, B., and Thiede, J. 1985. Stable isotope data and depositional environments in the Late Quaternary Arctic Ocean. Nature 314, 433-435.

GEOMAR REPORTS

1 GEOMAR FORSCHUNGSZENTRUM FÜR MARINE GEOWISSENSCHAFTEN DER CHRISTIAN-ALBRECHTS-UNIVERSITÄT ZU KIEL
BERICHT FÜR DIE JAHRE 1987 UND 1988. 1989. 71 + 6 pp.
In German

2 GEOMAR FORSCHUNGSZENTRUM FÜR MARINE GEOWISSENSCHAFTEN DER CHRISTIAN-ALBRECHTS-UNIVERSITÄT ZU KIEL
JAHRESBERICHT / ANNUAL REPORT 1989. 1990. 96 pp.
In German and English

3 GEOMAR FORSCHUNGSZENTRUM FÜR MARINE GEOWISSENSCHAFTEN DER CHRISTIAN-ALBRECHTS-UNIVERSITÄT ZU KIEL
JAHRESBERICHT / ANNUAL REPORT 1990. 1991. 212 pp.
In German and English

4 ROBERT F. SPIELHAGEN
DIE EISDRIFT IN DER FRAMSTRASSE WÄHREND DER LETZTEN 200.000 JAHRE. 1991. 133 pp.
In German with English summary

5 THOMAS C. W. WOLF
PALÄO-OZEANOGRAPHISCH-KLIMATISCHE ENTWICKLUNG DES NÖRDLICHEN NORDATLANTIKS SEIT DEM SPÄTEN NEOGEN
(ODP LEGS 105 UND 104, DSDP LEG 81). 1991. 92 pp.
In German with English summary

6 SEISMIC STUDIES OF LATERALLY HETEROGENOUS STRUCTURES - INTERPRETATION AND MODELLING OF SEISMIC DATA.
Edited by ERNST R. FLUEH
Commission on Controlled Source Seismology (CCSS), Proceedings of the 8th Workshop Meeting, held at
Kiel - Fellhorst (Germany), August 27-31, 1990. 1991. 359 pp.
In English

7 JENS MATTHIESSEN
DINOFLAGELLATEN-ZYSTEN IM SPÄTQUARTÄR DES EUROPÄISCHEN NORDMEERES: PALÖKOLOGIE UND PALÄO-OZEANOGRAPHIE. 1991. 104 pp.
In German with English summary

8 DIRK NÜRNBERG
HAUPT- UND SPURENELEMENTE IN FORAMINIFERENGEHÄUSEN - HINWEISE AUF KLIMATISCHE UND OZEANOGRAPHISCHE ÄNDERUNGEN
IM NÖRDLICHEN NORDATLANTIK WÄHREND DES SPÄTQUARTÄRS. 1991. 117 pp.
In German with English summary

9 KLAS S. LACKSCHEWITZ
SEDIMENTATIONSPROZESSE AM AKTIVEN MITTELOZEANISCHEN KOLBEINSEY RÜCKEN (NÖRDLICH VON ISLAND). 1991. 133 pp.
In German with English summary

10 UWE PAGELS
SEDIMENTOLOGISCHE UNTERSUCHUNGEN UND BESTIMMUNG DER KARBONATLÖSUNG IN SPÄTQUARTÄREN SEDIMENTEN DES ÖSTLICHEN
ARKTISCHEN OZEANS. 1991. 106 pp.
In German with English summary

11 FS POSEIDON - EXPEDITION 175 (9.10.-1.11.1990)
175/1: OSTGRÖNLÄNDISCHER KONTINENTALRAND (65° N)
175/2: SEDIMENTATION AM KOLBEINSEYRÜCKEN (NÖRDLICH VON ISLAND)
Hrsg. von J. MIENERT und H.-J. WALLRABE-ADAMS. 1992. 56 pp. + app.
In German with some English chapters

12 GEOMAR FORSCHUNGSZENTRUM FÜR MARINE GEOWISSENSCHAFTEN DER CHRISTIAN-ALBRECHTS-UNIVERSITÄT ZU KIEL
JAHRESBERICHT / ANNUAL REPORT 1991. 1992. 152 pp.
In German and English

13 SABINE E. I. KÖHLER
SPÄTQUARTÄRE PALÄO-OZEANOGRAPHISCHE ENTWICKLUNG DES NORDPOLARMEERES UND EUROPÄISCHEN NORDMEERES ANHAND VON
SAUERSTOFF- UND KOHLENSTOFF- ISOTOTPENVERHÄLTNISSEN DER PLANKTISCHEN FORAMINIFERE
Neogloboquadrina pachyderma (sin.). 1992. 104 pp.
In German with English summary

14 FS SONNE - FAHRTBERICHT SO 78 PERUVENT: BALBOA, PANAMA - BALBOA, PANAMA, 28.2.1992-16.4.1992
Hrsg. von ERWIN SUESS. 1992. 120 pp.
In German with some English chapters

15 FOURTH INTERNATIONAL CONFERENCE ON PALEOCEANOGRAPHY (ICP IV): SHORT- AND LONG-TERM GLOBAL CHANGE:
RECORDS AND MODELLING 21-25 SEPTEMBER 1992, KIEL/GERMANY
PROGRAM & ABSTRACTS. 1992. 351 pp.
In English

16 MICHAELA KUBISCH
DIE EISDRIFT IM ARKTISCHEN OZEAN WÄHREND DER LETZTEN 250.000 JAHRE. 1992. 100 pp.
In German with English summary

17 PERSISCHER GOLF: UMWELTGEFÄHRDUNG, SCHADENSERKENNUNG, SCHADENSBEWERTUNG AM BEISPIEL DES MEERESBODENS; ERKENNEN
EINER ÖKOSYSTEMVERÄNDERUNG NACH ÖLEINTRÄGEN. Schlußbericht zu den beiden BMFT-Forschungsvorhaben 03F0055 A + B. 1993. 108 pp.
In German with English summary

18 TEKTONISCHE ENTWÄSSERUNG AN KONVERGENTEN PLATTENRÄNDERN / DEWATERING AT CONTINENTAL MARGINS.
Hrsg. von/ed. by ERWIN SUESS. 1993. 106 + 32 + 68 + 16 + 22 + 38 + 4 + 19 pp.
Some chapters in English, some in German

19 THOMAS DICKMANN
DAS KONZEPT DER POLARISATIONSMETHODE UND SEINE ANWENDUNGEN AUF DAS SEIMISCHE VEKTORWELLENFELD IM WEITWINKELBEREICH. 1993. 121 pp.
In German with English summary

20 GEOMAR FORSCHUNGSZENTRUM FÜR MARINE GEOWISSENSCHAFTEN DER CHRISTIAN-ALBRECHTS-UNIVERSITÄT ZU KIEL
JAHRESBERICHT / ANNUAL REPORT 1992. 1993. 139 pp.
In German and English

21 KAI UWE SCHMIDT
PALYNOMORPHE IM NEOGENEN NORDATLANTIK - HINWEISE ZUR PALÄO-OZEANOGRAPHIE UND PALÄOKLIMATOLOGIE. 1993. 104 + 7 + 41 pp.
In German with English summary

22 UWE JÜRGEN GRÜTZMACHER
DIE VERÄNDERUNGEN DER PALÄOGEOGRAPHISCHEN VERBREITUNG VON *BOLBOFORMA* - EIN BEITRAG ZUR REKONSTRUKTION UND DEFINITION VON WASSERMASSEN IM TERTIÄR. 1993. 104 pp.
In German with English summary

23 RV PROFESSOR LOGACHEV - Research Cruise 09 (August 30 - September 17, 1993): SEDIMENT DISTRIBUTION ON THE REYKJANES RIDGE NEAR 59°N
Edited by H.-J. WALLRABE-ADAMS & K.S. LACKSCHEWITZ. 1993. 66 + 30 pp.
In English

24 ANDREAS DETTMER
DIATOMEEN-TAPHOZÖNOSEN ALS ANZEIGER PALÄO-OZEANOGRAPHISCHER ENTWICKLUNGEN IM PLIOZÄNEN UND QUARTÄREN NORDATLANTIK. 1993. 113 + 10 + 25 pp.
In German with English summary

25 GEOMAR FORSCHUNGSZENTRUM FÜR MARINE GEOWISSENSCHAFTEN DER CHRISTIAN-ALBRECHTS-UNIVERSITÄT ZU KIEL
JAHRESBERICHT / ANNUAL REPORT 1993. 1994. 69 pp.
In German and English

26 JÖRG BIALAS
SEISMISCHE MESSUNGEN UND WEITERE GEOPHYSIKALISCHE UNTERSUCHUNGEN AM SÜD-SHETLAND TRENCH UND IN DER BRANSFIELD STRASSE - ANTARKTISCHE HALBINSEL. 1994. 113 pp.
In German with English summary

27 JANET MARGARET SUMNER
THE TRANSPORT AND DEPOSITIONAL MECHANISM OF HIGH GRADE MIXED-MAGMA IGNIMBRITE TL, GRAN CANARIA: THE MORPHOLOGY OF A LAVA-LIKE FLOW. 1994. 224 pp.
In English with German summary

28 GEOMAR LITHOTHEK. Edited by JÜRGEN MIENERT. 1994. 12 pp + app.
In English

29 FS SONNE - FAHRTBERICHT SO 97 KODIAK-VENT: KODIAK - DUTCH HARBOR - TOKYO - SINGAPUR, 27.7. - 19.9.1994
Hrsg. von ERWIN SUESS. 1994.
Some chapters in German, some in English

30 CRUISE REPORTS:
RV LIVONIA CRUISE 92, KIEL-KIEL, 21.8.-17.9.1992: GLORIA STUDIES OF THE EAST GREENLAND CONTINENTAL MARGIN BETWEEN 70° AND 80°N
RV POSEIDON PO200/10, LISBON-BREST-BREMERHAVEN, 7.-23.8.1993: EUROPEAN NORTH ATLANTIC MARGIN: SEDIMENT PATHWAYS, PROCESSES AND FLUXES
RV AKADEMIK ALEKSANDR KARPINSKIY, KIEL-TROMSØ, 5.-25.7.1994: GAS HYDRATES ON THE NORTHERN EUROPEAN CONTINENTAL MARGIN
Edited by JÜRGEN MIENERT. 1994.
In English; report of RV AKADEMIK ALEKSANDR KARPINSKIY cruise in English and Russian

31 MARTIN WEINELT
BECKENENTWICKLUNG DES NÖRDLICHEN WIKING-GRABENS IM KÄNOZOIKUM - VERSENKUNGSGESCHICHTE, SEQUENZSTRATIGRAPHIE, SEDIMENTZUSAMMENSETZUNG. 1994. 86 pp.
In German with English summary

32 GEORG A. HEISS
CORAL REEFS IN THE RED SEA: GROWTH, PRODUCTION AND STABLE ISOTOPES. 1994. 141 pp.
In English with German summary

33 JENS A.HÖLEMANN
AKKUMULATION VON AUTOCHTHONEM UND ALLOCHTHONEM ORGANISCHEM MATERIAL IN DEN KÄNOZOISCHEN SEDIMENTEN DER NORWEGISCHEN SEE (ODP LEG 104). 1994. 78 pp.
In German with English summary

34 CHRISTIAN HASS
SEDIMENTOLOGISCHE UND MIKROPALÄONTOLOGISCHE UNTERSUCHUNGEN ZUR ENTWICKLUNG DES SKAGERRAKS (NE NORDSEE) IM SPÄTHOLOZÄN. 1994.
In German with English summary

35 BRITTA JÜNGER
TIEFENWASSERERNEUERUNG IN DER GRÖNLANDSEE WÄHREND DER LETZTEN 340.000 JAHRE.
DEEP WATER RENEWAL IN THE GREENLAND SEA DURING THE PAST 340,000 YEARS. 1994. 6 + 109 pp.
In German with English summary

36 JÖRG KUNERT
UNTERSUCHUNGEN ZU MASSEN- UND FLUIDTRANSPORT ANHAND DER BEARBEITUNG REFLEXIONSSEISMISCHER DATEN AUS DER KODIAK-SUBDUKTIONSZONE, ALASKA. 1995. 129 pp.
In German with English summary

37 CHARLOTTE M. KRAWCZYK
DETACHMENT TECTONICS DURING CONTINENTAL RIFTING OFF THE WEST IBERIA MARGIN: SEISMIC REFLECTION AND DRILLING CONSTRAINTS. 1995. 133 pp.
In English with German summary

38 CHRISTINE CAROLINE NÜRNBERG
BARIUMFLUSS UND SEDIMENTATION IM SÜDLICHEN SÜDATLANTIK - HINWEISE AUF PRODUKTIVITÄTSÄNDERUNGEN IM QUARTÄR. 1995. 6 + 108pp.
In German with English summary

39 JÜRGEN FRÜHN
TEKTONIK UND ENTWÄSSERUNG DES AKTIVEN KONTINENTALRANDES SÜDÖSTLICH DER KENAI-HALBINSEL, ALASKA. 1995. 93 pp.
In German with English summary

40 GEOMAR FORSCHUNGSZENTRUM FÜR MARINE GEOWISSENSCHAFTEN DER CHRISTIAN-ALBRECHTS-UNIVERSITÄT ZU KIEL
JAHRESBERICHT / ANNUAL REPORT 1994. 1995.
In German and English

41 FS SONNE - FAHRTBERICHT / CRUISE REPORT SO 103 CONDOR 1 B: VALPARAISO-VALPARAISO, 2.-21.7.1995.
Hrsg. von ERNST R. FLUEH. 1995. 140 pp.
Some chapters in German, some in English

42 R/V PROFESSOR BOGOROV CRUISE 37: CRUISE REPORT "POSETIV": Vladivostok - Vladivostok, September 23 - October 22, 1994.
Edited by CHRISTOPH GAEDICKE, BORIS BARANOV and EVGENIY LELIKOV. 1995. 48 + 33 pp.
In English

43 CHRISTOPH GAEDICKE
DEFORMATION VON SEDIMENTEN IM NANKAI-AKKRETIONSKEIL, JAPAN. BILANZIERUNG TEKTONISCHER VORGÄNGE ANHAND VON SEISMISCHEN PROFILEN UND ERGEBNISSEN DER ODP-BOHRUNG 808. II + 89 pp.
In German with English summary

44 MARTIN ANTONOW
SEDIMENTATIONSMUSTER UM DEN VESTERIS SEAMOUNT (ZENTRALE GRÖNLANDSEE) IN DEN LETZTEN 250.000 JAHREN. 1995.
In German with English summary

45 INTERNATIONAL CONGRESS: CORING FOR GLOBAL CHANGE - ICGC '95. KIEL, 28 - 30 June, 1995.
Edited by JÜRGEN MIENERT and GEROLD WEFER. 1996.
In English

46 JENS GRÜTZNER
ZUR PHYSIKALISCHEN ENTWICKLUNG VON DIAGENETISCHEN HORIZONTEN IN DEN SEDIMENTBECKEN DES ATLANTIKS. 1995. 96 pp.
In German with English summary

47 INGO A. PECHER
SEISMIC STUDIES OF BOTTOM SIMULATING REFLECTORS AT THE CONVERGENT MARGINS OFFSHORE PERU AND COSTA RICA. 1996. 159 pp.
In English with German summary

48 XIN SU
DEVELOPMENT OF LATE TERTIARY AND QUATERNARY COCCOLITH ASSEMBLAGES IN THE NORTHEAST ATLANTIC. 1996. 120 pp. + 7 pl.
In English with German summary

49 FS SONNE - FAHRTBERICHT / CRUISE REPORT SO 108 ORWELL: SAN FRANCISCO - ASTORIA, 14.4. - 23.5.1996
Edited by ERNST R. FLUEH and MICHAEL A. FISHER. 1996.

50 GEOMAR FORSCHUNGSZENTRUM FÜR MARINE GEOWISSENSCHAFTEN DER CHRISTIAN-ALBRECHTS-UNIVERSITÄT ZU KIEL
JAHRESBERICHT / ANNUAL REPORT 1995. 1996. 93 pp.
In German and English

51 THOMAS FUNCK
STRUCTURE OF THE VOLCANIC APRON NORTH OF GRAN CANARIA DEDUCED FROM REFLECTION SEISMIC, BATHYMETRIC AND BOREHOLE DATA. 1996. VI, 144 pp.
In English with German summary

52 PETER BRUNS
GEOCHEMISCHE UND SEDIMENTOLOGISCHE UNTERSUCHUNGEN ÜBER DAS SEDIMENTATIONSVERHALTEN IM BEREICH BIOSTRATIGRAPHISCHER DISKONTINUITÄTEN IM NEOGEN DES NORDATLANTIK, ODP LEG 104, SITES 642B UND 643A. 1993. V, 73 pp.
n German with English summary

53 CHRISTIANE C. WAGNER
COLD SEEPS AN KONVERGENTEN PLATTENRÄNDERN VOR OREGON UND PERU: BIOGEOCHEMISCHE BESTANDSAUFNAHME. 1996. 108, XXXVI pp.
In German with English summary

54 FRAUKE KLINGELHÖFER
MODEL CALCULATIONS ON THE SPREADING OF SUBMARINE LAVA FLOWS. 1996. 98 pp.
In English with German summary

55 HANS-JÜRGEN HOFFMANN
OBJEKTORIENTIERTE ANALYSE UND MIGRATION DIFFRAKTIERTER WELLENFELDER UNTER VERWENDUNG DER STRAHLENMETHODE UND DER EDGE-WAVE-THEORIE. 1996. XXI, 153 pp.
In German with English summary

56 DIRK KLÄSCHEN
STRAHLENSEISMISCHE MODELLIERUNG UNTER BERÜCKSICHTIGUNG VON MEHRFACHDIFFRAKTIONEN MIT HILFE DER EDGE-WAVES: THEORIE UND ANWENDUNGSBEISPIELE. 1996. X, 159 pp.
In German with English summary

57 NICOLE BIEBOW
DINOFLAGELLATENZYSTEN ALS INDIKATOREN DER SPÄT- UND POSTGLAZIALEN ENTWICKLUNG DES AUFTRIEBSGESCHEHENS VOR PERU. 1996. IV, 100, 17, 14 (7 pl.) pp.
In German with English summary

58 RV SONNE - CRUISE REPORT SO109: HYDROTRACE. ASTORIA-VICTORIA-ASTORIA-VICTORIA. MAY 23 - JULY 8, 1996.
Ed. by PETER HERZIG, ERWIN SUESS, and PETER LINKE. 1997.
In English

59 RV SONNE - CRUISE REPORT SO110: SO - RO (SONNE - ROPOS). VICTORIA-KODIAK-VICTORIA. JULY 9 - AUGUST 19, 1996.
Ed. by ERWIN SUESS and GERHARD BOHRMANN. 1997.
In English

60 RV AKADEMIK M. A. LAVRENTYEV CRUISE 27. CRUISE REPORT: GREGORY. VLADIVOSTOK-PUSAN-OKHOTSK SEA-PUSAN-VLADIVOSTOK. SEPTEMBER 7 - OCTOBER 12, 1996. Ed. by DIRK NÜRNBERG, BORIS BARANOV, and BORIS KARP. 1997. 143 pp.
In English

62 FS SONNE - FAHRTBERICHT/CRUISE REPORT SO123: MAMUT (MAKRAN MURRAY TRAVERSE - GEOPHYSIK PLATTENTEKTONISCHER EXTREMFÄLLE). Maskat - Maskat, 07.09 - 03.10.1997.
Ed. by ERNST R. FLUEH, NINA KUKOWSKI, and CHRISTIAN REICHERT

63 RAINER ZAHN
NORTH ATLANTIC THERMOHALINE CIRCULATION DURING THE LAST GLACIAL PERIOD: EVIDENCE FOR COUPLING BETWEEN MELTWATER EVENTS AND CONVECTIVE INSTABILITY. 1997. 133 pp.
In English

64 FS SONNE - FAHRTBERICHT/CRUISE REPORT SO112 HIRESBAT (HIGH RESOLUTION BATHYMETRY).
Victoria, B.C., Canada - Apra Harbor, Guam. 17.09 - 08.10.1996.
Hrsg. von WILHELM WEINREBE. 1997. 90 pp.
Some chapters in German, some in English

65 NIELS NØRGAARD-PEDERSEN
LATE QUATERNARY ARCTIC OCEAN SEDIMENT RECORDS: SURFACE OCEAN CONDITIONS AND PROVENANCE OF ICE-RAFTED DEBRIS. 1997. 115 pp.
In English with German summary

66 THOMAS NÄHR
AUTHIGENER KLINOPTILOLITH IN MARINEN SEDIMENTEN - MINERALCHEMIE, GENESE UND MÖGLICHE ANWENDUNG ALS GEOTHERMOMETER. 1997. 119, 43 pp.
In German with English summary